ROLE OF HISTONE H1 IN NEURAL DIFFERENTIATION OF EMBRYONIC STEM CELLS

A Dissertation
Presented to
The Academic Faculty

By

Chenyi Pan

In Partial Fulfillment
of the Requirements for the Degree of
Doctor of Philosophy in the School of Biology

Georgia Institute of Technology
August 2015

ROLE OF HISTONE H1 IN NEURAL DIFFERENTIATION OF EMBRYONIC STEM CELLS

Approved by:

Dr. Yuhong Fan, Advisor
School of Biology
Georgia Institute of Technology

Dr. Alfred H. Merrill
School of Biology
Georgia Institute of Technology

Dr. Francesca Storici
School of Biology
Georgia Institute of Technology

Dr. Joseph M. Le Doux
Wallace H. Coulter Department of Biomedical Engineering
Georgia Institute of Technology

Dr. Adegboyega "Yomi" Oyelere
School of Chemistry and Biochemistry
Georgia Institute of Technology

Date Approved: February 10, 2015

To my parents and my family for their love, faith, and support

ACKNOWLEDGEMENTS

I would like to express my sincerest thankfulness to my thesis advisor, Dr. Yuhong Fan, from whom I have been fortunate enough to receive patient guidance and constant support, not only in scientific research but also in personal life. Without her accepting me into her lab and training me on critical thinking, experimental skills, and scientific writing, I would never be able to accomplish all the work and make it this far. Her enthusiasm and perseverance on solving scientific problems have guided me through tough times and will continue to encourage me to strive for success.

I want to show my appreciation to my committee members – Dr. Alfred Merrill, Dr. Francesca Storici, Dr. Joseph Le Doux, and Dr. Adegboyega (Yomi) Oyelere. Their guidance and help are valuable for my PhD study and future career.

One group of people I'll always remember and be grateful is the Fan lab at Georgia Tech including its past and current members. Dr. Yunzhe Zhang is a master in lab techniques and took care of everyone in the lab. She helped to derive a few H1 knockout ES cell lines used in my thesis, and also taught me a variety of techniques. I will never forget the scene that Dr. Yunzhe Zhang taught me lab techniques like preparing samples for PCR and running gel electrophoresis when I first joined the lab. Dr. Kaixiang Cao is such a wonderful buddy and helped me enormously in and outside research, especially on establishment of stable ES cell lines. I spent most of these years together with Dr. Yunzhe Zhang, Dr. Kaixiang Cao, and Dr. Magdalena Medrzycki. They are the ones to whom I always turn for help and advice, and I cannot thank them enough. I greatly appreciate Po-Yi Ho, Ting Wu, Zhiqiang Lin, Dr. Zheng Liu, Dr.

Shiraj Panjwani, Samantha Lasater, and those helpful undergrads I've worked with, for all their help throughout these years. I am particularly grateful to Ting Wu for her help in research. This is a wonderful family filled with happiness, teamwork, and mutual support within and outside research. Because of these wonderful people, these years have become an unforgettable memory in my life.

I thank Dr. Jessica Okosun and Dr. Jude Fitzgibbon at Queen Mary University of London and Dr. Hanjoong Jo at Georgia Tech/Emory University for fruitful collaborations.

I want to thank the wonderful staffs in IBB at Georgia Tech for their technical support and advice including Steve Woodard, James "Allen" Echols, Nadia Boguslavsky, Andrew Shaw, and Aqua Asberry. They were always there to offer help whenever I needed.

I am grateful to my friends at Georgia Tech community including Dr. Ziming Zhao, Dr. Jianrong Wang, Dr. Yu Zhang, Drs. Lee and Samantha Katz, Dr. Patrick Ruff, Dr. He Gong, Ziwei Sheng, Dr. Yongzhi Qiu, Dr. Ming Ruan, Dr. Danjue Chen, Dr. Yike Hu, and Li Zheng. I have been so fortunate to meet these amazing individuals and I appreciate their help along the way.

Finally, to my parents, my sister, and members of my extended family, I cannot express how much I appreciate their support and encouragement. Their whole-hearted love and faith in me motivate me to overcome difficulties, to thrive, and to strive for success. I am forever indebted to them.

TABLE OF CONTENTS

LIST OF FIGURES

LIST OF ABBREVIATIONS

A_{214}	absorbence at 214 nm
BCL2	B-cell lymphoma 2
bFGF	basic fibroblast growth factor
bp	base pair
BrdU	5-bromo-2'-deoxyuridine
C-terminal	carboxyl-terminal
C305T	cytosine to thymidine mutation at nucleotide position 305
cDNA	complementary DNA
CDS	coding DNA sequence
CHD8	chromodomain-helicase-DNA-binding protein 8
CREBBP	CREB binding protein
Cul4A	Cullin-4A
DNA	deoxyribonucleic acid
DLBCL	diffuse large B-cell lymphoma
DMEM	Dulbecco's modified Eagle's medium
DNMT1	DNA (cytosine-5)-methyltransferase 1
DNMT3B	DNA (cytosine-5)-methyltransferase 3B
Dox	doxycycline
E8.5	embryonic day 8.5
EB	embryoid body
EDTA	ethylenediaminetetraacetic acid
EP300	E1A binding protein p300
ESC	embryonic stem cell
FBS	fetal bovine serum
FL	follicular lymphoma
FLAG-H1d	FLAG-tagged H1d
FRAP	fluorescence recovery after photobleaching

GAPDH	glyceraldehyde 3-phosphate dehydrogenase
GFAP	glial fibrillary acidic protein
GFP	green fluorescent protein
GH5	globular domain of chicken histone H5
H1/nuc	H1 to nucleosome
$H1^0$ KO	$H1^0$ knockout
H1 TKO	H1c/H1d/H1e triple knockout
H1 QKO	H1c/H1d/H1e/$H1^0$ quadruple knockout
H3K4me3	histone H3 lysine 4 tri-methylation
H3K9Ac	histone H3 lysine 9 acetylation
H3K9me2	histone H3 lysine 9 di-methylation
H3K9me3	histone H3 lysine 9 tri-methylation
H3K27	histone H3 lysine 27
H3K27me3	histone H3 lysine 27 tri-methylation
H4K12	histone H4 lysine 12
H4K16Ac	histone H4 lysine 16 acetylation
H4K20	histone H4 lysine 20
H4K20me2	histone H4 lysine 20 di-methylation
H4K31	histone H4 lysine 31
hH1c	Human H1c
HP1	heterochromatin protein 1
HPLC	high-performance liquid chromatography
IgG	immunoglobulin G
IL-1β	interleukin 1β
JAK	Janus kinase
Kb	kilo base pairs
LIF	leukemia inhibitory factor
LTR	long terminal repeat
mAU	milli-absorbency units

miR-30	microRNA 30
MLL2	myeloid/lymphoid or mixed-lineage leukemia protein 2, also known as histone-lysine N-methyltransferase 2D (KMT2D)
Msx1	Msh homeobox 1
MyoD	Myogenic differentiation 1
N-terminal	amine-terminal
NF-κB	nuclear factor kappa-light-chain-enhancer of activated B cells
NHL	non-Hodgkin lymphoma
NRL	nucleosome repeat length
NSC	neural stem cell
Oct4	octamer-binding transcription factor 4, as known as POU domain, class 5, transcription factor 1 (Pou5f1)
p53	tumor protein 53
PAF1	RNA polymerase II-associated factor 1 homolog
PARP-1	poly(ADP-ribose) polymerase-1
PBS	phosphate buffered saline
PCR	polymerase chain reaction
PLO	poly-L-ornithine
poly-A	polyadenylation
PRC2	Polycomb Repressive Complex 2
QKO/abi	embryonic stem cells with H1c/H1d/H1e knockout and inducible knockdown of H1a and H1b
QKO/abi/H1^{res}	H1d overexpression in embryonic stem cells with H1c/H1d/H1e knockout and inducible knockdown of H1a and H1b
QKO/abi/Oct4i	embryonic stem cells with H1c/H1d/H1e knockout and inducible knockdown of H1a, H1b, and Oct4
QKO/sci	H1c/H1d/H1e knockout embryonic stem cells transduced with scramble shRNA
qRT-PCR	quantitative reverse transcription-PCR
RA	retinoic acid
RNA	ribonucleic acid

RNAi	RNA interference
RP-HPLC	reversed phase HPLC
rRNA	ribosomal RNA
S>F	serine to phenylalanine mutation
S102F	serine to phenylalanine mutation at amino acid 102
SA-β-Gal	senescence-associated β-galactosidase
S.D.	standard deviation
shRNA	short hairpin RNA
SirT1	NAD-dependent deacetylase sirtuin-1
STAT	signal transduction and transcription protein
Su(var)3-9	suppressor of variegation 3-9
Tet-On	tetracycline-controlled transcriptional activation
tFL	transformed follicular lymphoma
TH	tyrosine hydroxylase
TNF-α	tumor necrosis factor alpha
TUBB3	β-tubulin isotype III
WT	wildtype

SUMMARY

Linker histone H1 is a key structural protein facilitating the formation of higher order chromatin structures and regulates specific gene expression. In mammals, there exist 11 closely related H1 variants. Previous studies show that H1 depletion by 50% impairs specific gene regulation and differentiation of embryonic stem cells (ESCs). However, the mechanisms by which H1 and its variants regulate ESC differentiation remain elusive. Here, we demonstrate a dosage effect of H1 variants in mouse ESCs through severe H1 depletion and mutation analysis. We establish ultra-low H1 ESCs by sequential depletion of six somatic H1 variants. These cells exhibit normal ESC morphology and self-renewal. During neural differentiation, the total H1 level gradually increases, and H1 depletion reveals a dosage effect in neurite formation, induction of neural lineage-specific genes, and silencing of pluripotency-associated genes such as *Oct4* and *Nanog*. In addition, severe H1 depletion causes reduced cell proliferation and cellular senescence in neural lineages. Significantly, *Oct4* knockdown effectively restores neural differentiation and partially rescues the reduction in cell proliferation and cellular senescence. These results suggest that H1 is crucial for neural differentiation of ESCs and its regulation in the process acts in a dosage dependent, rather than a variant specific, manner.

Another part of this thesis centers on analysis of H1 mutations frequently occurred in follicular lymphoma or transformed follicular lymphoma. These mutations in H1 are clustered in the globular and C-terminal domains directly involved in chromatin binding. By comparing the properties of wild-type human H1c (hH1c) and mutant

hHc^{S102F} expressed in H1c/H1d/H1e triple knockout mouse ESCs, we find that S102F mutation dramatically impairs the association of hH1c with chromatin. These results suggest that the identified H1 mutations in follicular lymphoma most likely result in a loss-of-function phenotype by reducing the binding affinity of H1 for chromatin, thus compromising chromatin compaction and the regulation of specific genes.

CHAPTER 1

INTRODUCTION

1.1 Linker Histone H1 Family

In eukaryotic nuclei, DNA is packaged into chromatin by binding to histone proteins, a family of positively charged proteins, including H1, H2A, H2B, H3, and H4. The fundamental repeating unit of chromatin is the nucleosome (van Holde, 1988; Wolffe and Kurumizaka, 1998), which consists of about 147 base pairs of DNA wrapped approximately 1.7 turns around a core histone octamer (Davey et al., 2002; Luger et al., 1997). The DNA between nucleosomes is called "linker DNA", which together with nucleosome core particles form the extended chromatin fiber, the 10 nm "beads-on-a-string" fiber observed under the electron microscope (Olins and Olins, 1974; Woodcock et al., 1976). The linker histone H1 seals the nucleosomes at the entry and exit sites of DNA to stabilize the nucleosomes and facilitate the folding of the 30 nm chromatin fiber (Ramakrishnan, 1997; Thoma et al., 1979; Wolffe, 1997).

All metazoan histone H1s share a generic tri-partite structure consisting of a short, flexible N-terminal tail, a highly conserved globular domain with a winged-helix motif, and a long extended lysine rich C-terminal tail (Allan et al., 1980; Chapman et al., 1976; Ramakrishnan et al., 1993). The structure of H1s from unicellular eukaryotes, yeast and *Tetrahymena*, however, is rather different from metazoan H1s. *Tetrahymena* H1 lacks the most conserved globular domain found in multicellular organisms (Brown and Sittman, 1993; Wolffe, 1997; Wu et al., 1986), whereas the yeast H1, Hho1, consists of two such structured globular domains (Ushinsky et al., 1997). The central globular

domain of H1 is highly conserved and necessary for interaction with nucleosomal DNA (Brown et al., 2006). Both the globular and the C-terminal domains are involved in high affinity binding of H1 to chromatin (Brown et al., 2006; Hendzel et al., 2004; Stasevich et al., 2010; Syed et al., 2010). *In vivo* studies using H1-GFP fusion proteins and FRAP (Fluorescence Recovery after Photobleaching) assays show that the binding of H1 to chromatin is dynamic with a rapid exchange rate (Lever et al., 2000; Misteli et al., 2000).

The H1 histone family is the most divergent and heterogeneous group of histones among the highly conserved histone protein families. In mammals, as many as 11 closely related nonallelic H1 variants have been characterized, including 7 somatic H1s (H1a, H1b, H1c, H1d, H1e, $H1^0$, and H1x), 3 testicular H1s (H1t, H1T2, and HILS1), and one oocyte-specific H1 (H1oo) (Happel and Doenecke, 2009) (Figure 1.1). Each H1 variant is encoded by a single copy gene. While H1a-e are replication-dependent, mainly expressed in the S phase of the cell cycle, the replacement histone $H1^0$ is replication-independent, enriched in terminally differentiated cell types that have stopped dividing (Izzo et al., 2008; Khochbin, 2001; Sekeri-Pataryas and Sourlingas, 2007; Zlatanova and Doenecke, 1994). The mRNA messages of replication-dependent H1 genes lack introns and a poly-A tail, but possess a stem-loop sequence at the 3' end instead, and their proteins are mainly synthesized during S phase (Dominski and Marzluff, 1999). The replication-dependent H1a-e and H1t genes are clustered together with multiple core histone genes on human chromosome 6 and murine chromosome 13, whereas other H1 genes are scattered in the genome and expressed as polyadenylated mRNA messages throughout cell cycle independent of DNA replication. The most newly characterized variant, H1x, is quite divergent, sharing only 30% similarity in amino acid sequence with

other H1 variants (Happel et al., 2005; Yamamoto and Horikoshi, 1996). The expression of H1 variants is tightly regulated in development and cellular differentiation, and their composition differs in different tissues (Fan et al., 2003; Wang et al., 1997; Woodcock et al., 2006; Zhang et al., 2012). For example, while $H1^0$ and H1e are the major H1 variants in adult mouse liver, constituting ~30% and ~40% of total H1 respectively, these two variants only account for approximately 2% and 10% of total H1 in mouse thymus (Fan et al., 2003).

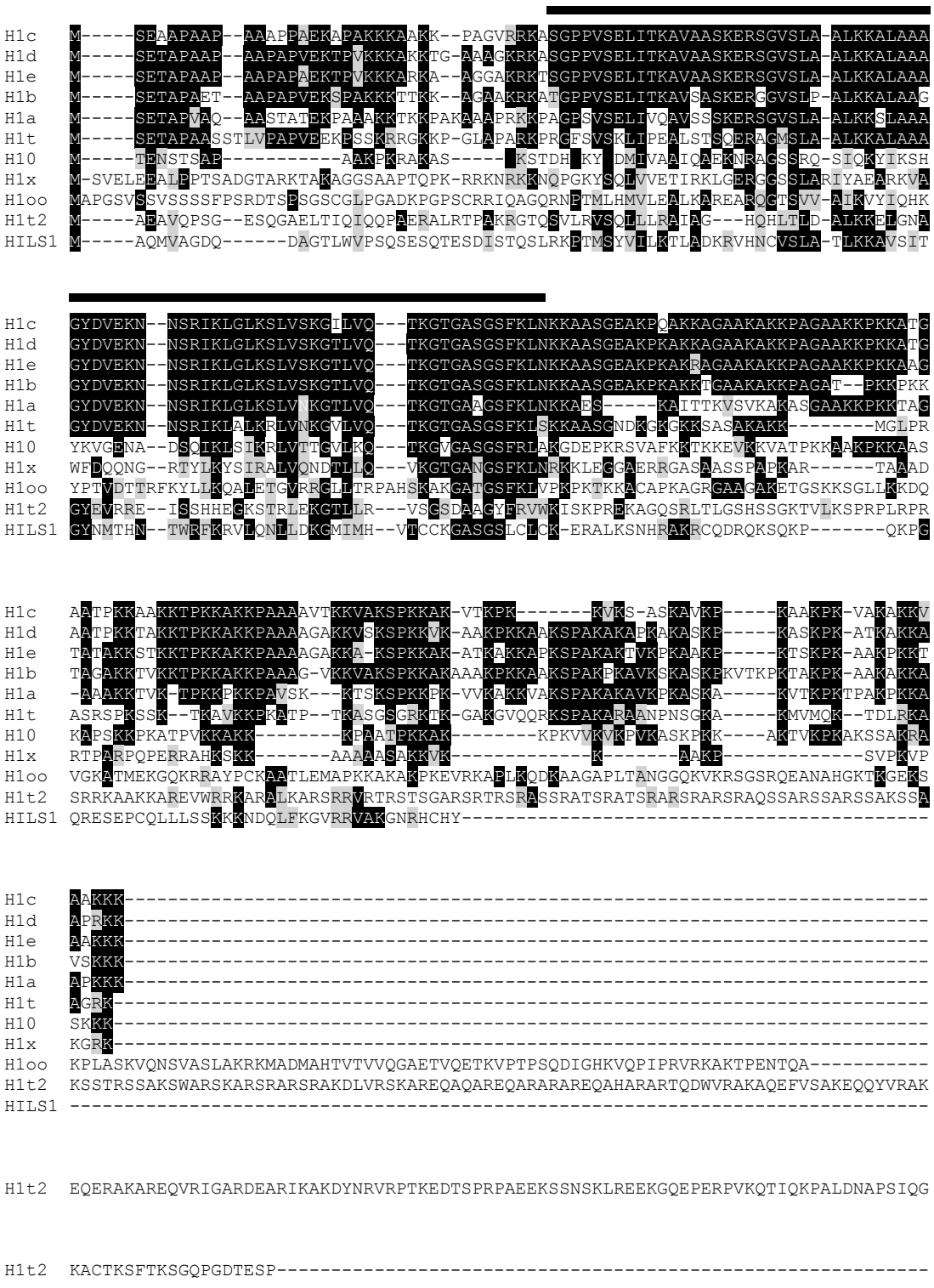

Figure 1.1 Multiple alignment of mouse histone H1 variants.

The black line on top of amino acid sequences marks the globular domain. Conversed residues are highlighted in black color and similar residues are highlighted in grey.

1.2 Histone H1 Depletion in Protists and Metazoans

Depletion of specific H1 variants has been performed in various protists and metazoans (Figure 1.2). The complete H1 elimination in protozoans such as *Saccharomyces cerevisiae* (Patterton et al., 1998), *Tetrahymena theromophila* (Shen et al., 1995), *Aspergillus nidulans* (Ramon et al., 2000), *Ascobolus immersus* (Barra et al., 2000), doesn't affect growth and viability, but it gives rise to distinct phenotypes. H1 deletion in *Tetrahymena* leads to enlarged nuclei (Shen and Gorovsky, 1996). Up- or down- regulation of specific genes is also observed in *Tetrahymena* (Shen and Gorovsky, 1996) and yeast (Hellauer et al., 2001) with H1 deletion, suggesting that linker histone H1 is a fine-tuner of specific genes rather than a global transcriptional regulator in unicellular organisms. Loss of H1 in *Ascobolus immersus* causes an abrupt stop of growth and increased accessibility of micrococcal nuclease to chromatin, indicating that H1 is necessary for long life span and chromatin organization (Barra et al., 2000). Similarly, another study finds that loss of the yeast H1 homolog, Hho1p, results in shortened life span in *Saccharomyces cerevisiae,* likely owing to a role of histone H1 in DNA repair by inhibiting homologous recombination (Downs et al., 2003). These findings indicate that, although histone H1 is not essential for survival of protists, it may function in chromatin compaction, gene expression, and DNA repair in these organisms.

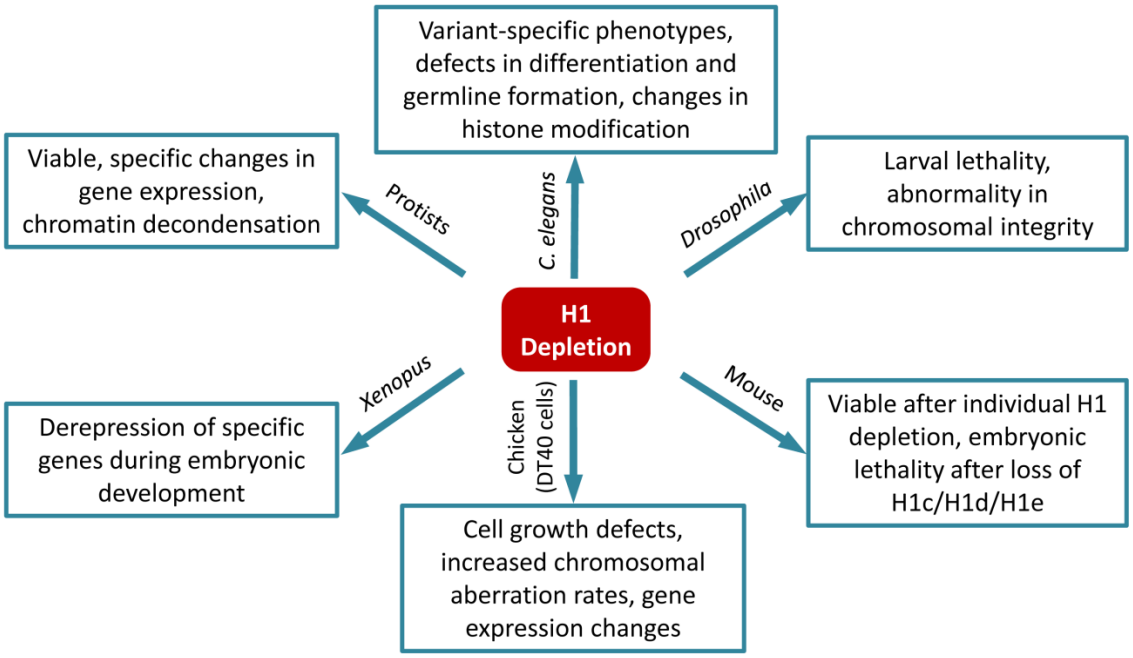

Figure 1.2 Overview of histone H1 depletion studies in multiple organisms.

In contrast to unicellular organisms, metazoans generally have multiple histone H1 variants, elimination of which gives rise to diverse phenotypes (Figure 1.2). *Caenorhabditis elegans* has eight H1 isoforms. *HIS-24* (an ortholog of mammalian *HIST1H1A*) depletion leads to severe abnormalities in germline proliferation and differentiation of hermaphrodites, as well as changes in H3K4 methylation and H3K9 methylation (Jedrusik and Schulze, 2001, 2007). In *Xenopus,* the oocyte- and embryo-specific H1 variant (named B4 or H1M) is replaced by somatic H1 variants during the transition from mid-blastula to neurulation (Andrews et al., 1991; Bouvet et al., 1994). This transition of H1 variants is the rate-limiting step for the loss of mesodermal competence, and ribozyme-mediated depletion of a somatic H1 variant leads to derepression of 5S rRNA expression and the regulatory genes required for loss of mesodermal competence during embryonic development (Bouvet et al., 1994; Kandolf, 1994; Steinbach et al., 1997). These studies suggest important roles of H1 variants in germline formation and embryogenesis of these organisms.

Drosophila melanogaster differs from other metazoans in that there have been only two H1 variants identified, a somatic H1, dH1 (Nagel and Grossbach, 2000), and a recently identified embryonic H1, dBigH1 (Perez-Montero et al., 2013). The reduced histone H1 complexity makes *Drosophila* an attractive system for investigating its *in vivo* functions. RNA interference (RNAi)-mediated dH1 depletion by 80% causes larval lethality and abnormalities in major pericentric heterochromatin-associated histone marks including H3K9me2 and H4K20me2 (Lu et al., 2009). The other fly H1 variant, dBigH1, mainly expressed during early embryogenesis and in germlines, shares the characteristic tripartite structure of the H1 family, showing a high degree of homology in the globular

and the C-terminal domains with dH1, but it distinguishes itself with an unusual long N-terminal domain enriched in negatively charged residues, suggesting a unique regulatory mechanism for dBigH1 (Perez-Montero et al., 2013). Indeed, abrogation of dBigH1 causes embryonic lethality at early development stages, likely due to a disruption in developmental programs by premature zygotic genome activation (Perez-Montero et al., 2013).

The first H1-null vertebrate cell line has been created by progressive deletion of all six H1 variants in DT40 chicken B lymphocytes. Individual H1-deficient mutants exhibit enhanced expression of the remaining H1 genes and distinct changes in gene expression (Takami et al., 2000). Complete H1 null DT40 cells display severe growth defects, decreased chromatin compaction, and increased chromosome aberration rates, as well as gene expression changes (Hashimoto et al., 2010). In this study, however, 17 core histone alleles were also removed by bulk deletion, making it difficult to assess whether the observed effects are solely attributable to the loss of histone H1.

In mammals, there are 11 nonallelic H1 variants identified. Gene targeting studies of H1 in mice have unveiled interesting features of H1. Due to compensation of other H1 variants, mice with single or double knockout of somatic H1s (H1a, H1c, H1d, H1e, and $H1^0$) are viable and develop normally (Fan et al., 2001; Lin et al., 2004; Sirotkin et al., 1995). Nonetheless, further investigation reveals distinct phenotypes in certain single or double H1 knockouts. For example, $H1^0$ expression is found to be associated with production of dendritic cells, a type of antigen-presenting cells in the immune system, and $H1^0$ deletion significantly impairs this process, suggesting a specific function of $H1^0$ in certain immune cells (Gabrilovich et al., 2002). Another interesting

phenomenon raised in certain single H1 knockout mice is the position effect variegation, defined as variations in the expression of a transgene caused by changes in the local chromatin structure in different cell types. Loss of H1d and H1e, but not H1a, H1c, or $H1^0$ attenuates age-dependent silencing of transgenes (Alami et al., 2003), indicating that H1 variants can differentially modulate higher order chromatin structures and gene expression. Beside somatic H1 variants, knockout studies have also been performed in testis-specific H1 variants in mice. Elimination of the most abundant H1 variant in spermatocyte, H1t, doesn't have apparent effects on spermatogenesis (Drabent et al., 2000; Fantz et al., 2001; Lin et al., 2000). Yet, another testis-specific variant, H1T2, is found to be required for chromatin packaging and spermatid elongation during spermiogenesis (Martianov et al., 2005; Tanaka et al., 2005). These studies establish both redundancy and specificity of the histone H1 family in mammals.

An impressive progress on the study of histone H1 comes from compound deletion of three H1 variants, H1c, H1d, and H1e, in mice, which causes a 50% reduction in the total H1 level and embryonic lethality (Fan et al., 2003). H1c/H1d/H1e triple knockout (H1 TKO) embryonic stem cells (ESCs) derived thereof show reduced chromatin compaction and nucleosome repeat length (Fan et al., 2005). Interestingly, only a small number of genes are found to be affected in these cells, overrepresented by imprinted genes normally regulated by DNA methylation. Marked reduction in the H1 content in ESCs affects specific DNA methylation patterns at the regulatory regions of the affected genes which may be particularly sensitive to changes in H1 occupancy (Fan et al., 2005). This level of H1 depletion also leads to a reduction in both H4K12 acetylation and H3K27 methylation in ESCs. The change in H4K12 acetylation is likely

to neutralize negative DNA charges in response to dramatic loss of H1, allowing for tighter chromatin compaction (Fan et al., 2005).

Taken together, these studies on H1 disruption have shed significant light on the *in vivo* functions of histone H1 in various organisms. H1 is not essential for protists, but play important developmental roles in metazoans. Furthermore, both functional redundancy and specificity of H1 variants have been observed these studies.

1.3 The Role of Histone H1 in Chromatin Compaction and Gene Regulation

Histone H1 binds to nucleosomes and linker DNA to protect additional ~20 bp of DNA (Meyer et al., 2011; Simpson, 1978; Syed et al., 2010), and the binding of H1 dramatically affects nucleosomal spacing, with the total H1 level positively correlated with the nucleosome repeat length (NRL) (Woodcock et al., 2006). Cells with a higher H1 to nucleosome ratio tend to have a longer NRL and more organized and compact chromatin fibers, and a reduction in H1 content leads to a reduced NRL and less compact chromatin (Fan et al., 2005; Hashimoto et al., 2010; Popova et al., 2013; Woodcock et al., 2006). Among the three domains, the globular and intrinsically disordered C-terminal domains are essential for chromatin binding and compaction (Allan et al., 1980; Allan et al., 1986; Hendzel et al., 2004; Luque et al., 2014). Although the N-terminal domain appears to be nonessential for higher order chromatin compaction, its deletion or swapping between different H1 variants changes the binding affinity of the respective H1 for chromatin (Allan et al., 1986; Hendzel et al., 2004; Oberg and Belikov, 2012; Vyas and Brown, 2012).

Different H1 variants exhibit significant sequence divergence from one another, especially in the C-terminal domain, suggesting distinct functions for these variants in chromatin compaction. Indeed, FRAP studies have shown that H1 variants differ in chromatin binding affinity and residence time dependent on the length of the C-terminal tail, as well as on the density of basic residues and the number of S/TPXK phosphorylation sites (Th'ng et al., 2005). Human H1a and H1c have the shortest C-terminal domain and also residence time, whereas the variants with longer tails, namely H1b and H1e, show higher binding affinity for chromatin. Recently, striking differences of H1 variants in the binding affinity for chromatin have also been demonstrated by *in vitro* and *in vivo* chromatin assembly studies (Oberg et al., 2012; Orrego et al., 2007). Given that H1 variants bind to DNA with distinct affinities and vary in their abilities in chromatin condensation (Clausell et al., 2009), the dramatically different compositions of H1 variants in various tissues could result in fine tuning chromatin condensation in both bulk chromatin and at specific regions in the genome.

Because of its role in chromatin folding and its hyperphosphorylation as a hallmark of mitosis (Boggs et al., 2000; Hansen, 2002), histone H1 has been hypothesized to be a pivotal determinant of the mitotic chromosome structure. Indeed, H1 has been shown to be essential for *in vitro* assembly of mitotic chromosomes in *Xenopus* egg extracts (Maresca et al., 2005). In *Drosophila*, H1 is required for proper alignment of sister chromatids and the establishment of pericentric heterochromatin, likely mediated through recruitment of the heterochromatin-specific histone H3 lysine 9 methyltransferase Su(var)3-9 (Lu et al., 2009; Lu et al., 2013). The direct interaction of H1 with heterochromatin protein HP1 may also contribute to heterochromatin formation

(Daujat et al., 2005; Hale et al., 2006; Nielsen et al., 2001; Studencka et al., 2012). While H1x has been reported to be required for correct mitotic progression in HeLa cells, chicken lymphocytes with complete H1 knockout are not affected in mitotic chromosomal structure (Hashimoto et al., 2010; Takata et al., 2007). Therefore, more evidence is needed to define the role of H1 in chromosomal integrity and mitotic chromosome structure.

As an important component of eukaryotic chromatin, H1 is also engaged in epigenetic regulation including DNA methylation and histone modifications in multiple organisms. In *Ascobolus immersus* and *Arabidoposis thaliana*, H1 abolishment leads to global DNA hypermethylation and stochastic alterations in DNA methylation respectively (Wendt et al., 2008; Wierzbicki and Jerzmanowski, 2005). In mammals, compound loss of three H1 variants causes loci-specific DNA hypomethylation in mouse ESCs (Fan et al., 2005). This study for the first time establishes a connection between H1 and DNA methylation in mammals. More recently, H1 is shown to promote and maintain DNA methylation by recruiting DNA methyltransferases, DNMT1 and DNMT3B, to specific regions in the genome (Kashiwagi et al., 2011; Yang et al., 2013).

Beside its interaction with DNMT's, both *in vitro* and *in vivo* studies have identified physical interactions of H1 with enzymes responsible for specific histone modifications, including PRC2-EZH2 complex (Martin et al., 2006), which catalyzes H3K27 di- and tri- methylation (Cao et al., 2002; Margueron et al., 2008; Shen et al., 2008), and SirT1, a histone deacetylase preferentially targeting to H3K9Ac and H4K16Ac (Vaquero et al., 2004). Histone marks affected by H1 depletion include H3K4 methylation and H3K9 methylation in *C. elegans* (Jedrusik and Schulze, 2001), H3K9

dimethylation and H4K20 dimethylation in *Drosophila* (Lu et al., 2009), and H4K12 acetylation and H3K27 trimethylation in mouse ESCs (Fan et al., 2005). These results reinforce the role of H1 in epigenetic regulation of genes.

A plethora of studies unravel H1 to be gene-specific regulators. For example, H1 forms a complex with CHD8 to suppress p53-mediated transcription and apoptosis during early embryogenesis (Nishiyama et al., 2009). In addition, H1 is shown to modulate the expression of specific genes in ESCs, which is mediated at least partially through its effects on DNA methylation (Fan et al., 2005; Giambra et al., 2008; Maclean et al., 2011). In human promonocytes, H1 coordinates with HMGB1, a member of non-histone chromatin-associated proteins, to silence proinflammatory tumor necrosis factor alpha (TNF-α) and interleukin 1β (IL-1β) after the initiation of severe systemic inflammation (Cato et al., 2008; El Gazzar et al., 2009). H1 has also been shown to compete with PARP-1 (poly(ADP-ribose) polymerase-1) in regulating gene expression in human breast cancer cells (Krishnakumar et al., 2008; Shan et al., 2014).

Other lines of evidence demonstrate variant specificities of H1 in gene regulation. Msx1 specifically interacts with H1b at a key regulatory element of *MyoD*, a central regulator of skeletal muscle differentiation, to suppress myogenesis during embryonic development (Lee et al., 2004). Overexpression of $H1^0$ and H1c elicits different effects in gene expression in 3T3 cells and knockdown of individual H1 variants in human breast cancer cell line T47D also causes expression changes in specific genes (Brown et al., 1997; Gunjan and Brown, 1999; Sancho et al., 2008). Using a set of single H1 variant knockout mice, Alami *et al.* find that H1 variants can differentially affect transgene expression as modifiers for position effect variegation of β-globin transgenes *in vivo*

(Alami et al., 2003). H1c specifically interacts with Cul4A E3 ubiquitin ligase and PAF1 elongation complexes to activate gene transcription by inducing H4K31 ubiquitination, H3K4me3, and H3K79me2 (Kim et al., 2013). Recently, we also demonstrated that overexpression of H1d, but not other H1 variants, potently represses the noncoding oncogene *H19* in ovarian cancer cells (Medrzycki et al., 2014). Modulation of the expression levels of specific H1 variants inhibits cell growth, which is likely due to, at least partially, the effects of H1 on gene expression. The difference of H1 variants in gene regulation is probably owing to their different affinities for chromatin and capacities for DNA compaction, as well as the divergent C-terminal domain (Clausell et al., 2009; Th'ng et al., 2005).

Recent genome-wide profiling studies on epitope-tagged H1 variants take a different approach to elucidate H1 functions, which show that H1 is generally depleted at GC-rich and gene-rich regions and active promoters, as well as regulatory elements controlling transcription (Cao et al., 2013; Izzo et al., 2013; Millan-Arino et al., 2014). In particular, H1 occupancy at transcription start sites appears to be positively correlated with the repressive histone mark H3K9me3 and in negative correlation with the active histone mark H3K4me3. Taken together, these studies indicate that H1 variants are important in regulating specific gene expression.

In addition to the aforementioned functions, H1 is also implicated in genome surveillance and DNA repair. An intriguing example is the direct involvement of H1c in double-strand break induced apoptosis (Konishi et al., 2003). When initiated by X-ray- or etoposide- induced DNA double-strand breaks, H1c (but not other H1 variants) translocates to the cytoplasm and functions as a cytochrome C-releasing factor to

stimulate cell apoptosis (Konishi et al., 2003). H1 also has been reported to suppress p53-mediated transcription and apoptosis through association with other cofactors (Kim et al., 2008; Nishiyama et al., 2009). Moreover, H1 can serve as a stimulating factor for non-homologous end-joining and homologous recombination mediated DNA repair (Hashimoto et al., 2007; Rosidi et al., 2008), and H1 depletion increases DNA damage response in yeast and mouse ESCs (Downs et al., 2003; Murga et al., 2007). These findings suggest additional functions of H1 in chromatin and gene regulation.

1.4 Objectives

Previous studies have shown that compound depletion of H1c/H1d/H1e leads to specific changes in gene regulation (Fan et al., 2005) and impaired ESCs differentiation (Zhang et al., 2012). However, there is still 50% H1 remaining in these cells. Therefore, one goal of this study is to determine if H1 is essential for ESC self-renewal and differentiation by depleting the remaining H1 variants in ESCs and to investigate the underlying regulatory mechanisms. On the other hand, recurrent mutations in multiple H1 variants have been identified in follicular lymphoma (Li et al., 2014; Lohr et al., 2012; Morin et al., 2011; Okosun et al., 2014). Therefore, the other goal of this study is to elucidate how H1 mutations will affect their *in vivo* functions and contribute to tumorigenesis. Completion of this study is expected to provide new insights into the functions of histone H1 in chromatin compaction and gene regulation during development and tumorigenesis.

1.5 References

Alami, R., Fan, Y., Pack, S., Sonbuchner, T.M., Besse, A., Lin, Q., Greally, J.M., Skoultchi, A.I., and Bouhassira, E.E. (2003). Mammalian linker-histone subtypes differentially affect gene expression in vivo. Proc Natl Acad Sci U S A *100*, 5920-5925.

Allan, J., Hartman, P.G., Crane-Robinson, C., and Aviles, F.X. (1980). The structure of histone H1 and its location in chromatin. Nature *288*, 675-679.

Allan, J., Mitchell, T., Harborne, N., Bohm, L., and Crane-Robinson, C. (1986). Roles of H1 domains in determining higher order chromatin structure and H1 location. J Mol Biol *187*, 591-601.

Andrews, M.T., Loo, S., and Wilson, L.R. (1991). Coordinate inactivation of class III genes during the Gastrula-Neurula Transition in Xenopus. Dev Biol *146*, 250-254.

Barra, J.L., Rhounim, L., Rossignol, J.L., and Faugeron, G. (2000). Histone H1 is dispensable for methylation-associated gene silencing in Ascobolus immersus and essential for long life span. Mol Cell Biol *20*, 61-69.

Boggs, B.A., Allis, C.D., and Chinault, A.C. (2000). Immunofluorescent studies of human chromosomes with antibodies against phosphorylated H1 histone. Chromosoma *108*, 485-490.

Bouvet, P., Dimitrov, S., and Wolffe, A.P. (1994). Specific regulation of Xenopus chromosomal 5S rRNA gene transcription in vivo by histone H1. Genes Dev *8*, 1147-1159.

Brown, D.T., Gunjan, A., Alexander, B.T., and Sittman, D.B. (1997). Differential effect of H1 variant overproduction on gene expression is due to differences in the central globular domain. Nucleic Acids Res *25*, 5003-5009.

Brown, D.T., Izard, T., and Misteli, T. (2006). Mapping the interaction surface of linker histone H1(0) with the nucleosome of native chromatin in vivo. Nat Struct Mol Biol *13*, 250-255.

Brown, D.T., and Sittman, D.B. (1993). Identification through overexpression and tagging of the variant type of the mouse H1e and H1c genes. J Biol Chem *268*, 713-718.

Cao, K., Lailler, N., Zhang, Y., Kumar, A., Uppal, K., Liu, Z., Lee, E.K., Wu, H., Medrzycki, M., Pan, C., *et al.* (2013). High-resolution mapping of h1 linker histone variants in embryonic stem cells. PLoS Genet *9*, e1003417.

Cao, R., Wang, L., Wang, H., Xia, L., Erdjument-Bromage, H., Tempst, P., Jones, R.S., and Zhang, Y. (2002). Role of histone H3 lysine 27 methylation in Polycomb-group silencing. Science *298*, 1039-1043.

Cato, L., Stott, K., Watson, M., and Thomas, J.O. (2008). The interaction of HMGB1 and linker histones occurs through their acidic and basic tails. J Mol Biol *384*, 1262-1272.

Chapman, G.E., Hartman, P.G., and Bradbury, E.M. (1976). Studies on the role and mode of operation of the very-lysine-rich histone H1 in eukaryote chromatin. The isolation of the globular and non-globular regions of the histone H1 molecule. In Eur J Biochem, pp. 69-75.

Clausell, J., Happel, N., Hale, T.K., Doenecke, D., and Beato, M. (2009). Histone H1 subtypes differentially modulate chromatin condensation without preventing ATP-dependent remodeling by SWI/SNF or NURF. PLoS One *4*, e0007243.

Daujat, S., Zeissler, U., Waldmann, T., Happel, N., and Schneider, R. (2005). HP1 binds specifically to Lys26-methylated histone H1.4, whereas simultaneous Ser27 phosphorylation blocks HP1 binding. J Biol Chem *280*, 38090-38095.

Davey, C.A., Sargent, D.F., Luger, K., Maeder, A.W., and Richmond, T.J. (2002). Solvent mediated interactions in the structure of the nucleosome core particle at 1.9 a resolution. J Mol Biol *319*, 1097-1113.

Dominski, Z., and Marzluff, W.F. (1999). Formation of the 3' end of histone mRNA. Gene *239*, 1-14.

Downs, J.A., Kosmidou, E., Morgan, A., and Jackson, S.P. (2003). Suppression of homologous recombination by the Saccharomyces cerevisiae linker histone. Mol Cell *11*, 1685-1692.

Drabent, B., Saftig, P., Bode, C., and Doenecke, D. (2000). Spermatogenesis proceeds normally in mice without linker histone H1t. Histochem Cell Biol *113*, 433-442.

El Gazzar, M., Yoza, B.K., Chen, X., Garcia, B.A., Young, N.L., and McCall, C.E. (2009). Chromatin-specific remodeling by HMGB1 and linker histone H1 silences proinflammatory genes during endotoxin tolerance. Mol Cell Biol *29*, 1959-1971.

Fan, Y., Nikitina, T., Morin-Kensicki, E.M., Zhao, J., Magnuson, T.R., Woodcock, C.L., and Skoultchi, A.I. (2003). H1 linker histones are essential for mouse development and affect nucleosome spacing in vivo. Mol Cell Biol *23*, 4559-4572.

Fan, Y., Nikitina, T., Zhao, J., Fleury, T.J., Bhattacharyya, R., Bouhassira, E.E., Stein, A., Woodcock, C.L., and Skoultchi, A.I. (2005). Histone H1 depletion in mammals alters global chromatin structure but causes specific changes in gene regulation. Cell *123*, 1199-1212.

Fan, Y., Sirotkin, A., Russell, R.G., Ayala, J., and Skoultchi, A.I. (2001). Individual somatic H1 subtypes are dispensable for mouse development even in mice lacking the H1(0) replacement subtype. Mol Cell Biol *21*, 7933-7943.

Fantz, D.A., Hatfield, W.R., Horvath, G., Kistler, M.K., and Kistler, W.S. (2001). Mice with a targeted disruption of the H1t gene are fertile and undergo normal changes in structural chromosomal proteins during spermiogenesis. Biol Reprod *64*, 425-431.

Gabrilovich, D.I., Cheng, P., Fan, Y., Yu, B., Nikitina, E., Sirotkin, A., Shurin, M., Oyama, T., Adachi, Y., Nadaf, S., *et al.* (2002). H1(0) histone and differentiation of dendritic cells. A molecular target for tumor-derived factors. J Leukoc Biol *72*, 285-296.

Giambra, V., Volpi, S., Emelyanov, A.V., Pflugh, D., Bothwell, A.L., Norio, P., Fan, Y., Ju, Z., Skoultchi, A.I., Hardy, R.R., *et al.* (2008). Pax5 and linker histone H1 coordinate DNA methylation and histone modifications in the 3' regulatory region of the immunoglobulin heavy chain locus. Mol Cell Biol *28*, 6123-6133.

Gunjan, A., and Brown, D.T. (1999). Overproduction of histone H1 variants in vivo increases basal and induced activity of the mouse mammary tumor virus promoter. Nucleic Acids Res *27*, 3355-3363.

Hale, T.K., Contreras, A., Morrison, A.J., and Herrera, R.E. (2006). Phosphorylation of the linker histone H1 by CDK regulates its binding to HP1alpha. Mol Cell *22*, 693-699.

Hansen, J.C. (2002). Conformational dynamics of the chromatin fiber in solution: determinants, mechanisms, and functions. Annu Rev Biophys Biomol Struct *31*, 361-392.

Happel, N., and Doenecke, D. (2009). Histone H1 and its isoforms: contribution to chromatin structure and function. Gene *431*, 1-12.

Happel, N., Schulze, E., and Doenecke, D. (2005). Characterisation of human histone H1x. Biol Chem *386*, 541-551.

Hashimoto, H., Sonoda, E., Takami, Y., Kimura, H., Nakayama, T., Tachibana, M., Takeda, S., and Shinkai, Y. (2007). Histone H1 variant, H1R is involved in DNA damage response. DNA Repair (Amst) *6*, 1584-1595.

Hashimoto, H., Takami, Y., Sonoda, E., Iwasaki, T., Iwano, H., Tachibana, M., Takeda, S., Nakayama, T., Kimura, H., and Shinkai, Y. (2010). Histone H1 null vertebrate cells exhibit altered nucleosome architecture. Nucleic Acids Res *38*, 3533-3545.

Hellauer, K., Sirard, E., and Turcotte, B. (2001). Decreased expression of specific genes in yeast cells lacking histone H1. J Biol Chem *276*, 13587-13592.

Hendzel, M.J., Lever, M.A., Crawford, E., and Th'ng, J.P. (2004). The C-terminal domain is the primary determinant of histone H1 binding to chromatin in vivo. J Biol Chem *279*, 20028-20034.

Izzo, A., Kamieniarz-Gdula, K., Ramirez, F., Noureen, N., Kind, J., Manke, T., van Steensel, B., and Schneider, R. (2013). The genomic landscape of the somatic linker histone subtypes H1.1 to H1.5 in human cells. Cell reports *3*, 2142-2154.

Izzo, A., Kamieniarz, K., and Schneider, R. (2008). The histone H1 family: specific members, specific functions? Biol Chem *389*, 333-343.

Jedrusik, M.A., and Schulze, E. (2001). A single histone H1 isoform (H1.1) is essential for chromatin silencing and germline development in Caenorhabditis elegans. Development *128*, 1069-1080.

Jedrusik, M.A., and Schulze, E. (2007). Linker histone HIS-24 (H1.1) cytoplasmic retention promotes germ line development and influences histone H3 methylation in Caenorhabditis elegans. Mol Cell Biol *27*, 2229-2239.

Kandolf, H. (1994). The H1A histone variant is an in vivo repressor of oocyte-type 5S gene transcription in Xenopus laevis embryos. Proc Natl Acad Sci U S A *91*, 7257-7261.

Kashiwagi, K., Nimura, K., Ura, K., and Kaneda, Y. (2011). DNA methyltransferase 3b preferentially associates with condensed chromatin. Nucleic Acids Res *39*, 874-888.

Khochbin, S. (2001). Histone H1 diversity: bridging regulatory signals to linker histone function. Gene *271*, 1-12.

Kim, K., Choi, J., Heo, K., Kim, H., Levens, D., Kohno, K., Johnson, E.M., Brock, H.W., and An, W. (2008). Isolation and characterization of a novel H1.2 complex that acts as a repressor of p53-mediated transcription. J Biol Chem *283*, 9113-9126.

Kim, K., Lee, B., Kim, J., Choi, J., Kim, J.M., Xiong, Y., Roeder, R.G., and An, W. (2013). Linker Histone H1.2 cooperates with Cul4A and PAF1 to drive H4K31 ubiquitylation-mediated transactivation. Cell reports *5*, 1690-1703.

Konishi, A., Shimizu, S., Hirota, J., Takao, T., Fan, Y., Matsuoka, Y., Zhang, L., Yoneda, Y., Fujii, Y., Skoultchi, A.I., *et al.* (2003). Involvement of histone H1.2 in apoptosis induced by DNA double-strand breaks. Cell *114*, 673-688.

Krishnakumar, R., Gamble, M.J., Frizzell, K.M., Berrocal, J.G., Kininis, M., and Kraus, W.L. (2008). Reciprocal binding of PARP-1 and histone H1 at promoters specifies transcriptional outcomes. Science *319*, 819-821.

Lee, H., Habas, R., and Abate-Shen, C. (2004). MSX1 cooperates with histone H1b for inhibition of transcription and myogenesis. Science *304*, 1675-1678.

Lever, M.A., Th'ng, J.P., Sun, X., and Hendzel, M.J. (2000). Rapid exchange of histone H1.1 on chromatin in living human cells. Nature *408*, 873-876.

Li, H., Kaminski, M.S., Li, Y., Yildiz, M., Ouillette, P., Jones, S., Fox, H., Jacobi, K., Saiya-Cork, K., Bixby, D., *et al.* (2014). Mutations in linker histone genes HIST1H1 B, C, D, and E; OCT2 (POU2F2); IRF8; and ARID1A underlying the pathogenesis of follicular lymphoma. Blood *123*, 1487-1498.

Lin, Q., Inselman, A., Han, X., Xu, H., Zhang, W., Handel, M.A., and Skoultchi, A.I. (2004). Reductions in linker histone levels are tolerated in developing spermatocytes but cause changes in specific gene expression. J Biol Chem *279*, 23525-23535.

Lin, Q., Sirotkin, A., and Skoultchi, A.I. (2000). Normal spermatogenesis in mice lacking the testis-specific linker histone H1t. Mol Cell Biol *20*, 2122-2128.

Lohr, J.G., Stojanov, P., Lawrence, M.S., Auclair, D., Chapuy, B., Sougnez, C., Cruz-Gordillo, P., Knoechel, B., Asmann, Y.W., Slager, S.L., *et al.* (2012). Discovery and prioritization of somatic mutations in diffuse large B-cell lymphoma (DLBCL) by whole-exome sequencing. Proc Natl Acad Sci U S A *109*, 3879-3884.

Lu, X., Wontakal, S.N., Emelyanov, A.V., Morcillo, P., Konev, A.Y., Fyodorov, D.V., and Skoultchi, A.I. (2009). Linker histone H1 is essential for Drosophila development, the establishment of pericentric heterochromatin, and a normal polytene chromosome structure. Genes Dev *23*, 452-465.

Lu, X., Wontakal, S.N., Kavi, H., Kim, B.J., Guzzardo, P.M., Emelyanov, A.V., Xu, N., Hannon, G.J., Zavadil, J., Fyodorov, D.V., *et al.* (2013). Drosophila H1 regulates the genetic activity of heterochromatin by recruitment of Su(var)3-9. Science *340*, 78-81.

Luger, K., Mader, A.W., Richmond, R.K., Sargent, D.F., and Richmond, T.J. (1997). Crystal structure of the nucleosome core particle at 2.8 A resolution. Nature *389*, 251-260.

Luque, A., Collepardo-Guevara, R., Grigoryev, S., and Schlick, T. (2014). Dynamic condensation of linker histone C-terminal domain regulates chromatin structure. Nucleic Acids Res *42*, 7553-7560.

Maclean, J.A., Bettegowda, A., Kim, B.J., Lou, C.H., Yang, S.M., Bhardwaj, A., Shanker, S., Hu, Z., Fan, Y., Eckardt, S., *et al.* (2011). The rhox homeobox gene cluster is imprinted and selectively targeted for regulation by histone h1 and DNA methylation. Mol Cell Biol *31*, 1275-1287.

Maresca, T.J., Freedman, B.S., and Heald, R. (2005). Histone H1 is essential for mitotic chromosome architecture and segregation in Xenopus laevis egg extracts. J Cell Biol *169*, 859-869.

Margueron, R., Li, G., Sarma, K., Blais, A., Zavadil, J., Woodcock, C.L., Dynlacht, B.D., and Reinberg, D. (2008). Ezh1 and Ezh2 maintain repressive chromatin through different mechanisms. Mol Cell *32*, 503-518.

Martianov, I., Brancorsini, S., Catena, R., Gansmuller, A., Kotaja, N., Parvinen, M., Sassone-Corsi, P., and Davidson, I. (2005). Polar nuclear localization of H1T2, a histone H1 variant, required for spermatid elongation and DNA condensation during spermiogenesis. Proc Natl Acad Sci U S A *102*, 2808-2813.

Martin, C., Cao, R., and Zhang, Y. (2006). Substrate preferences of the EZH2 histone methyltransferase complex. J Biol Chem *281*, 8365-8370.

Medrzycki, M., Zhang, Y., Zhang, W., Cao, K., Pan, C., Lailler, N., McDonald, J.F., Bouhassira, E.E., and Fan, Y. (2014). Histone h1.3 suppresses h19 noncoding RNA expression and cell growth of ovarian cancer cells. Cancer Res *74*, 6463-6473.

Meyer, S., Becker, N.B., Syed, S.H., Goutte-Gattat, D., Shukla, M.S., Hayes, J.J., Angelov, D., Bednar, J., Dimitrov, S., and Everaers, R. (2011). From crystal and NMR structures, footprints and cryo-electron-micrographs to large and soft structures: nanoscale modeling of the nucleosomal stem. Nucleic Acids Res *39*, 9139-9154.

Millan-Arino, L., Islam, A.B., Izquierdo-Bouldstridge, A., Mayor, R., Terme, J.M., Luque, N., Sancho, M., Lopez-Bigas, N., and Jordan, A. (2014). Mapping of six somatic linker histone H1 variants in human breast cancer cells uncovers specific features of H1.2. Nucleic Acids Res *42*, 4474-4493.

Misteli, T., Gunjan, A., Hock, R., Bustin, M., and Brown, D.T. (2000). Dynamic binding of histone H1 to chromatin in living cells. Nature *408*, 877-881.

Morin, R.D., Mendez-Lago, M., Mungall, A.J., Goya, R., Mungall, K.L., Corbett, R.D., Johnson, N.A., Severson, T.M., Chiu, R., Field, M., *et al.* (2011). Frequent mutation of histone-modifying genes in non-Hodgkin lymphoma. Nature *476*, 298-303.

Murga, M., Jaco, I., Fan, Y., Soria, R., Martinez-Pastor, B., Cuadrado, M., Yang, S.M., Blasco, M.A., Skoultchi, A.I., and Fernandez-Capetillo, O. (2007). Global chromatin compaction limits the strength of the DNA damage response. J Cell Biol *178*, 1101-1108.

Nagel, S., and Grossbach, U. (2000). Histone H1 genes and histone gene clusters in the genus Drosophila. Journal of molecular evolution *51*, 286-298.

Nielsen, A.L., Oulad-Abdelghani, M., Ortiz, J.A., Remboutsika, E., Chambon, P., and Losson, R. (2001). Heterochromatin formation in mammalian cells: interaction between histones and HP1 proteins. Mol Cell *7*, 729-739.

Nishiyama, M., Oshikawa, K., Tsukada, Y., Nakagawa, T., Iemura, S., Natsume, T., Fan, Y., Kikuchi, A., Skoultchi, A.I., and Nakayama, K.I. (2009). CHD8 suppresses p53-mediated apoptosis through histone H1 recruitment during early embryogenesis. Nat Cell Biol *11*, 172-182.

Oberg, C., and Belikov, S. (2012). The N-terminal domain determines the affinity and specificity of H1 binding to chromatin. Biochem Biophys Res Commun *420*, 321-324.

Oberg, C., Izzo, A., Schneider, R., Wrange, O., and Belikov, S. (2012). Linker histone subtypes differ in their effect on nucleosomal spacing in vivo. J Mol Biol *419*, 183-197.

Okosun, J., Bodor, C., Wang, J., Araf, S., Yang, C.Y., Pan, C., Boller, S., Cittaro, D., Bozek, M., Iqbal, S., *et al.* (2014). Integrated genomic analysis identifies recurrent mutations and evolution patterns driving the initiation and progression of follicular lymphoma. Nat Genet *46*, 176-181.

Olins, A.L., and Olins, D.E. (1974). Spheroid chromatin units (v bodies). Science *183*, 330-332.

Orrego, M., Ponte, I., Roque, A., Buschati, N., Mora, X., and Suau, P. (2007). Differential affinity of mammalian histone H1 somatic subtypes for DNA and chromatin. BMC biology *5*, 22.

Patterton, H.G., Landel, C.C., Landsman, D., Peterson, C.L., and Simpson, R.T. (1998). The biochemical and phenotypic characterization of Hho1p, the putative linker histone H1 of Saccharomyces cerevisiae. J Biol Chem *273*, 7268-7276.

Perez-Montero, S., Carbonell, A., Moran, T., Vaquero, A., and Azorin, F. (2013). The embryonic linker histone H1 variant of Drosophila, dBigH1, regulates zygotic genome activation. Developmental cell *26*, 578-590.

Popova, E.Y., Grigoryev, S.A., Fan, Y., Skoultchi, A.I., Zhang, S.S., and Barnstable, C.J. (2013). Developmentally regulated linker histone H1c promotes heterochromatin condensation and mediates structural integrity of rod photoreceptors in mouse retina. J Biol Chem *288*, 17895-17907.

Ramakrishnan, V. (1997). Histone structure and the organization of the nucleosome. Annu Rev Biophys Biomol Struct *26*, 83-112.

Ramakrishnan, V., Finch, J.T., Graziano, V., Lee, P.L., and Sweet, R.M. (1993). Crystal structure of globular domain of histone H5 and its implications for nucleosome binding. Nature *362*, 219-223.

Ramon, A., Muro-Pastor, M.I., Scazzocchio, C., and Gonzalez, R. (2000). Deletion of the unique gene encoding a typical histone H1 has no apparent phenotype in Aspergillus nidulans. Mol Microbiol *35*, 223-233.

Rosidi, B., Wang, M., Wu, W., Sharma, A., Wang, H., and Iliakis, G. (2008). Histone H1 functions as a stimulatory factor in backup pathways of NHEJ. Nucleic Acids Res *36*, 1610-1623.

Sancho, M., Diani, E., Beato, M., and Jordan, A. (2008). Depletion of human histone H1 variants uncovers specific roles in gene expression and cell growth. PLoS Genet *4*, e1000227.

Sekeri-Pataryas, K.E., and Sourlingas, T.G. (2007). The differentiation-associated linker histone, H1.0, during the in vitro aging and senescence of human diploid fibroblasts. Ann N Y Acad Sci *1100*, 361-367.

Shan, L., Li, X., Liu, L., Ding, X., Wang, Q., Zheng, Y., Duan, Y., Xuan, C., Wang, Y., Yang, F., *et al.* (2014). GATA3 cooperates with PARP1 to regulate CCND1 transcription through modulating histone H1 incorporation. Oncogene *33*, 3205-3216.

Shen, X., and Gorovsky, M.A. (1996). Linker histone H1 regulates specific gene expression but not global transcription in vivo. Cell *86*, 475-483.

Shen, X., Liu, Y., Hsu, Y.J., Fujiwara, Y., Kim, J., Mao, X., Yuan, G.C., and Orkin, S.H. (2008). EZH1 mediates methylation on histone H3 lysine 27 and complements EZH2 in maintaining stem cell identity and executing pluripotency. Mol Cell *32*, 491-502.

Shen, X., Yu, L., Weir, J.W., and Gorovsky, M.A. (1995). Linker histones are not essential and affect chromatin condensation in vivo. Cell *82*, 47-56.

Simpson, R.T. (1978). Structure of the chromatosome, a chromatin particle containing 160 base pairs of DNA and all the histones. Biochemistry *17*, 5524-5531.

Sirotkin, A.M., Edelmann, W., Cheng, G., Klein-Szanto, A., Kucherlapati, R., and Skoultchi, A.I. (1995). Mice develop normally without the H1(0) linker histone. Proc Natl Acad Sci U S A *92*, 6434-6438.

Stasevich, T.J., Mueller, F., Brown, D.T., and McNally, J.G. (2010). Dissecting the binding mechanism of the linker histone in live cells: an integrated FRAP analysis. EMBO J *29*, 1225-1234.

Steinbach, O.C., Wolffe, A.P., and Rupp, R.A. (1997). Somatic linker histones cause loss of mesodermal competence in Xenopus. Nature *389*, 395-399.

Studencka, M., Konzer, A., Moneron, G., Wenzel, D., Opitz, L., Salinas-Riester, G., Bedet, C., Kruger, M., Hell, S.W., Wisniewski, J.R., *et al.* (2012). Novel roles of Caenorhabditis elegans heterochromatin protein HP1 and linker histone in the regulation of innate immune gene expression. Mol Cell Biol *32*, 251-265.

Syed, S.H., Goutte-Gattat, D., Becker, N., Meyer, S., Shukla, M.S., Hayes, J.J., Everaers, R., Angelov, D., Bednar, J., and Dimitrov, S. (2010). Single-base resolution mapping of H1-nucleosome interactions and 3D organization of the nucleosome. Proc Natl Acad Sci U S A *107*, 9620-9625.

Takami, Y., Nishi, R., and Nakayama, T. (2000). Histone H1 variants play individual roles in transcription regulation in the DT40 chicken B cell line. Biochem Biophys Res Commun *268*, 501-508.

Takata, H., Matsunaga, S., Morimoto, A., Ono-Maniwa, R., Uchiyama, S., and Fukui, K. (2007). H1.X with different properties from other linker histones is required for mitotic progression. FEBS Lett *581*, 3783-3788.

Tanaka, H., Iguchi, N., Isotani, A., Kitamura, K., Toyama, Y., Matsuoka, Y., Onishi, M., Masai, K., Maekawa, M., Toshimori, K., *et al.* (2005). HANP1/H1T2, a novel histone H1-like protein involved in nuclear formation and sperm fertility. Mol Cell Biol *25*, 7107-7119.

Th'ng, J.P., Sung, R., Ye, M., and Hendzel, M.J. (2005). H1 family histones in the nucleus. Control of binding and localization by the C-terminal domain. J Biol Chem *280*, 27809-27814.

Thoma, F., Koller, T., and Klug, A. (1979). Involvement of histone H1 in the organization of the nucleosome and of the salt-dependent superstructures of chromatin. J Cell Biol *83*, 403-427.

Ushinsky, S.C., Bussey, H., Ahmed, A.A., Wang, Y., Friesen, J., Williams, B.A., and Storms, R.K. (1997). Histone H1 in Saccharomyces cerevisiae. Yeast *13*, 151-161.

van Holde, K.E. (1988). Chromatin (Springer Series in Molecular and Cell Biology) (Springer), pp. 497.

Vaquero, A., Scher, M., Lee, D., Erdjument-Bromage, H., Tempst, P., and Reinberg, D. (2004). Human SirT1 interacts with histone H1 and promotes formation of facultative heterochromatin. Mol Cell *16*, 93-105.

Vyas, P., and Brown, D.T. (2012). N- and C-terminal domains determine differential nucleosomal binding geometry and affinity of linker histone isotypes H1(0) and H1c. J Biol Chem *287*, 11778-11787.

Wang, Z.F., Sirotkin, A.M., Buchold, G.M., Skoultchi, A.I., and Marzluff, W.F. (1997). The mouse histone H1 genes: gene organization and differential regulation. J Mol Biol *271*, 124-138.

Wendt, K.S., Yoshida, K., Itoh, T., Bando, M., Koch, B., Schirghuber, E., Tsutsumi, S., Nagae, G., Ishihara, K., Mishiro, T., *et al.* (2008). Cohesin mediates transcriptional insulation by CCCTC-binding factor. Nature *451*, 796-801.

Wierzbicki, A.T., and Jerzmanowski, A. (2005). Suppression of histone H1 genes in Arabidopsis results in heritable developmental defects and stochastic changes in DNA methylation. Genetics *169*, 997-1008.

Wolffe, A.P. (1997). Histone H1. Int J Biochem Cell Biol *29*, 1463-1466.

Wolffe, A.P., and Kurumizaka, H. (1998). The nucleosome: a powerful regulator of transcription. Progress in nucleic acid research and molecular biology *61*, 379-422.

Woodcock, C.L., Safer, J.P., and Stanchfield, J.E. (1976). Structural repeating units in chromatin. I. Evidence for their general occurrence. Experimental cell research *97*, 101-110.

Woodcock, C.L., Skoultchi, A.I., and Fan, Y. (2006). Role of linker histone in chromatin structure and function: H1 stoichiometry and nucleosome repeat length. Chromosome Res *14*, 17-25.

Wu, M., Allis, C.D., Richman, R., Cook, R.G., and Gorovsky, M.A. (1986). An intervening sequence in an unusual histone H1 gene of Tetrahymena thermophila. Proc Natl Acad Sci U S A *83*, 8674-8678.

Yamamoto, T., and Horikoshi, M. (1996). Cloning of the cDNA encoding a novel subtype of histone H1. Gene *173*, 281-285.

Yang, S.M., Kim, B.J., Norwood Toro, L., and Skoultchi, A.I. (2013). H1 linker histone promotes epigenetic silencing by regulating both DNA methylation and histone H3 methylation. Proc Natl Acad Sci U S A *110*, 1708-1713.

Zhang, Y., Cooke, M., Panjwani, S., Cao, K., Krauth, B., Ho, P.Y., Medrzycki, M., Berhe, D.T., Pan, C., McDevitt, T.C., *et al.* (2012). Histone h1 depletion impairs embryonic stem cell differentiation. PLoS Genet *8*, e1002691.

Zlatanova, J., and Doenecke, D. (1994). Histone H1 zero: a major player in cell differentiation? FASEB J *8*, 1260-1268.

CHAPTER 2

ROLE OF HISTONE H1 IN NEURAL DIFFERENTIATION OF ESCS

2.1 Abstract

Linker histone H1, a key structural protein involved in the formation of higher order chromatin structures, is emerging as an important epigenetic mark and regulator for gene expression and cell differentiation. Here, we establish embryonic stem cells (ESCs) with an ultra-low histone H1 level by sequential depletion of H1 variants. ESCs with severe H1 depletion display normal ESC morphology and self-renewal, as well as specific changes in epigenetic marks. The total H1 level gradually increases during neural differentiation, which corresponds to a global chromatin condensation in differentiating cells. *In vitro* neural differentiation of ESCs with sequential H1 depletion revealed a dosage effect of H1 on neural differentiation of embryonic stem cells, as indicated by neurite outgrowth, induction of neural lineage-specific genes, and repression of pluripotency genes such as *Oct4* and *Nanog*. Moreover, severe H1 depletion causes a reduction in cell proliferation and cellular senescence in neural lineages. Significantly, *Oct4* knockdown effectively rescues the defects in neural differentiation and partially reverses the reduction in cell proliferation and cellular senescence. Our results suggest that, despite a global impact of histone H1 on chromatin condensation, the regulation of H1 on neural differentiation of ESCs may act locally at specific loci.

2.2 Introduction

In eukaryotic nuclei, ~147 base pairs of DNA is wrapped around an octamer of core histones to form a fundamental unit called a nucleosome (Davey et al., 2002; Luger et al., 1997). The linker histone H1 seals the nucleosomes at the entry and exit sites of DNA to facilitate and stabilize the folding of the 30 nm chromatin fiber (Ramakrishnan, 1997; Thoma et al., 1979; Wolffe, 1997). Histone H1 has a generic tri-partite structure consisting of a short, flexible N-terminal tail, a highly conserved globular domain with a winged-helix motif, and a long extended lysine-rich C-terminal tail (Allan et al., 1980; Chapman et al., 1976; Ramakrishnan et al., 1993).

A prominent characteristic of the histone H1 family is its heterogeneity. In mammals, 11 closely related non-allelic H1 variants have been identified, including 7 somatic H1 isoforms ($H1^0$, H1a-e, and H1x), 3 testicular isoforms (H1t, H1T2, and HILS1), and one oocyte-specific isoform (H1oo) (Happel and Doenecke, 2009). Among somatic H1 variants, H1a-e are replication-dependent and mainly expressed in the S phase of the cell cycle, whereas the replacement variant, $H1^0$, is replication-independent and enriched in terminally differentiated cells that have stopped dividing (Khochbin, 2001; Zlatanova and Doenecke, 1994). The most divergent variant, H1x, shares only 30% similarity in amino acid sequence with other H1 variants and is the least characterized member (Happel et al., 2005; Yamamoto and Horikoshi, 1996). Ample evidence suggests that histone H1 plays specific roles in gene regulation during embryogenesis and in various cell types (Alami et al., 2003; El Gazzar et al., 2009; Fan et al., 2005; Giambra et al., 2008; Krishnakumar et al., 2008; Nishiyama et al., 2009). The differences of H1

variants in gene expression are likely owing to their different binding affinities for chromatin and capacities for DNA compaction, as well as the divergent C-terminal domain (Clausell et al., 2009; Th'ng et al., 2005).

ESCs possess the capacity to self-renew indefinitely and differentiate into almost all cell lineages, offering great promise in regenerative medicine and cellular therapies. ESCs maintain an open and relaxed chromatin structure, with hyperdynamic binding of structural chromatin proteins and hyperactive global transcriptional activity as hallmarks (Efroni et al., 2008; Meshorer et al., 2006). During differentiation, ESCs undergo dramatic molecular changes, including silencing of pluripotency genes such as *Oct4* (also known as *Pou5f1*) and *Nanog*, and activation of lineage-specific genes (Loebel et al., 2003). In addition, the genome of differentiating ESCs undergoes global chromatin remodeling and epigenetic reprogramming (Jaenisch and Bird, 2003; Rasmussen, 2003).

Mouse ESCs have an H1/nucleosome ratio of 0.46 (Fan et al., 2005), approximately 1 H1 per 2 nucleosomes, versus that up to 0.75~0.8 in adult cells (Fan et al., 2003; Woodcock et al., 2006), also suggesting an open chromatin state in pluripotent stem cells versus a compact chromatin state in differentiated cells. ESCs with a compound deletion of 3 somatic H1 variants (H1c, H1d, and H1e) (H1 TKO) have on average only 1 H1 per 4 nucleosomes (H1/nucleosome ratio at 0.25) (Fan et al., 2003; Fan et al., 2005). H1 TKO ESCs display decondensed structure in bulk chromatin but specific changes in gene expression (Fan et al., 2003; Fan et al., 2005). Subsequent investigations reveal that H1 TKO ESCs are impaired in ESC differentiation and that pluripotency genes such as *Oct4* and *Nanog* are not efficiently repressed during differentiation of H1 TKO ESCs (Zhang et al., 2012a). These findings indicate that the

total H1 level is critical for ESC differentiation. However, it remains elusive if H1 is essential for ESC self-renewal and how high order chromatin packaging modulates ESC differentiation.

In the current study, we established ESCs with an ultra-low H1 level by sequential depletion of H1 variants, which had an H1/nucleosome ratio of ~0.11, approximately one fourth of that in wildtype (WT) ESCs. By studying ESCs with different levels of H1 depletion, we uncovered a dosage effect of H1 on ESC differentiation, as indicated by neurite outgrowth, induction of neural lineage-specific genes, and repression of pluripotency genes such as *Oct4* and *Nanog*. Surprisingly, ESCs with severe H1 depletion were not affected in ESC morphology and self-renewal. However, severe H1 depletion caused a reduction in cell proliferation and cellular senescence in neural lineages. Finally we found that *Oct4* knockdown effectively rescued the defects in neural differentiation and partially reversed the reduction in cell proliferation and cellular senescence.

2.3 Materials and Methods

2.3.1 Generation of H1c/H1d/H1e/H1^0 quadruple knockout ESCs

Mice of H1c$^{+/-}$H1d$^{+/-}$H1e$^{+/-}$ and H1$^{0-/-}$ genotypes were intercrossed to generate H1c$^{+/-}$H1d$^{+/-}$H1e$^{+/-}$H10$^{+/-}$ quadruple heterozygotes, and breeding of these mice generated H1c$^{+/-}$H1d$^{+/-}$H1e$^{+/-}$H1$^{0-/-}$ mice. *E3.5* blastocysts were isolated from pregnant mice after intercross of H1c$^{+/-}$H1d$^{+/-}$H1e$^{+/-}$H1$^{0-/-}$ mice, cultured *in vitro* to establish ESC lines, and genotyped to screen for H1c/H1d/H1e/H1^0 quadruple knockout (H1 QKO) ESCs as previously described (Fan et al., 2003; Fan et al., 2005). Animal breeding and experimental procedures were approved by Georgia Tech Institutional Animal Care and Use Committee.

2.3.2 Cell culture and growth curve assay

ESCs were propagated on mitotically inactivated mouse embryonic fibroblast feeder layers in tissue culture dishes (Corning) coated with 0.1% gelatin (Sigma-Aldrich). Prior to experiments such as HPLC analysis, ESCs were grown on feeder-free culture dishes for feeder removal. ESC culture media consisted of Dulbecco's modified Eagle's medium (DMEM) (Life Technologies) supplemented with 15% fetal bovine serum (FBS) (Gemini), 100 U/ml penicillin (Life Technologies), 100 μg/ml streptomycin (Life Technologies), 1X MEM nonessential amino acids (Life Technologies), 0.1 mM β-mercaptoethanol (Life Technologies), and 103 U/ml of leukemia inhibitory factor (LIF; ESGRO, Chemicon). Cultures were re-fed with fresh media every other day, and passaged every 2-3 days when reaching 70-80% confluence. For the inducible

expression of shRNAs, ESC culture media were supplemented with 1 μg/ml doxycycline (Dox) (Sigma-Aldrich). For growth curve assay, ESCs were seeded without feeder cells on 12-well plates at a density of 1 x 10^4 cells/well. The cells were trypsinized with 0.25% trypsin-EDTA solution and counted on a hemocytometer in triplicates every 2 days for up to 6 days.

2.3.3 Construction of the inducible vector for H1a and H1b knockdown and generation of ESCs with an ultra-low H1 level (QKO/abi ESCs)

The Tet-On inducible shRNA expression vector pTRIPZ and the TransLenti viral packaging system were purchased from Open Biosystems. One copy of H1a shRNA and two copies of H1b shRNA embedded in the miR-30 backbone were inserted into the pTRIPZ vector. The shRNA-miR-30 sequences are as follows: H1a shRNA-miR-30, 5'-aagaaggtatattgctgttgacagtgagcgACAGGCAGTTTCTTCTTCCAAAtagtgaagccacagatgta-TTTGGAAGAAGAAACTGCCTGCtgcctactgcctcggacttcaaggg-3'; H1b shRNA-miR-30, 5'-aagaaggtatattgctgttgacagtgagcgACTCTGGTTCCTTCAAGCTTAAtagtgaagccacagat-gtaTTAAGCTTGAAGGAACCAGAGGtgcctactgcctcggacttcaaggg-3'. Capital letters indicate the sense and antisense sequences. Viral particles containing the re-constituted vector were produced according to the manufacturer's manual, and transduced into H1 QKO ESCs for growth into colonies. The resulting ESC clones were propagated and induced with 1 μg/ml Dox for HPLC analysis to confirm the depletion of H1a and H1b. Positive clones were designated as QKO/abi ESC lines.

2.3.4 Histone extraction and HPLC analysis

Chromatin and histones were prepared from ESCs and embryoid bodies (EBs) according to protocols described previously (Cao et al., 2013; Fan and Skoultchi, 2004; Medrzycki et al., 2012). Approximately 50 μg of total histones were injected into a C18 reverse phase column (Vydac) on an Äktapurifier UPC 900 system (GE Healthcare). Linker histones and core histones were fractionated with an increasing acetonitrile gradient as described previously (Medrzycki et al., 2012). The effluent was monitored at 214 nm wavelength, and the peak areas were analyzed with AKTA UNICORN 5.11 software (GE Healthcare). The areas of A_{214} peaks of H1 variants and H2B were normalized by the number of peptide bonds of respective histone proteins, and the normalized values were used for calculation of H1 to nucleosome (H1/nuc) ratio (Fan and Skoultchi, 2004; Medrzycki et al., 2012).

2.3.5 *In vitro* neural differentiation of ESCs

Neural differentiation of ESCs was performed following a protocol established previously with some modifications (Zhang et al., 2012a). Briefly, ESCs were trypsinized with 0.25% trypsin-EDTA solution, depleted of feeder cells, and resuspended in differentiation media at 5 x 10^4 cells/ml. The differentiation media had the same composition as ESC culture media but without LIF. EBs were formed in hanging drops of 20 μl volume (containing 1000 cells) and incubated for 5 days. Subsequently, EBs were collected into ultra-low attachment dishes (Corning) and treated with 1 μM *all-trans* retinoic acid (Sigma-Aldrich) for additional 3 days. For neural differentiation, day 8 EBs were seeded on tissue culture dishes coated with 5 μg/ml poly-L-ornithine (Sigma-Aldrich) and laminin (Life Technologies) and cultured in NeuroCult NSC proliferation

medium (StemCell Technologies) supplemented with 100 ng/ml bFGF (GenScript) for up to 15 days. Day 8+5, 8+10, and 8+15 EBs were taken for subsequent analyses as indicated. 1 μg/ml Dox was supplemented during neural differentiation as needed. For QKO/abi/Oct4i+Dox EBs, Dox was added on day 5. Statistical analysis of neurite numbers was performed using GraphPad Prism 4 software (GraphPad Software).

2.3.6 Antibodies

The following antibodies were used for Western blotting and immunocytochemistry: anti-Oct4 (Santa Cruz, sc-8628), anti-GAPDH (Millipore, MAB374), anti-β-actin (Sigma-Aldrich, A5316), anti-FLAG (Sigma-Aldrich, F1804), anti-H3K4me3 (Millipore, 07-473), anti-H3K9me2 (Abcam, ab1220), anti-H3K9me3 (Abcam, ab8898), anti-H3K27me3 (Millipore, 07-449), anti-H3 (Abcam, ab1791), anti-GFAP (Dako, Z0334), anti-TUBB3 (Millipore, MAB1637); anti-Nestin (Millipore, MAB353), anti-BrdU (Abcam, ab1893).

2.3.7 Immunocytochemistry

Immunostaining of day 8+5 and 8+10 EBs was performed as previously described (Zhang et al., 2012a). Briefly, EBs grown on glass coverslips were fixed with 4% paraformaldehyde for 20 min and permeabilized with 0.2% Triton X-100/PBS for 30 min at room temperature, followed by blocking with 10% FBS/PBS for 1 h at room temperature. EBs were then immunostained with primary and secondary antibodies. The following secondary antibodies were used: Cy3-conjugated donkey anti-rabbit IgG (Jackson Immuno Research Laboratories, 711-165-152), Alexa Fluor 488-conjugated

donkey anti-mouse IgG (Life Technologies, A-21202). Nuclei were counter-stained with Hoechst 33342 (Molecular Probes). Images were collected on an Olympus Fluorescence Microscope with a Q-Color 3 CCD camera (Olympus).

2.3.8 RNA extraction and quantitative RT-PCR

RNA extraction and quantitative RT-PCR (qRT-PCR) were performed as previously described (Medrzycki et al., 2012; Zhang et al., 2012a). Briefly, total RNA from ESCs and EBs were extracted using the Allprep DNA/RNA Mini Kit (Qiagen) following the manufacturer's instruction. RNA samples were reverse transcribed with the SuperScript III First-Strand Synthesis System (Life Technologies). Real-time quantitative PCR was performed using iQ SYBR Green Supermix on the MyIQ Single Color Real-Time PCR Detection System (Bio-Rad). The following primers were used: *Oct4*: forward 5'-GCTCACCCTGGGCGTTCTC-3', reverse 5'-GGCCGCAGCTTACACATGTTC-3'; *Tyrosine hydroxylase*: forward 5'-GATTGCAGAGATTGCCTTCC-3', reverse 5-GGGTAGCATAGAGGCCCTTC-3'; *Nestin*: forward 5'-GCCTATAGTTCAACGC CCCC-3', reverse 5'-AGAC AGGCAGGGCTAGCAAG-3'; *GFAP*: forward 5'-GCCACCAGTAACATGCAAGA-3', reverse 5'-GGCGATAGTCGTTAGCTTCG-3'; *GAPDH*: forward 5'-TTCACCACCATGGAGAAGGC-3', reverse 5'-GGCATGGACT GTGGTCATGA-3'; *TUBB3*: forward 5'-CATGGACAGTGTTCGGTCTG-3', reverse 5'-CGCACGACATCTAGGACTGA-3'.

2.3.9 Generation of H1d rescue (QKO/abi/H1^{res}) ESCs

An expression vector containing H1d CDS and 5 kb mouse H1d upstream and downstream regulatory regions and the blasticidin resistant gene were established previously (Zhang et al., 2012a). 20 μg of plasmid DNA was transfected into 2 x 10^7 QKO/abi ESCs by electroporation and a total of 24 clones resistant to blasticidin (Life Technologies) were picked and screened by Western blotting using an anti-FLAG antibody. Two cell lines with the highest levels of H1d were selected as QKO/abi/$H1^{res}$ cell lines for further analysis.

2.3.10 Generation of ESCs with inducible *Oct4* knockdown

Similar to construction of the vector for inducible H1a and H1b knockdown, Oct4 shRNA-miR-30 cassettes were inserted between XhoI and EcoRI sites in the pTRIPZ vector. Oct4 shRNA-miR30's are as follows: 5'-ccagccttaagaacatgtgtaatagtgaagcc-acagatgtattacacatgttcttaaggctga-3', 5'-acccggaagagaaagcgaactatagtgaagccacagatgtatagttc-gctttctcttccgggc-3'. The puromycin resistant gene in the pTRIPZ vector was replaced with the blasticidin resistant gene for clone selection. The re-constituted viral vector was packaged into virus and transduced into QKO/abi ESCs. Blasticidin resistant clones were picked, induced with 1 μg/ml Dox, and screened for *Oct4* knockdown by Western blotting using an anti-Oct4 antibody. Two clones with highest knockdown efficiency were selected as QKO/abi/Oct4i ESC lines for further analysis.

2.3.11 Measurement of EB size

Day 5 EBs were collected from hanging drops and phase contrast images were taken with an AxioVision microscope (Carl Zeiss). EB size was measured by the

AxioVision software as area and EB diameters were then calculated. Over 150 EBs for each line from 3 independent experiments were pooled and statistically analyzed with GraphPad Prism 4 software.

2.3.12 BrdU incorporation assay of EBs

Day 8+5 EBs grown on glass coverslips were pulsed with 10 μg/ml 5-bromo-2'-deoxyuridine (BrdU; BD Pharmingen) for 2 h, then washed 3 times with PBS, and fixed with 4% paraformaldehyde for 20 min, followed by permeabilization with 0.2% Triton X-100/PBS for 20 min at room temperature. Subsequently, EBs were treated with 2N hydrochloric acid (HCl) for 30 min, and neutralized with 100 mM Tris-HCl buffer, pH8.0, for 20 min at room temperature. For immunostaining of BrdU, EBs were hybridized with an anti-BrdU antibody, and Cy3-conjugated Donkey anti-Sheep IgG (Jackson ImmunoResearch Laboratories, 713-165-147). Images were collected at 60X on an Olympus fluorescence microscope.

2.3.13 Senescence associated β-Galactosidase staining of EBs

ESCs and Day 8+5 EBs cultured on 6-well plates were stained for β-Galactosidase activity using the Senescence β-Galactosidase Staining Kit (Cell Signaling, #9860) following the manufacturer's manual. Images were taken with a Carl Zeiss AxioVision system.

2.3.14 Digestion of ESC genomic DNA with methylation-sensitive restriction enzymes

1 μg genomic DNA extracted from ESCs was completely digested with the methylation-insensitive restriction enzyme, MspI, and methylation-sensitive restriction enzymes, HpaII and MaeII. The digested DNA samples were separated by gel electrophoresis and stained with ethidium bromide (AMRESCO).

2.3.15 Cell cycle analysis of ESCs

ESCs in exponential expansion phase were trypsinized and washed with PBS, followed by fixation with 75% ethanol. For cell cycle analysis, fixed cells were resuspended in PBS and stained with 1 μg/ml Hoechst 33342 for 20 min at room temperature. Data were collected on a BD LSRII Flow Cytometer (BD Biosciences) and analyzed with FlowJo V10 (FLOWJO).

2.4 Results

2.4.1 Generation of H1c/H1d/H1e/H1^0 quadruple knockout ESCs

To begin to make ultra-low H1 ESCs, we first set out to generate H1c/H1d/H1e/H1^0 quadruple H1 knockout ESCs. Using previously reported H1c$^{+/-}$ H1d$^{+/-}$H1e$^{+/-}$ and H1$^{0-/-}$ mice (Fan et al., 2003; Sirotkin et al., 1995), we generated H1c$^{+/-}$ H1d$^{+/-}$H1e$^{+/-}$H1$^{0+/-}$ quadruple heterozygotes (Figure 2.1). H1c$^{-/-}$H1d$^{-/-}$H1e$^{-/-}$H1$^{0-/-}$ embryos, generated from intercross of H1c$^{+/-}$H1d$^{+/-}$H1e$^{+/-}$H1$^{0-/-}$ mice, were embryonic lethal and died by embryonic day 8.5 (*E8.5*), earlier than those with triple-H1 deficiency (Fan et al., 2003). From the outgrowth of quadruple-H1 null blastocysts, we derived H1c/H1d/H1e/H1^0 quadruple H1 knockout ESCs (H1 QKO ESCs) (Figure 2.1).

H1c$^{-/-}$H1d$^{-/-}$H1e$^{-/-}$H1$^{0-/-}$ ESCs displayed normal ESC morphology and comparable expression of pluripotency gene *Oct4* as WT ESCs, as well as growth rate and cell cycle distribution (Figure 2.2). Total histones were extracted from wildtype (WT) and H1 QKO ESCs and subjected to reverse phase (RP)-HPLC analysis. The HPLC profile of H1 QKO ESCs showed the absence of H1c, H1d, H1e, and H1^0 variants, demonstrating the deletion of these four H1 variants (Figure 2.3A). Calculation of H1/nucleosome (H1/nuc) ratio from H1 and H2B peaks showed that H1 QKO ESCs had an H1/nuc ratio of ~0.24 (Figure 2.3B), slightly lower than that of 0.25 in H1 TKO ESCs (Fan et al., 2005), which is consistent with the low/minimum levels of H1^0 (~2% of total H1) in WT ESCs. In H1 QKO ESCs, H1a and H1b accounted for 30% and 70% of the total H1 level respectively. HPLC analysis was unable to detect the H1x peak, indicating that H1x

exists in a very low amount in ESCs and does not noticeably compensate for loss of other H1 variants.

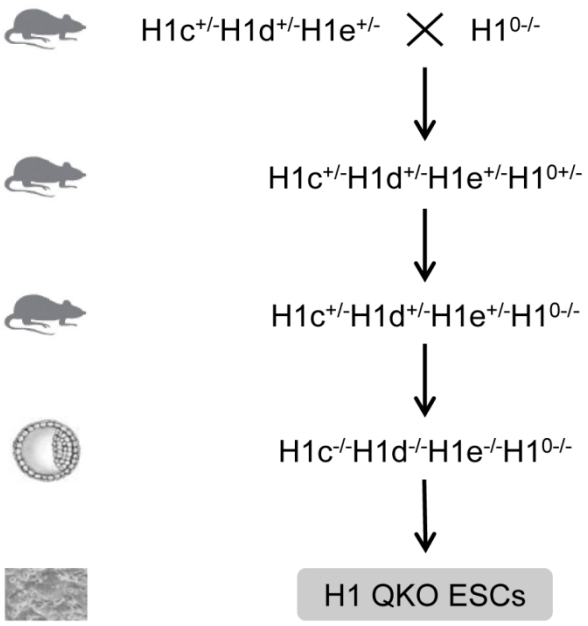

Figure 2.1 A schematic view of the process for generation of H1c/H1d/H1e/H1^0 quadruple knockout ESCs.

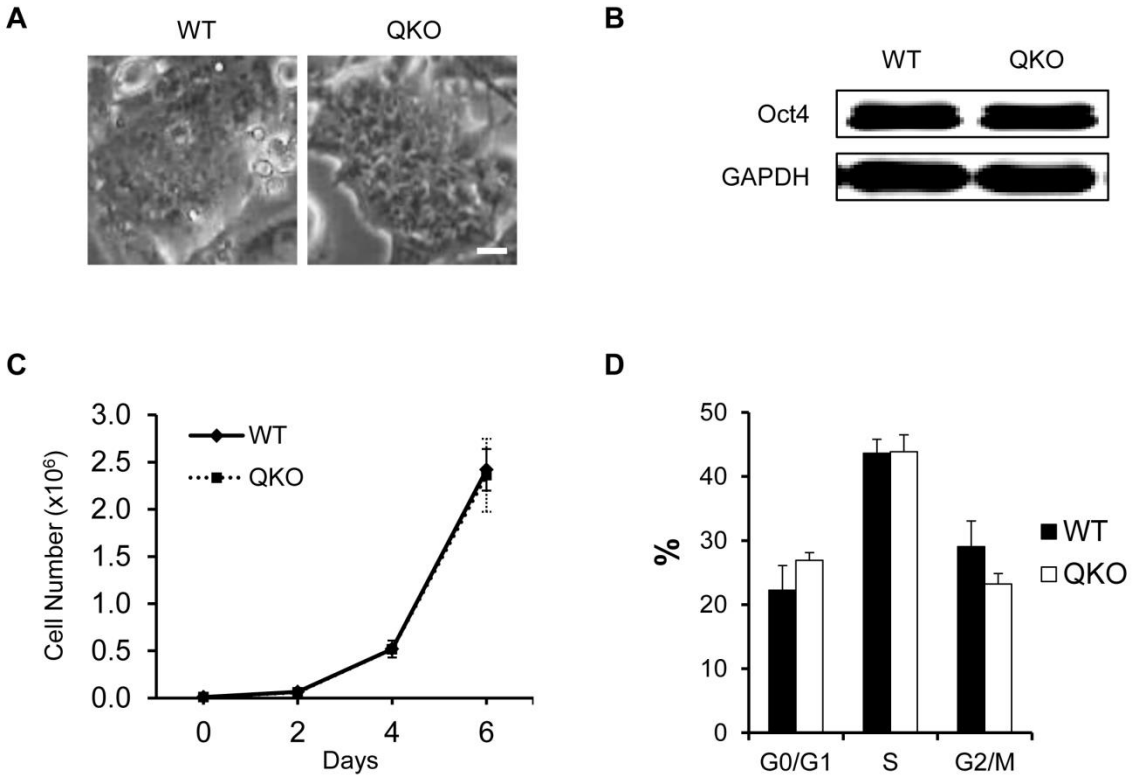

Figure 2.2 Characterization of H1 QKO ESCs.
H1 QKO ESCs exhibit similar colony morphology (A), *Oct4* expression (B), growth rate (C), and cell cycle distribution (D), as wildtype (WT) ESCs. Scale bar: 20 μm.

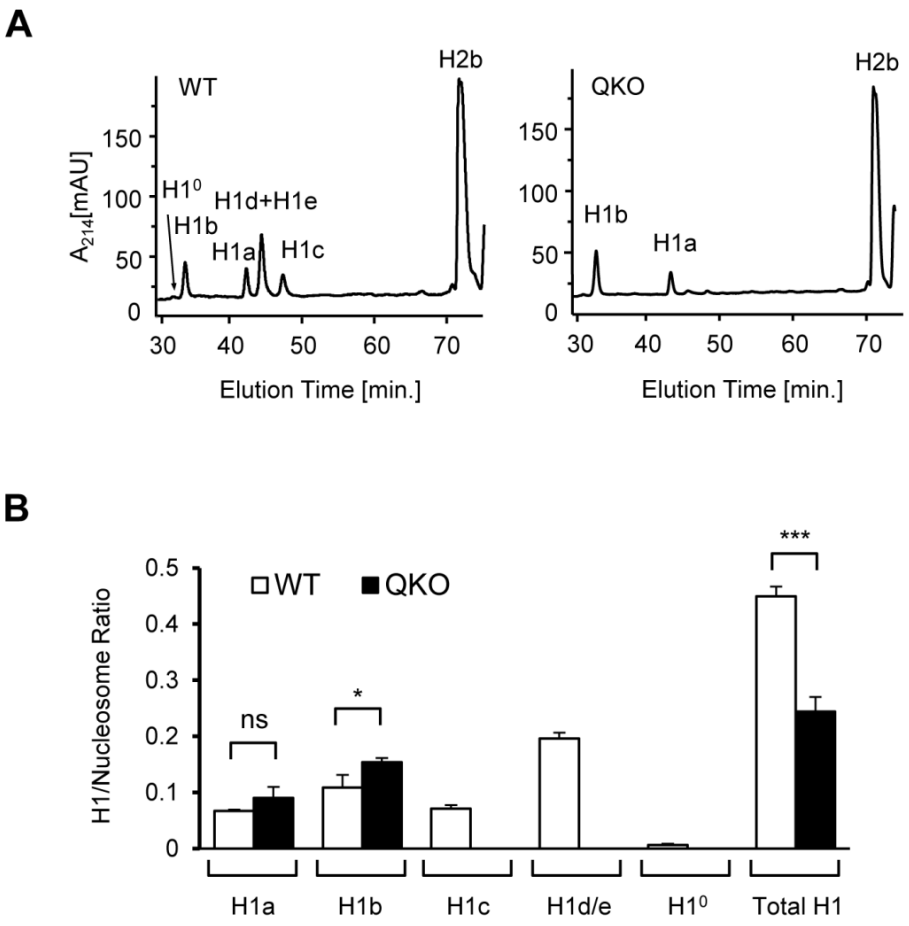

Figure 2.3 Reverse-phase HPLC analysis of H1 QKO ESCs.
A) HPLC profiles of wildtype (WT) and H1 QKO ESCs. X axis: elution time; Y axis: absorbency at A214; mAU, milli-absorbency units.
B) Quantification of H1 levels as H1 to nucleosome ratio according to HPLC profiles in (*A*). Values are shown in means ± S.D., n = 3. ns: not significant; *: $p<0.05$; ***: $p<0.001$.

2.4.2 Generation of ESCs with an ultra-low H1 level

To deplete the remaining H1a and H1b variants in H1 QKO ESCs and to avoid the potential deleterious effects on ESC viability by complete H1 elimination, we employed a Tet-On inducible RNAi vector, pTRIPZ. To simultaneously deplete both variants, one copy and two copies of H1a shRNA and H1b shRNA respectively were inserted into the shRNA-miR cassette of pTRIPZ vector (Figure 2.4) (Sun et al., 2006). Two copies of H1b shRNA were inserted for knockdown of H1b expression because of a higher percentage of H1b than H1a, 70% vs. 30%, in the remaining H1s. H1 QKO ESCs transduced with the reconstituted lentiviral vector were established as QKO/abi ESCs. The HPLC profile of histone extracts from QKO/abi ESCs showed a dramatic reduction in H1a and H1b upon induction with doxycycline (Dox) (Figure 2.5A). In the absence of Dox, QKO/abi (QKO/abi-Dox) ESCs had a similar H1 level as H1 QKO ESCs (Figures 2.3B and 2.5B). Upon induction with Dox, the total H1/nuc ratio in QKO/abi (QKO/abi+Dox) ESCs was reduced to ~0.11 4 days post induction. QKO/abi+Dox ESCs had ~25% total H1 remaining as compared with WT ESCs.

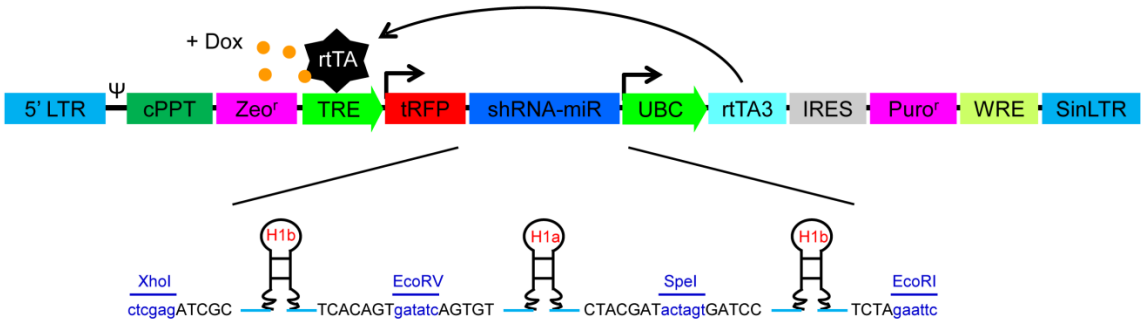

Figure 2.4 A schematic view of the lentiviral vector pTRIPZ encompassing H1a and H1b shRNA-miR-30 hairpins.

The reverse tetracycline transactivator 3 (rtTA3), which is ubiquitously expressed, can bind to the tetracycline responsive element (TRE) and activate the expression of TurboRFP (tRFP) and shRNA-miR hairpins in the presence of Dox. The shRNA-miR-30 cassette consists of one copy of H1a shRNA and two copies of H1b shRNA connected by artificial sequences and restriction sites. 5' LTR, 5' long terminal repeat; Ψ, retroviral Psi packaging element; cPPT, central polypurine tract; Zeo^r, Zeocin resistant gene; UBC, ubiquitin C promoter; IRES, internal ribosome entry site; Puro^r, puromycin resistant gene; WRE, woodchuck hepatitis virus posttranscriptional regulatory element; SinLTR, self-inactivating long terminal repeat.

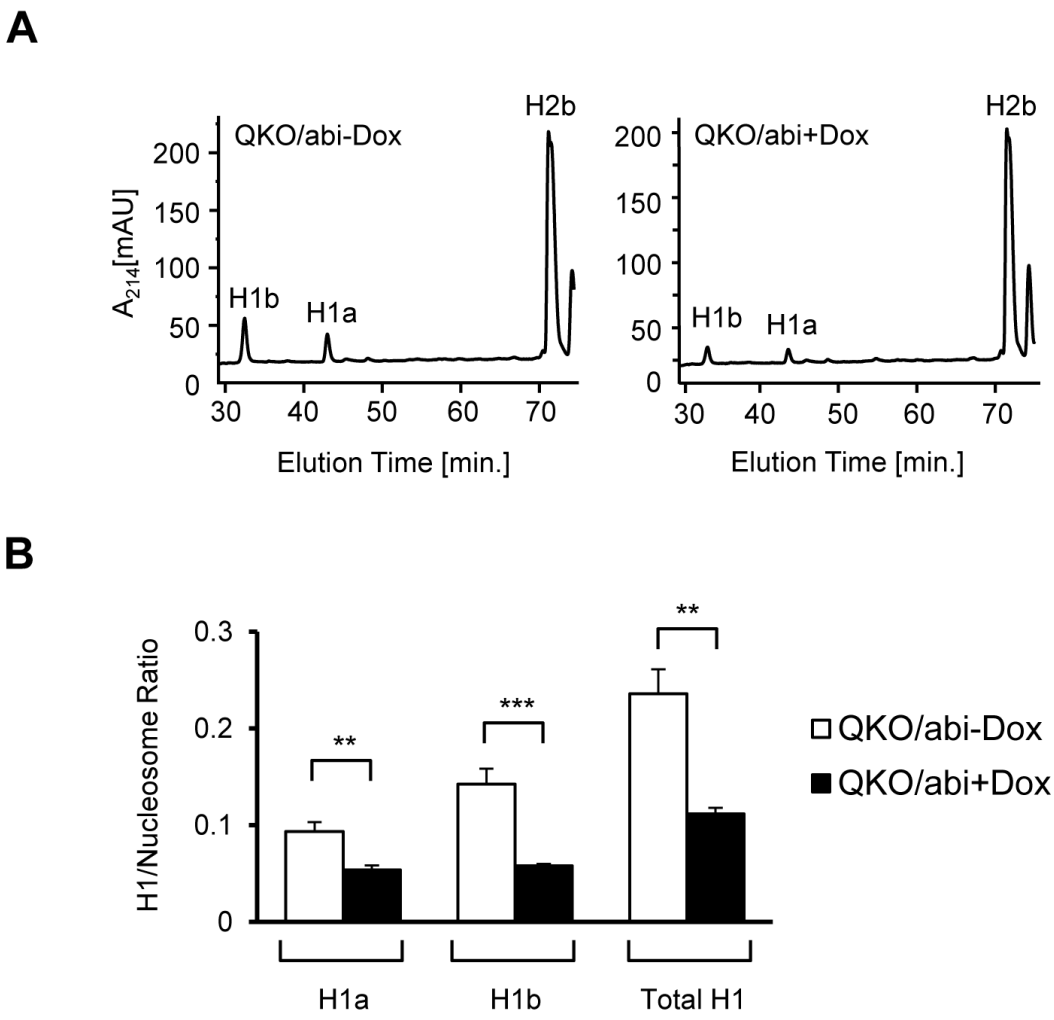

Figure 2.5 Reverse-phase HPLC analysis of QKO/abi ESCs.
A) HPLC profiles of uninduced and induced QKO/abi ESCs. X axis: elution time; Y axis: absorbency at A214; mAU, milli-absorbency units.
B) Quantification of H1 levels as H1 to nucleosome ratio according to HPLC profiles in (*A*). Values are shown in means ± S.D., n = 3. **: $p<0.01$; ***: $p<0.001$.

2.4.3 Phenotypic analysis of ESCs with an ultra-low H1 level

To investigate the effects of severe H1 depletion in ESCs, we induced the expression of H1a shRNA and H1b shRNA using Dox. Upon induction, QKO/abi ESCs did not show noticeable changes in colony morphology, the expression of the pluripotency gene *Oct4*, growth rate, and cell cycle profile, as compared with WT ESCs (Figure 2.6). These results indicate that severe depletion of the H1 level to as few as 1 H1 per 9 nucleosomes does not affect the self-renewal of ESCs.

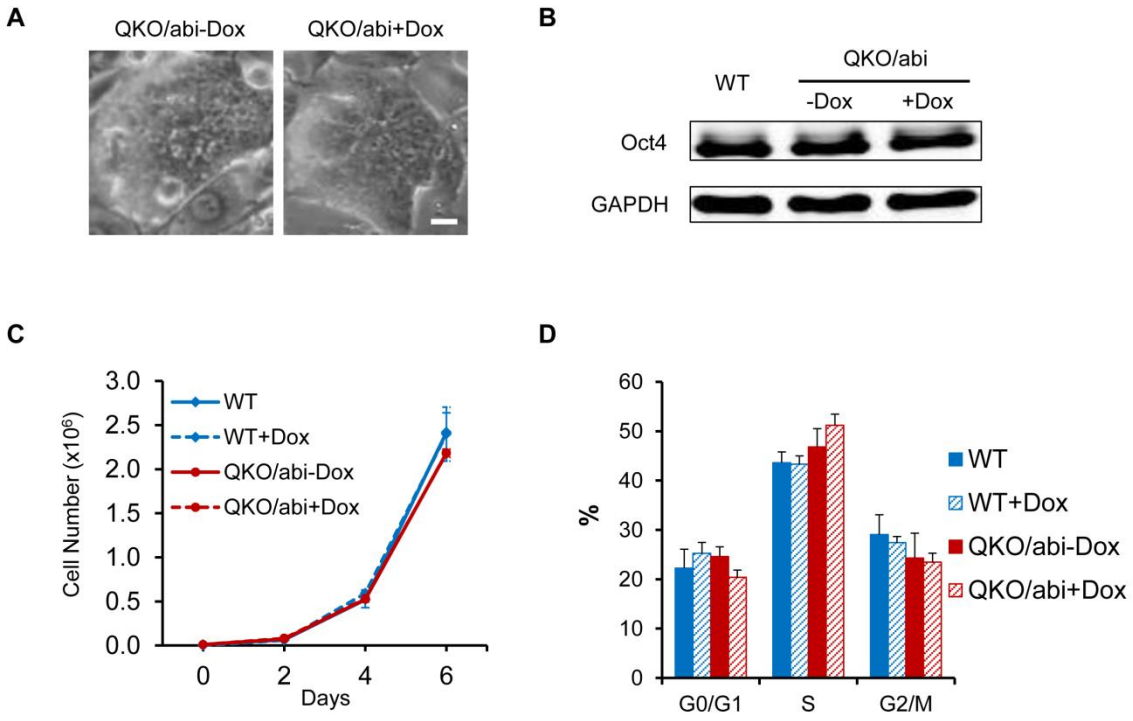

Figure 2.6 Characterization of QKO/abi ESCs.
QKO/abi+/-Dox ESCs exhibit similar colony morphology (A), *Oct4* expression (B), growth rate (C), and cell cycle profile (D), as wildtype (WT) ESCs. Scale bar: 20 μm.

2.4.4 Analysis of DNA methylation and histone modifications in bulk chromatin of ultra-low H1 ESCs

Previous studies show that triple-H1 deletion does not change the overall DNA methylation but causes reduction in certain histone marks in ESCs (Fan et al., 2005). To investigate how further H1 depletion affects epigenetic marks in ESCs, we first performed Western blotting to compare several key histone marks in WT ESCs and ESCs with sequential H1 depletion. While the overall levels of the active histone mark, H3K4me3, and the repressive histone marks, H3K9me2 and H3K9me3, remained unchanged, the level of H3K27me3 was progressively reduced after sequential H1 depletion (Figure 2.7). These results further support a role of H1 in regulating specific histone modifications in bulk chromatin.

To determine if a severe reduction of the H1 level causes DNA methylation changes in bulk chromatin, genomic DNA from WT and H1-depleted ESCs was digested with DNA methylation-sensitive restriction enzymes, HpaII or MaeII, which recognize CCGG and ACGT respectively. Both HpaII and MaeII are blocked by CpG methylation which occurs on the 5' of cytosine at CpG configuration. As a control, genomic DNA was digested with DNA methylation-insensitive restriction enzyme MspI, which recognizes the same recognition sequence as HpaII, CCGG. While genomic DNA was nearly fully digested by MspI, majority of DNA was resistant to the digestion by HpaII or MaeII, indicating that genomic DNA of these ultra-low H1 ESCs remain heavily methylated (Figure 2.8). These results suggest that severe H1 depletion does not significantly affect DNA methylation at the bulk level.

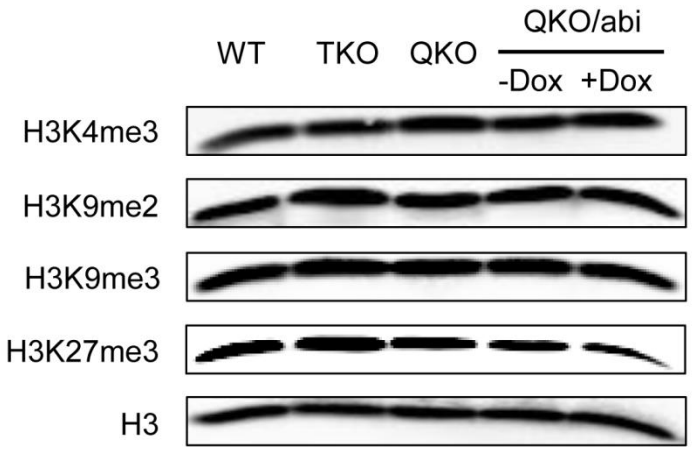

Figure 2.7 Overall levels of selective histone marks in ESCs with sequential H1 depletion.

Western blotting of the active histone mark, H3K4me3, and the repressive histone marks, H3K9me2, H3K9me3, and H3K27me3, in wildtype (WT), H1 TKO (TKO), H1 QKO (QKO), and QKO/abi+/-Dox ESCs. H3 serves as an internal control.

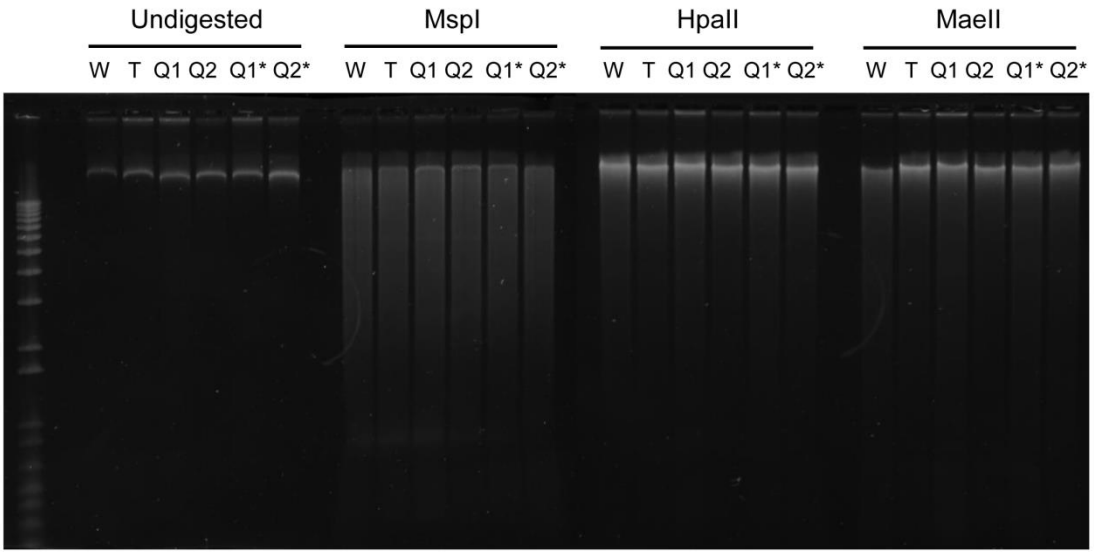

Figure 2.8 Severe H1 depletion doesn't affect the overall DNA methylation in ESCs. Genomic DNA extracted from ESC lines was digested with the methylation-insensitive restriction enzyme, MspI, and methylation-sensitive restriction enzymes, HpaII and MaeII, followed by gel electrophoresis. W, wildtype; T, H1 TKO; Q1, QKO/abi-Dox clone 1; Q2, QKO/abi-Dox clone 2; Q1*, QKO/abi+Dox clone 1; Q2*, QKO/abi+Dox clone 2.

2.4.5 A dosage effect of histone H1 on neural differentiation of ESCs

As we have previously shown, triple-H1 null ESCs are impaired, but not completely blocked, in neural differentiation (Zhang et al., 2012a). Having established ultra-low H1 ESCs, we set out to examine how further H1 depletion affects ESC differentiation. We employed an *in vitro* neural differentiation scheme (Figure 2.9) which we optimized based on a previous protocol (Kim et al., 2009; Zhang et al., 2012a). The neural differentiation regimen provides an ideal approach to study the regulatory mechanisms of ESC differentiation. Embryoid bodies (EBs) grown in hanging drops for 5 days were treated with *all-trans* retinoic acid (RA) for additional 3 days, followed by neural differentiation on poly-L-ornithine (PLO)- and laminin- coated culture dishes for up to 15 days. Of note, at day 5, QKO/abi EBs with Dox induction formed in hanging drops showed significantly smaller EB size (Figure 2.10), which was in sharp contrast to QKO/abi EBs without addition of Dox.

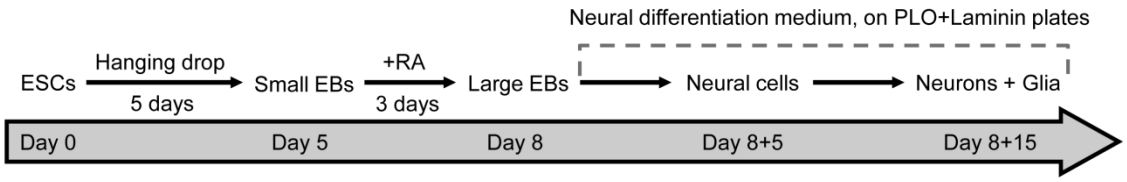

Figure 2.9 A schematic view of the optimized *in vitro* neural differentiation protocol.

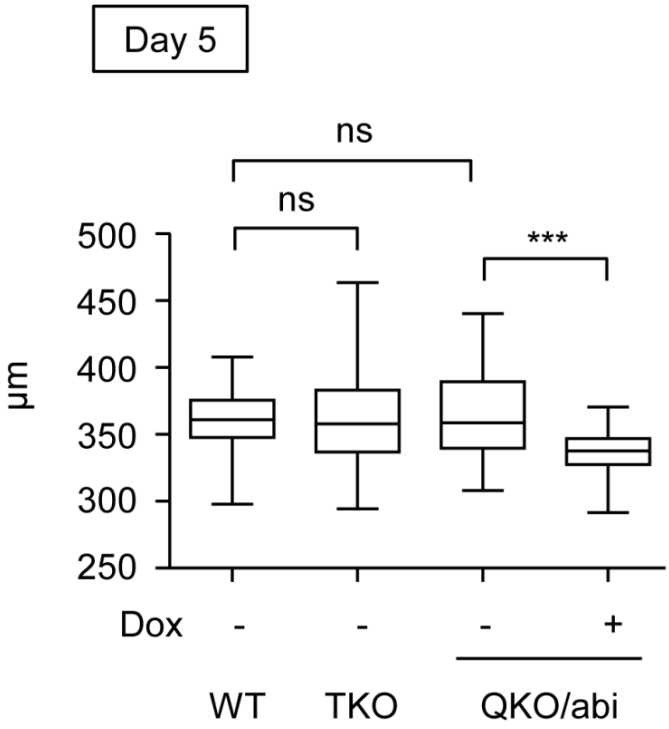

Figure 2.10 QKO/abi+Dox EBs exhibit significantly smaller size at day 5.
Day 5 EBs prepared from hanging drops were measured in diameters (µm). Data were collected from 3 independent experiments and are presented in Box-and-whisker plots, N ≥ 150. ns: not significant; ***: $p<0.001$.

During the development of the central nervous system, immature neurons migrate long distances to their destinations, form axons and dendrites, and are eventually orchestrated into neural networks. Upon differentiation following the neural differentiation protocol described above, by day 8+5, WT EBs sprouted numerous thick and extended neurites, and were surrounded by a radial monolayer of migrated neural cells (Figure 2.11A). Similar cell migration patterns were observed in H1 TKO and QKO/abi-Dox EBs, whereas QKO/abi+Dox EBs exhibited impaired migration of neural cells. Quantitative measurements showed that on average 79% of WT EBs formed neurite outgrowth with an average of 38 neurites per EB, versus 35% of H1 TKO EBs with an average of 14 neurites per EB (Figure 2.11B). Severe H1 depletion caused an enhanced hindrance in neurite outgrowth: 23% of QKO/abi-Dox EBs formed 9 neurites on average, with the numbers dropping to 19% and 3 in QKO/abi+Dox EBs, respectively. The dosage effect of H1 depletion on neurite outgrowth was confirmed by immunostaining of neuron-specific β-tubulin isotype III (TUBB3), which is rich in neurites. By day 8+5, WT EBs exhibited abundant thick bundles of microtubules with bright TUBB3 staining (Figure 2.12), whereas both the quantity and thickness of neurites were compromised in H1 TKO EBs, with a more drastic decrease in QKO/abi (±Dox) EBs. Collectively, our results suggest a dosage effect of histone H1 variants on ESC differentiation towards neuronal lineages, with progressively more severe defects with increasing deficiency of H1.

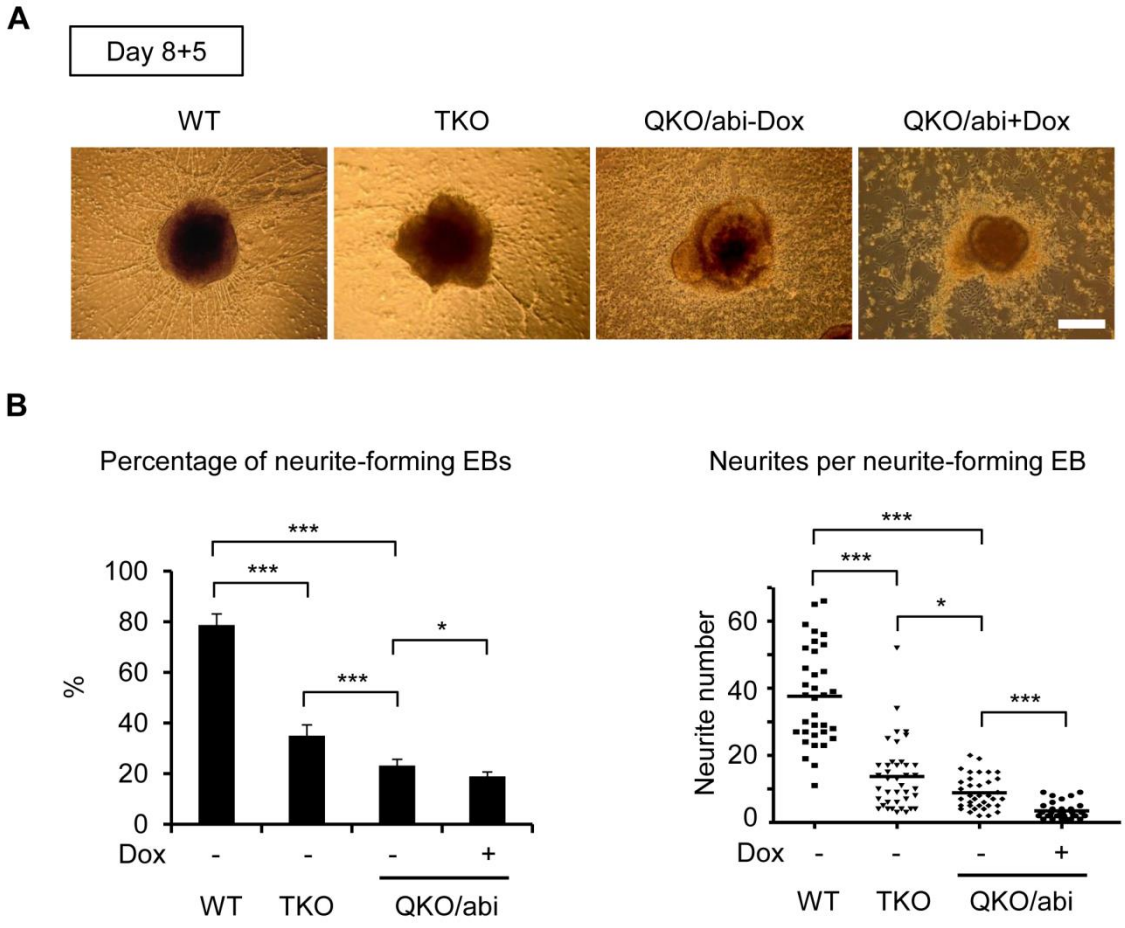

Figure 2.11 Sequential H1 depletion leads to a progressive decrease of neurite outgrowth in day 8+5 EBs.
A) Phase contrast images of day 8+5 EBs. Scale bar, 200 μm.
B) Left panel: percentage of neurite-forming EBs. Numbers were averaged from at least 4 experiments. Over 100 EBs were counted per experiment. Right panel: numbers of neurites per neurite-forming EB. Neurite number was counted from EBs that produced neurites. Dox was added to media when EB cultures were induced. All data are presented as means ± S.D. *: $p<0.05$; ***: $p<0.001$.

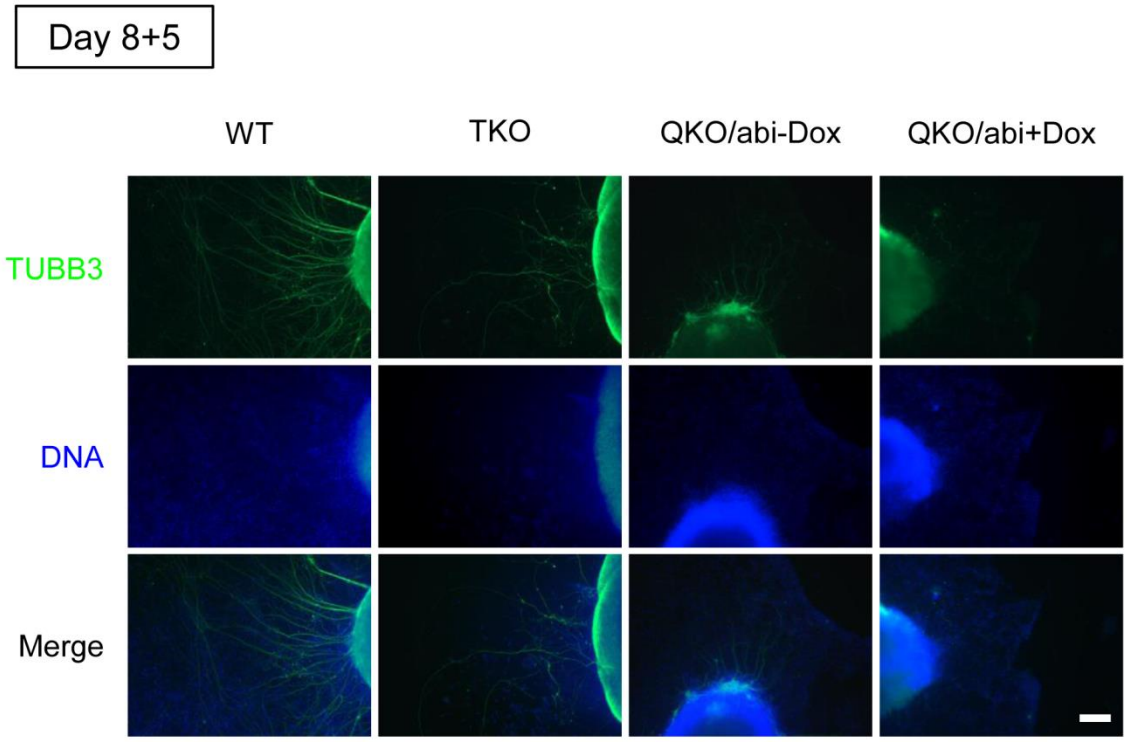

Figure 2.12 Immunostaining of TUBB3 in day 8+5 EBs.
TUBB3 was stained in green color and nuclei counterstained with Hoechst in blue. Scale bar: 200 μm.

Next we examined ESC differentiation towards other neural lineages. The early developmental stages of the nervous system are marked by neural stem cells (NSCs), which can differentiate into diverse neural lineages. To examine the production of NSCs, we immunostained the NSC marker Nestin in day 8+5 EB cultures. The results showed that WT EBs were enriched in cells with abundant Nestin filaments (Figure 2.13 upper panels). In contrast, H1 depletion progressively repressed *Nestin* expression, reaching a trace level in EBs with an ultra-low H1 level (QKO/abi+Dox EBs). In addition to neurogenesis, we further assessed gliogenesis by immunostaining of the astrocyte marker, glial fibrillary acidic protein (GFAP), in day 8+10 EB cultures, given that the gliogenic process occurs after neurogenesis during *in vivo* brain development (Qian et al., 2000). Remarkably, in sharp contrast to WT EB cultures, the number of glial cells was drastically decreased in H1 TKO EB cultures and no GFAP-positive cells were detected in QKO/abi (±Dox) EB cultures (Figure 2.13 lower panels). It is noteworthy that these defects in neural differentiation of ultra-low H1 ESCs were not observed in H1 QKO ESCs transduced with scramble shRNA (QKO/sci ESCs) and induced with Dox (Figures 2.14, 2.15, and 2.16), further suggesting that the blockage in neural differentiation of ultra-low H1 ESCs are caused specifically by the dramatic loss of H1.

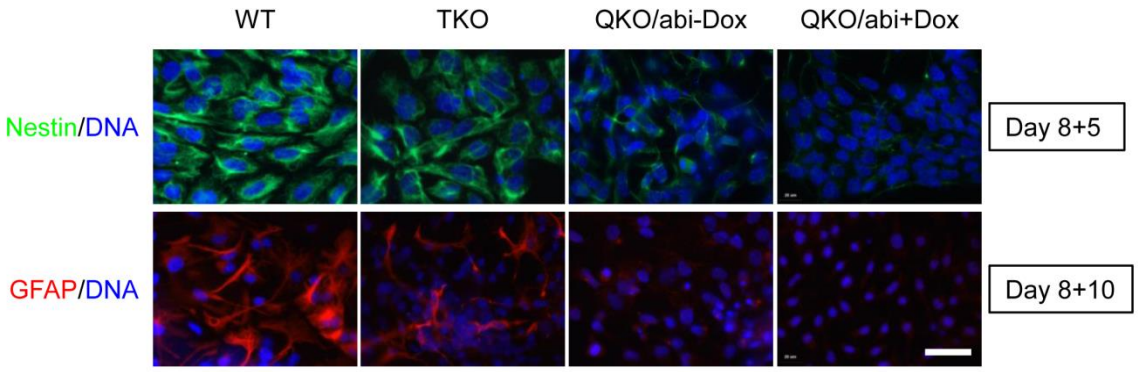

Figure 2.13 Sequential H1 depletion causes a progressive decrease in the expression of *Nestin* and *GFAP* in EB cultures.
Day 8+5 and 8+10 EBs were immunostained against the neural stem cell marker Nestin (upper panels) and the glial cell marker GFAP (lower panels), respectively. Nuclei were counterstained with Hoechst in blue color. Scale bar: 20 μm.

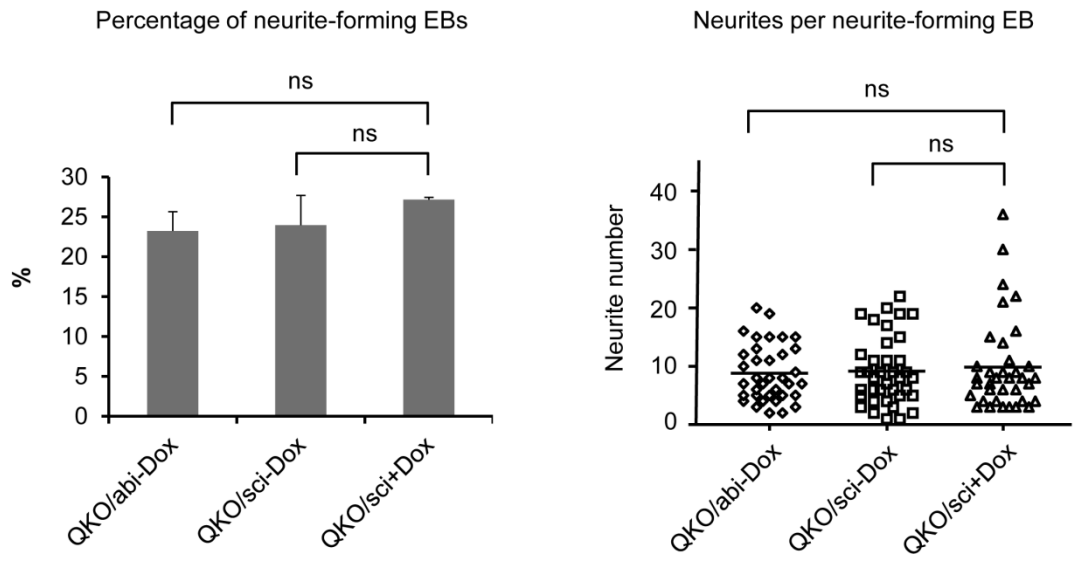

Figure 2.14 Neurite outgrowth is not affected by introduction of scramble shRNA and Dox.
Left panel: Percentage of neurite-forming EBs. Numbers were averaged from at least 4 experiments. Over 100 EBs were counted per experiment.
Right panel: Numbers of neurites per neurite-forming EB. Neurite number was counted from EBs that produced neurites. QKO/sci, EBs formed from H1 QKO ESCs transduced with scramble shRNA. ns: Not significant.

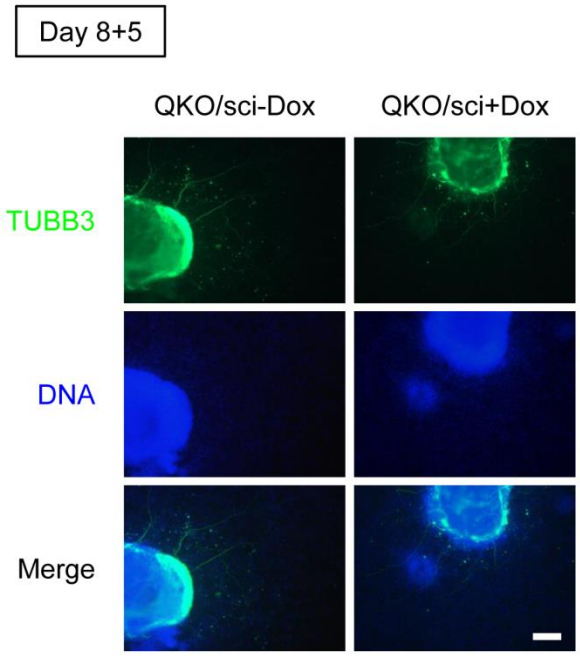

Figure 2.15 Scramble shRNA and Dox have no effect on *TUBB3* expression.
TUBB3 was stained in green color and nuclei were counterstained with Hoechst in blue. Scale bar: 200 μm.

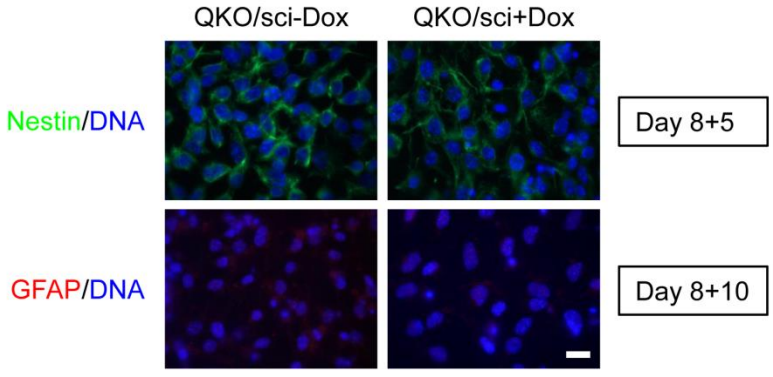

Figure 2.16 Scramble shRNA and Dox have no effect on the expression of *Nestin* and *GFAP* in EB cultures.
Day 8+5 and 8+10 EBs were immunostained against the neural stem cell marker Nestin (upper panels) and the glial cell marker GFAP (lower panels), respectively. Nuclei were counterstained with Hoechst in blue color. Scale bar: 20 μm.

Next, we examined the expression patterns of different neural markers throughout the course of neural differentiation by quantitative reverse-transcription PCR (qRT-PCR) to compare the temporal expression profiles of these markers in WT and ultra-low H1 cells. *Nestin* and *GFAP* expression was efficiently and progressively induced in WT EB cultures (Figure 2.17) and significant up-regulation of *GFAP* occurred starting from day 8+10, consistent with the notion that neurogenesis is followed by gliogenesis during the development of the central nervous system. The expression of *TUBB3* and tyrosine hydroxylase (*TH*) reached peak levels at day 8+5 and decreased after an extended culture. While the expression of these neural markers was compromised in H1 TKO EB cultures as we observed previously (Zhang et al., 2012a), their expression was largely blocked in QKO/abi (±Dox) EB cultures throughout the culture course. Collectively, our results indicate that a sufficient amount of histone H1 is required for the induction of neural lineage-specific genes during neural differentiation.

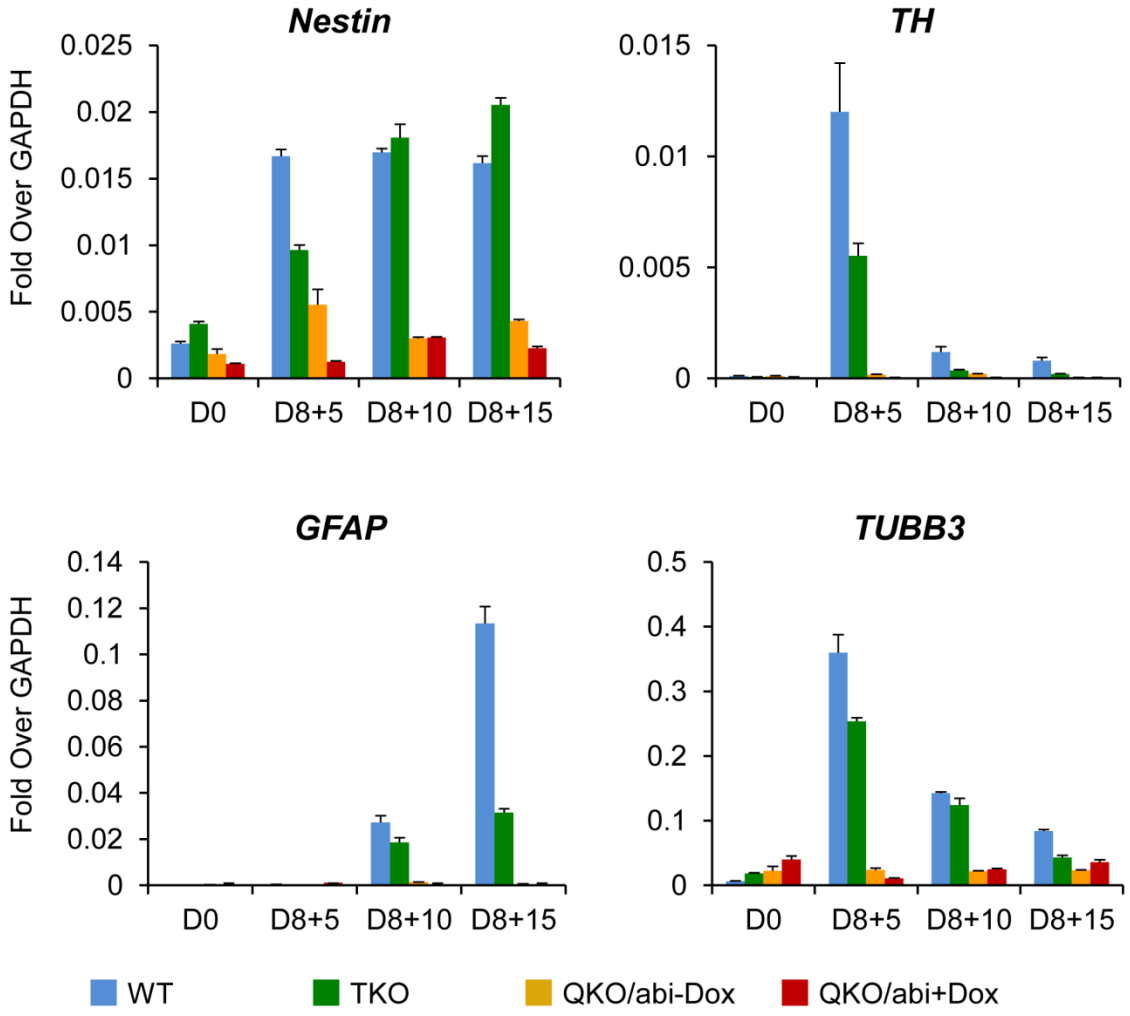

Figure 2.17 Sequential H1 depletion progressively impairs the induction of neural lineage-specific genes.

qRT-PCR analysis was performed to examine the expression of the neural stem cell marker *Nestin*, two neuronal markers *TUBB3* and tyrosine hydroxylase (*TH*), and the glial marker *GFAP* in ESCs and differentiating EBs. Data were normalized over the expression of *GAPDH* and are presented as means ± S.D.

2.4.6 H1 depletion causes dysregulation of pluripotency-associated genes during neural differentiation

ESCs express pluripotency-associated genes like *Oct4* and *Nanog* as hallmarks. These transcription factors play fundamental roles in maintaining ESC pluripotency and their downregulation is necessary for differentiation to occur (Liang et al., 2008; Loh et al., 2006; Mitsui et al., 2003; Niwa et al., 2000). We have previously reported that *Oct4* is not efficiently silenced in H1 TKO cells during embryogenesis and EB differentiation (Zhang et al., 2012a). We performed qRT-PCR analysis to determine if severe H1 depletion further compromised the repression of *Oct4* and *Nanog* expression during neural differentiation. While the expression of *Oct4* and *Nanog* was efficiently downregulated in WT EBs during neural differentiation, they remained at high levels in EBs with an ultra-low H1 level (QKO/abi+Dox EBs), even more drastic dysregulated than that in H1 TKO EBs. These results demonstrate that severe depletion of H1 does not affect the expression of *Oct4* and *Nanog* in ESCs but causes de-repression of these genes in a dose-dependent manner.

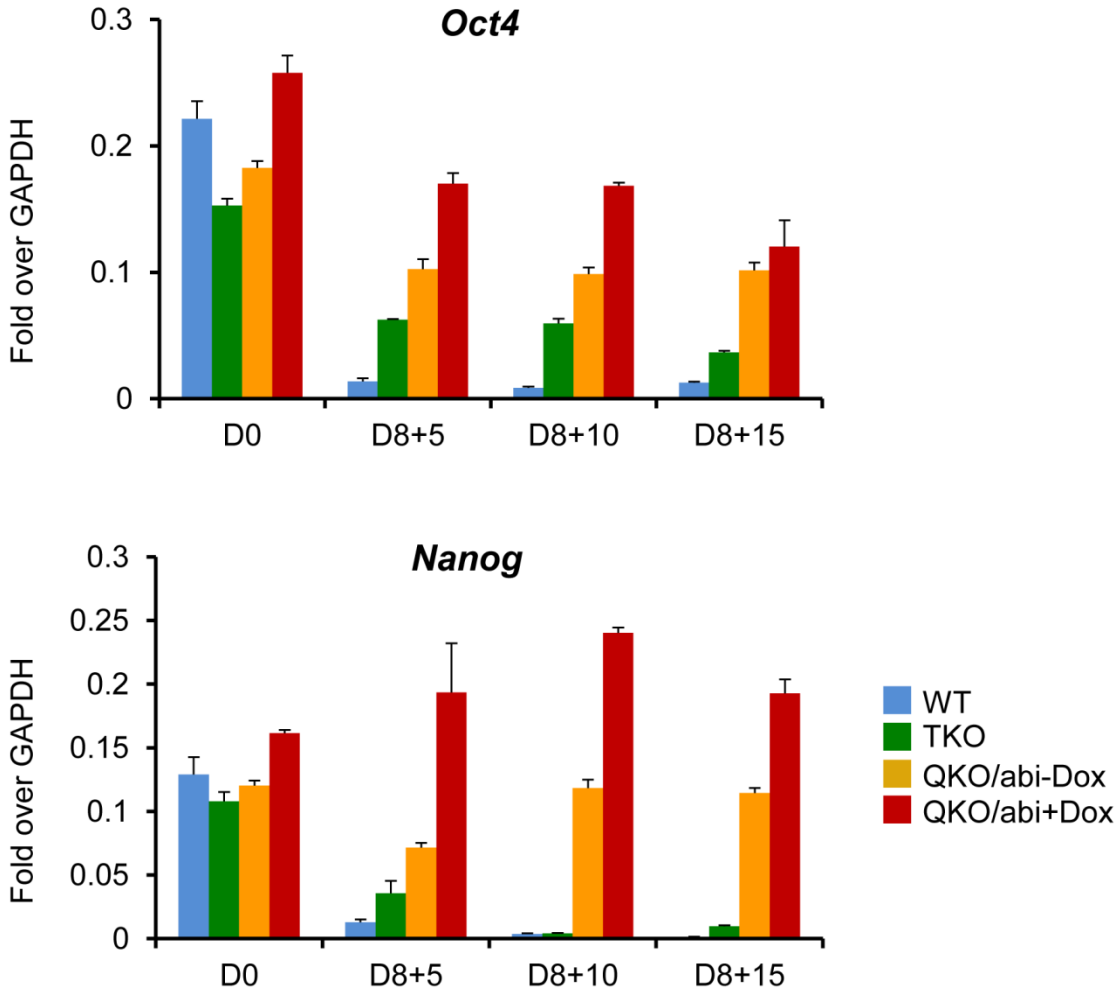

Figure 2.18 H1 depletion causes dysregulation of pluripotency-associated genes during neural differentiation.
qRT-PCR analysis was performed to examine the expression of *Oct4* and *Nanog* throughout the whole neural differentiation course. Data were normalized over the expression of *GAPDH* and are presented as means ± S.D.

2.4.7 The total H1 level progressively increases during neural differentiation

To ascertain how the H1 level can modulate neural differentiation, we examined the expression profiles of H1 variants throughout the course of neural differentiation. Total histone extracts from ESCs (day 0), day 8+5, day 8+10, and day 8+15 EBs were subjected to HPLC analysis. Upon neural differentiation, the total H1 level in WT EB cultures progressively increased over time, with the total H1/nuc ratio elevated nearly 60% from 0.45 in ESCs (day 0) to 0.71 in day 8+15 EB cultures (Figure 2.19). In contrast, the total H1 level was not significantly changed over time in QKO/abi-Dox EBs, remaining close to 0.24. By day 8+15, QKO/abi+Dox EB cultures had an H1/nuc ratio of ~0.17, only 24% of that in WT EBs (an H1/nuc ratio of ~0.71).

During neural differentiation, the increase in the levels of H1c, H1d, H1e, and $H1^0$ was responsible for the increase in the total H1 level (Figure 2.19). In H1 TKO EB cultures, $H1^0$ was dramatically upregulated, accounting for 54% of the total H1 level in day 8+15 EBs. The elevation in the $H1^0$ level during neural differentiation is in concert with previous findings which suggest an accumulation of $H1^0$ in postnatal brain in a period corresponding to neural terminal differentiation (Cestelli et al., 1992; Dominguez et al., 1992; Pina et al., 1984). However, $H1^0$ alone is not required for neural differentiation as shown by the similar extent of neurite formation and comparable expression levels of neural markers in $H1^0$ KO and WT EBs (Figures 2.20, 2.21, and 2.22).

These results indicate that the histone H1 level is progressively increased during ESC differentiation and that the severe reduction in total H1 level is responsible for the blockage in neural differentiation.

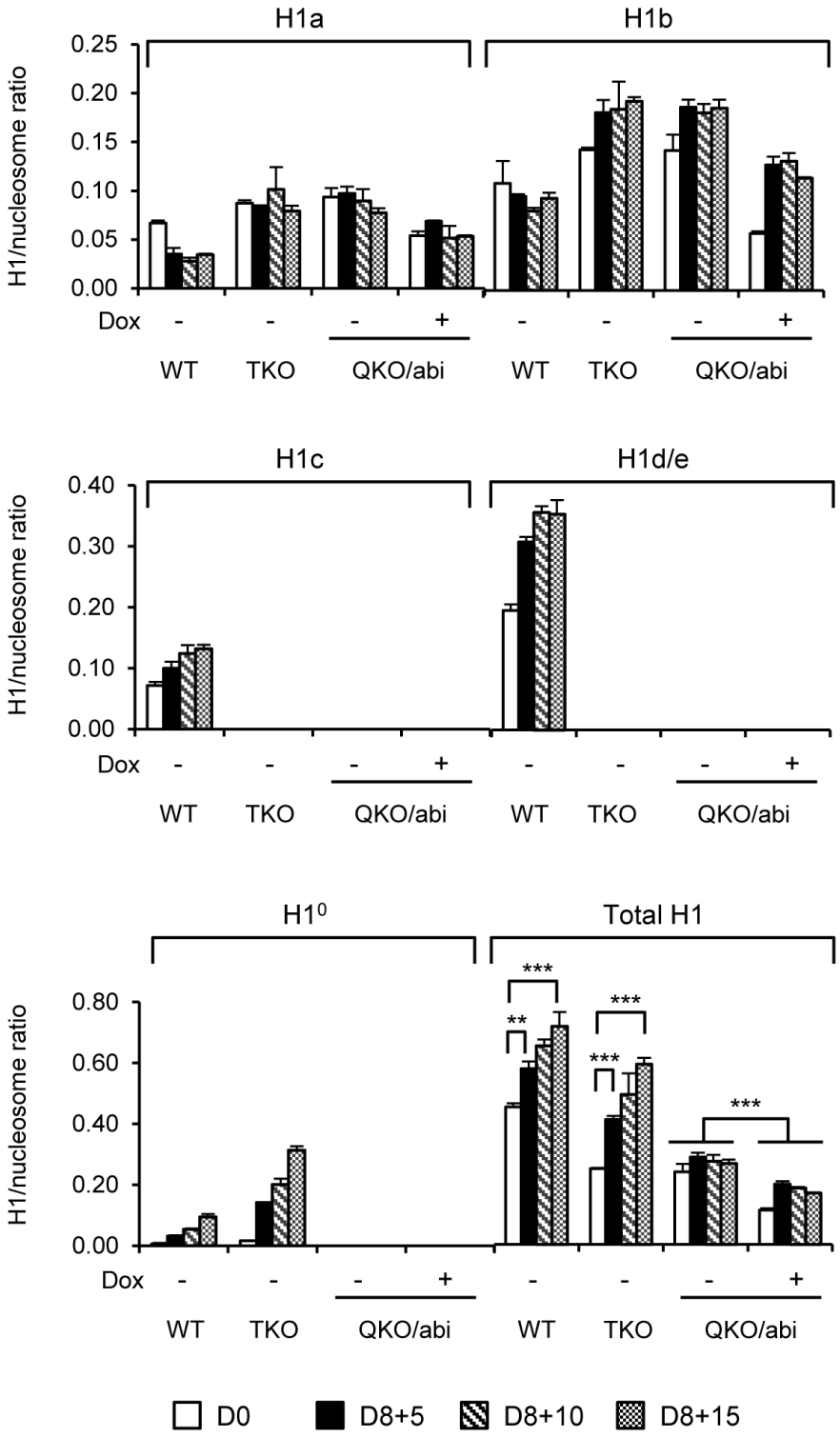

Figure 2.19 Expression profiles of histone H1 variants during neural differentiation. Individual and total H1 to nucleosome ratios were calculated according to HPLC analysis of ESCs and EB samples. Values are shown in means ± S.D., n = 3. **: $p<0.01$; ***: $p<0.001$.

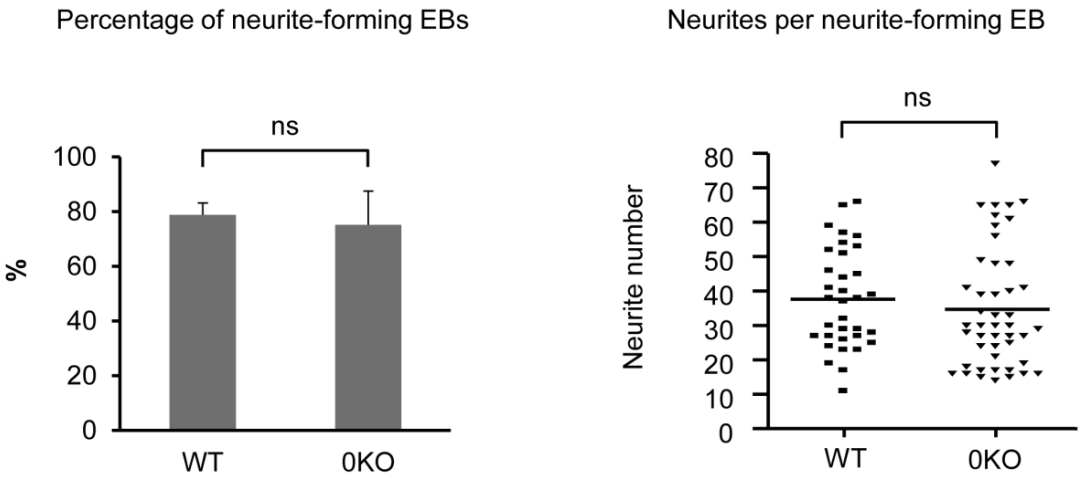

Figure 2.20 $H1^0$ knockout (0KO) EBs have similar neurite outgrowth ability as wildtype (WT) EBs.
Left panel: percentage of neurite-forming EBs. Numbers were averaged from at least 4 experiments. Over 100 EBs were counted per experiment. Right panel: numbers of neurites per neurite-forming EB. Neurite number was counted from EBs that produced neurites. ns: not significant.

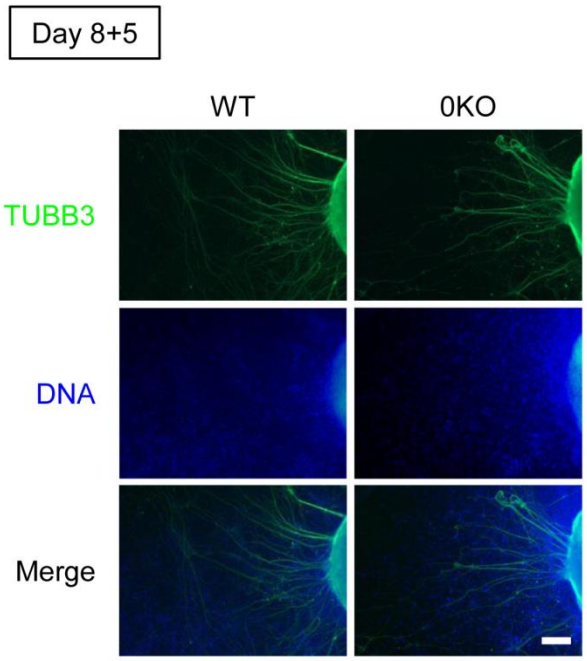

Figure 2.21 $H1^0$ knockout alone does not affect *TUBB3* expression in day 8+5 EBs.
TUBB3 was stained in green color and nuclei were counterstained with Hoechst in blue. 0KO, $H1^0$ knockout. Scale bar: 200 μm.

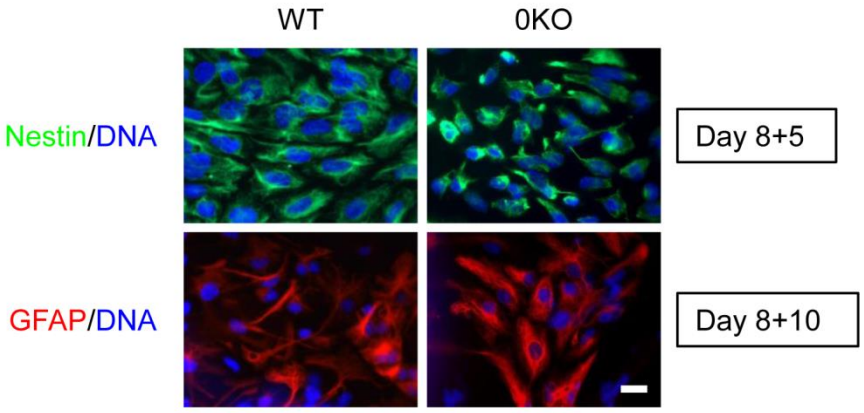

Figure 2.22 $H1^0$ knockout alone has no effect on the expression of *Nestin* and *GFAP* in EB cultures.
Day 8+5 and 8+10 EBs were immunostained against the neural stem cell marker Nestin (upper panels) and glial cell marker GFAP (lower panels), respectively. Nuclei were counterstained with Hoechst in blue color. Scale bar: 20 μm.

2.4.8 H1d overexpression restores the neural differentiation capacity of ESCs

To confirm the dosage effect of histone H1 on neural differentiation, we re-introduced H1d back into QKO/abi ESCs. H1d overexpression restored the total H1 level to 0.43, close to WT ESCs (Figure 2.23). These ESCs were designated as QKO/abi/H1^{res} ESCs. Neural differentiation of QKO/abi/H1^{res} ESCs was performed to examine if H1d overexpression could rescue the defects observed in QKO/abi ESCs. Indeed, over 68% of QKO/abi/H1^{res} EBs were able to form neurite outgrowth with an average of 20 neurites per EB (Figure 2.24), indicating that QKO/abi/H1^{res} ESCs surpassed H1 TKO ESCs in differentiation capacity. Similarly, the expression of *TUBB3*, *Nestin*, and *GFAP*, and the silencing of pluripotency genes, *Oct4* and *Nanog*, were restored in QKO/abi/H1^{res} EB cultures (Figures 2.25, 2.26, 2.27, and 2.28). Collectively, our results reveal a dosage effect of histone H1 on neural differentiation of ESCs rather than a variant specificity, and that severe depletion of histone H1 blocks differentiation.

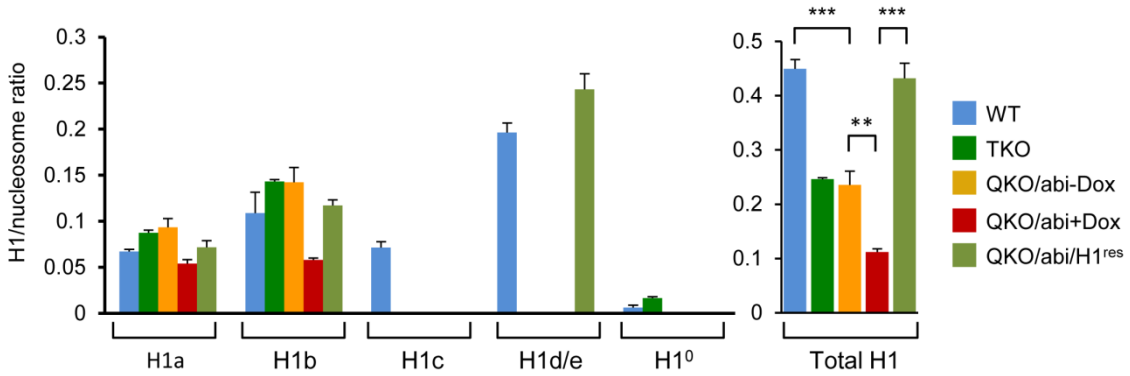

Figure 2.23 H1d overexpression in QKO/abi ESCs.
HPLC analysis and H1 quantification showed that overexpression of H1d in QKO/abi ESCs restored the total H1 level comparable to that in WT ESCs. Values are presented as means ± S.D. n = 3. **: $p<0.01$; ***: $p<0.001$.

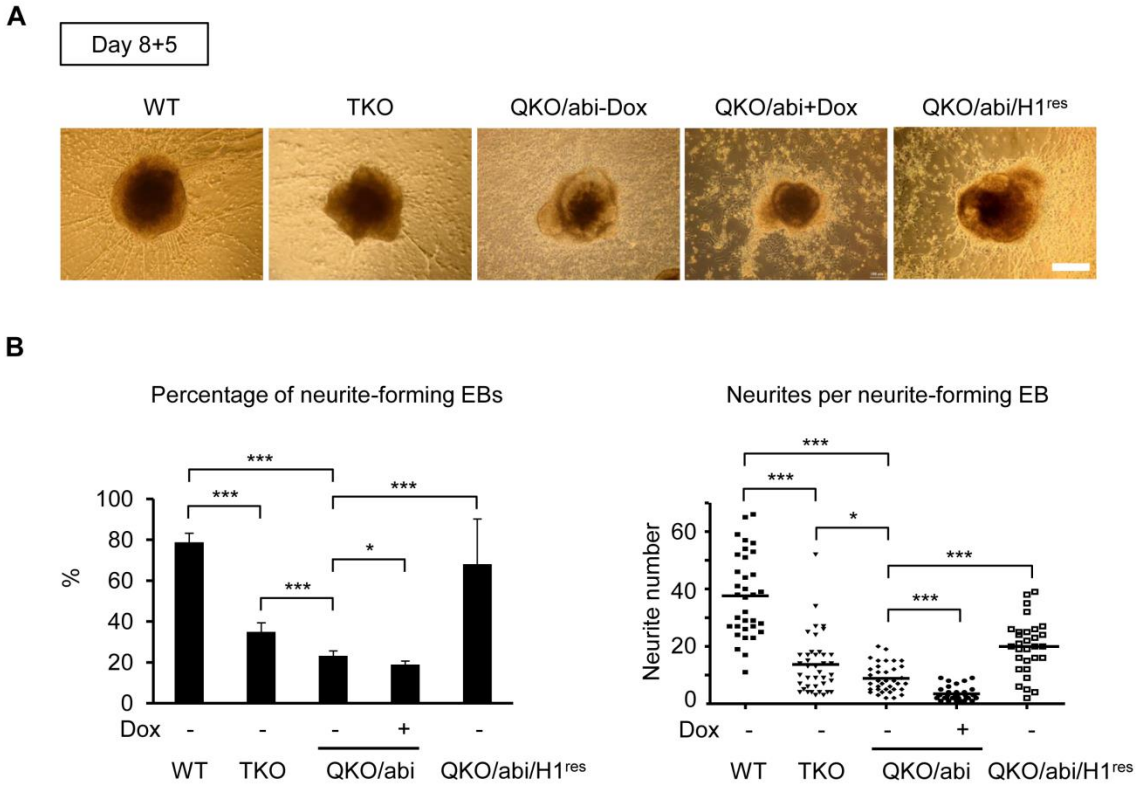

Figure 2.24 H1d overexpression rescues the defects in neurite outgrowth in day 8+5 EBs.
A) Phase contrast images of day 8+5 EBs. Scale bar, 200 μm.
B) Left panel: percentage of neurite-forming EBs. Numbers were averaged from at least 4 experiments. Over 100 EBs were counted per experiment. Right panel: numbers of neurites per neurite-forming EB. Neurite number was counted from EBs that produced neurites. Dox was added to media when EB cultures were induced. All data are presented as means ± S.D. QKO/abi/H1^{res}, H1d overexpression in QKO/abi ESCs. *: $p<0.05$; ***: $p<0.001$.

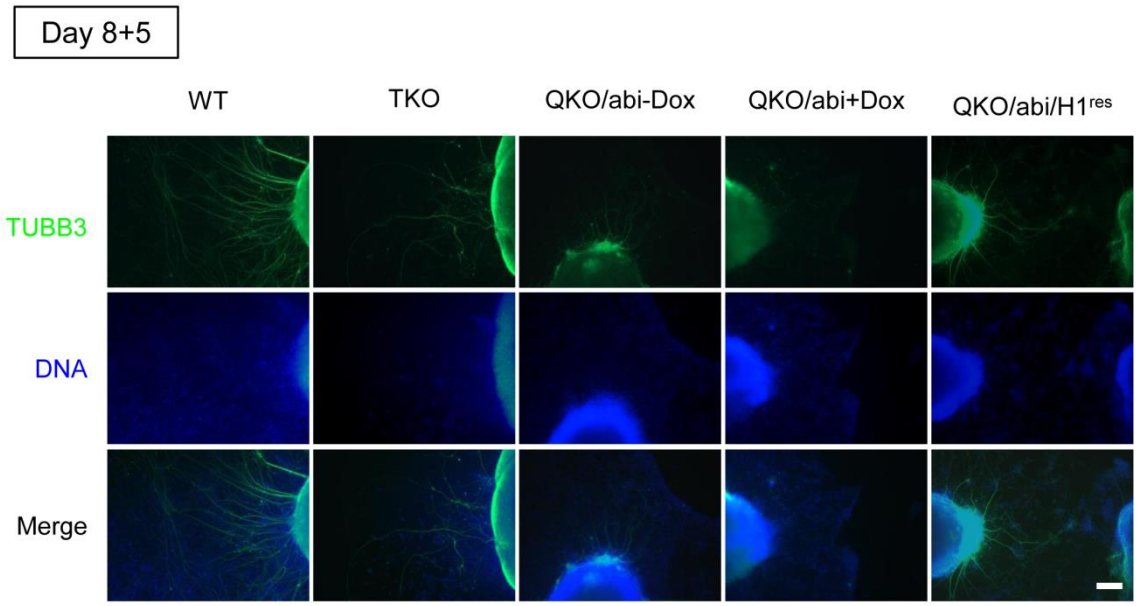

Figure 2.25 H1d overexpression rescues *TUBB3* expression in day 8+5 EBs.
TUBB3 was stained in green color and nuclei counterstained with Hoechst in blue. Scale bar: 200 μm.

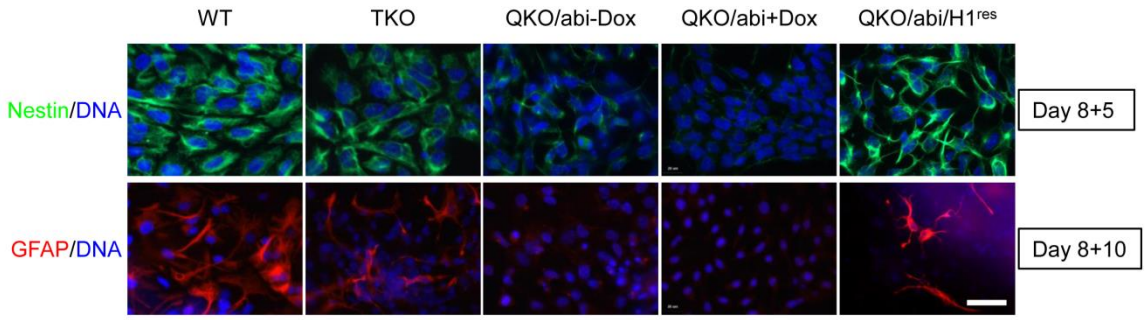

Figure 2.26 H1d overexpression restores the expression of *Nestin* and *GFAP* in QKO/abi/H1^{res} EB cultures.

Day 8+5 and 8+10 EBs were immunostained against the neural stem cell marker Nestin (upper panels) and the glial cell marker GFAP (lower panels), respectively. Nuclei were counterstained with Hoechst in blue color. Scale bar: 20 μm.

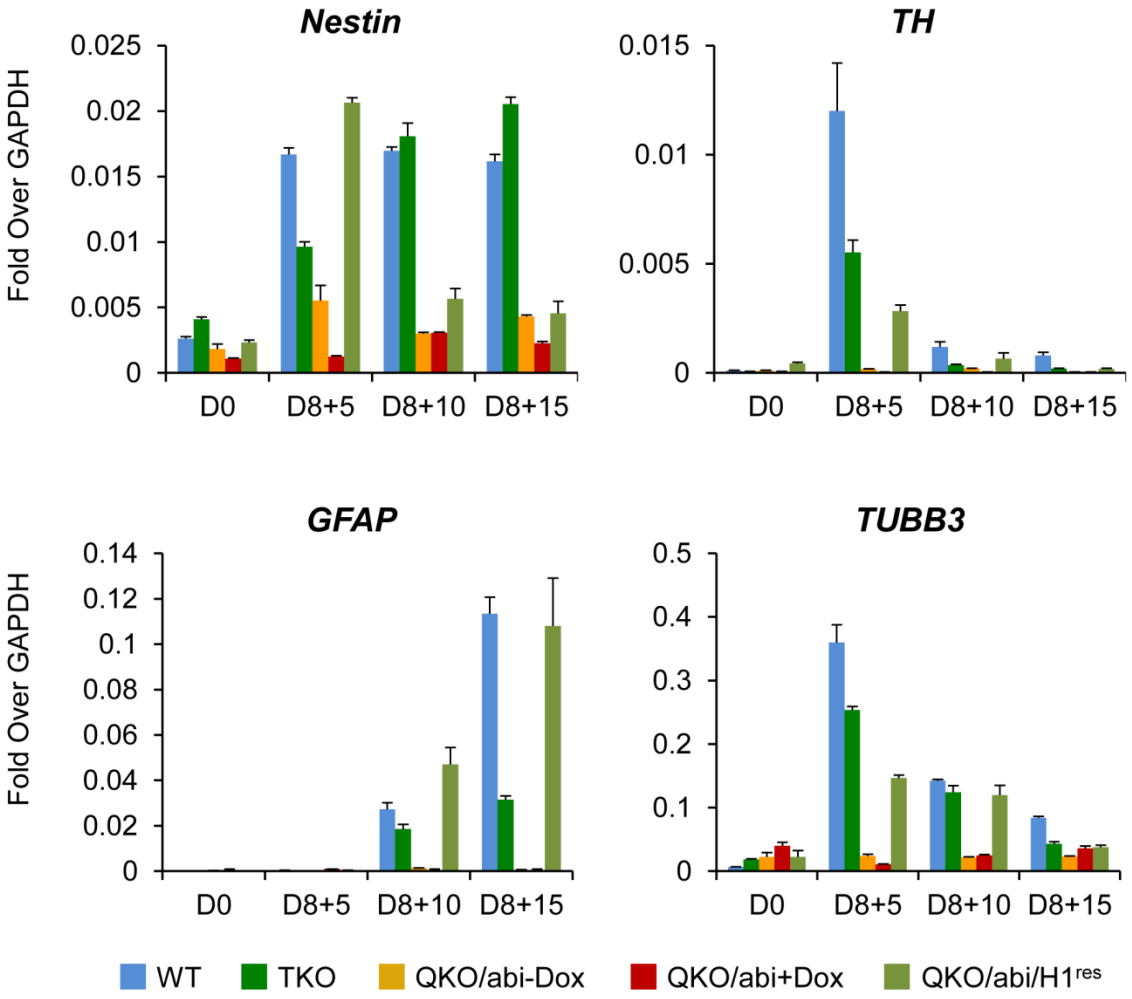

Figure 2.27 The induction of neural lineage-specific genes in QKO/abi/H1^{res} EB cultures during neural differentiation.

qRT-PCR analysis was performed to examine the expression of the neural stem cell marker *Nestin*, two neuronal markers *TUBB3* and tyrosine hydroxylase (*TH*), and the glial marker *GFAP* in ESCs and differentiating EBs. Data were normalized over the expression of *GAPDH* and are presented as means ± S.D.

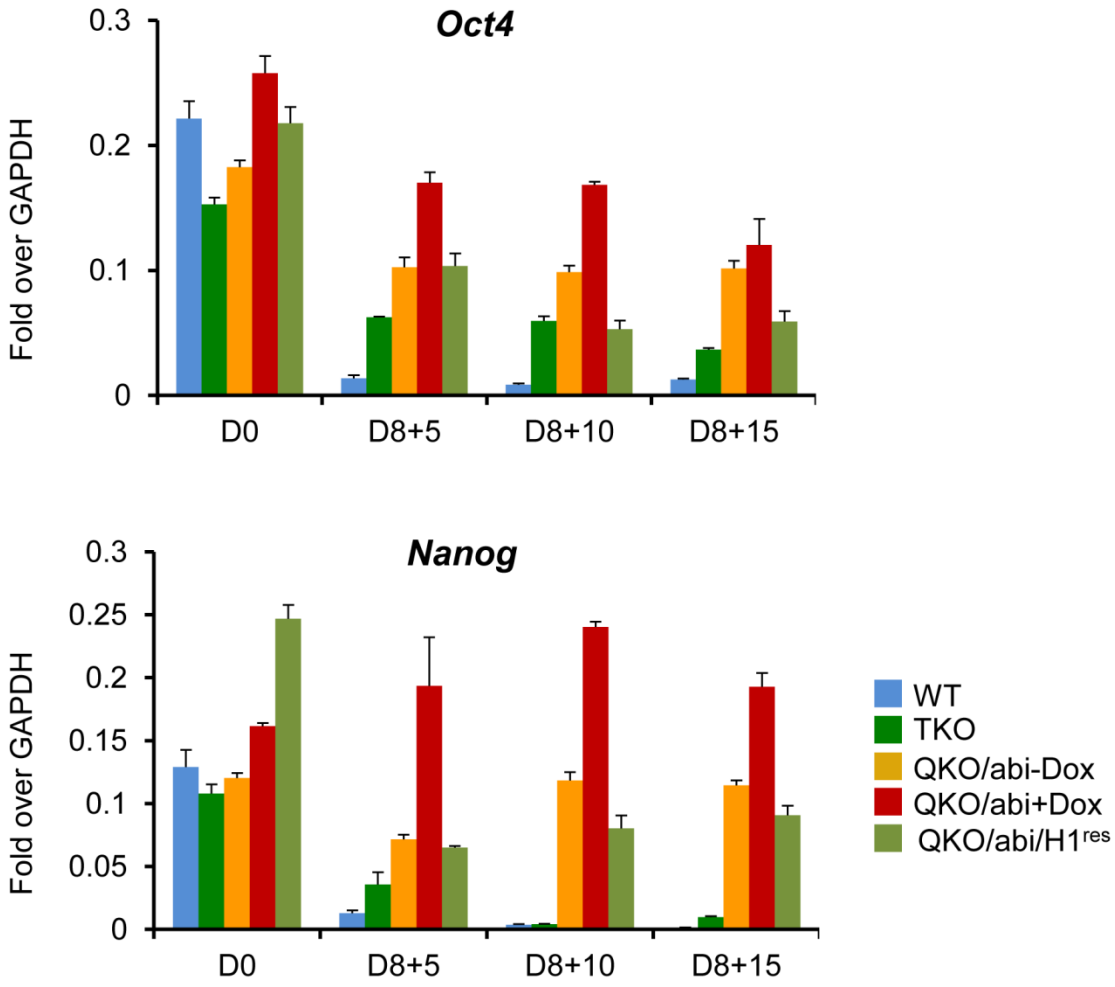

Figure 2.28 H1d overexpression represses *Oct4* and *Nanog* expression during neural differentiation.

qRT-PCR analysis was performed to examine the expression of *Oct4* and *Nanog* throughout the whole neural differentiation course. Data were normalized over the expression of *GAPDH* and are presented as means ± S.D.

2.4.9 Severe H1 depletion causes a reduction in cell proliferation and cellular senescence in neural lineages

While severe H1 depletion did not affect the proliferation of ESCs (Figures 2.2C and 2.6C), day 5 EBs with an ultra-low H1 level (QKO/abi+Dox EBs) showed a small but statistically significant reduction in EB size (Figure 2.10). This result suggests that fewer cells were present in day 5 ultra-low H1 EBs compared with WT counterparts. To test if cell proliferation is affected in QKO/abi+Dox EBs, we performed 5-bromo-2'-deoxyuridine (BrdU) incorporation assay in neural lineages. Day 8+5 EBs were pulsed with BrdU for 2 hours and assessed for BrdU incorporation by immunostaining. WT, H1 TKO, QKO/abi-Dox, and QKO/abi+Dox EB cultures displayed an increasingly reduced level of BrdU incorporation (Figure 2.29). Quantification of BrdU-positive cells revealed 47%, 38%, 30%, and 25% of BrdU-positive cells in WT, H1 TKO, QKO/abi-Dox, and QKO/abi+Dox EBs, respectively (Figure 2.30). H1d overexpression was able to rescue the defect in cell proliferation (Figures 2.29 and 2.30). These results establish a dosage effect of H1 depletion on cell proliferation in differentiating EBs.

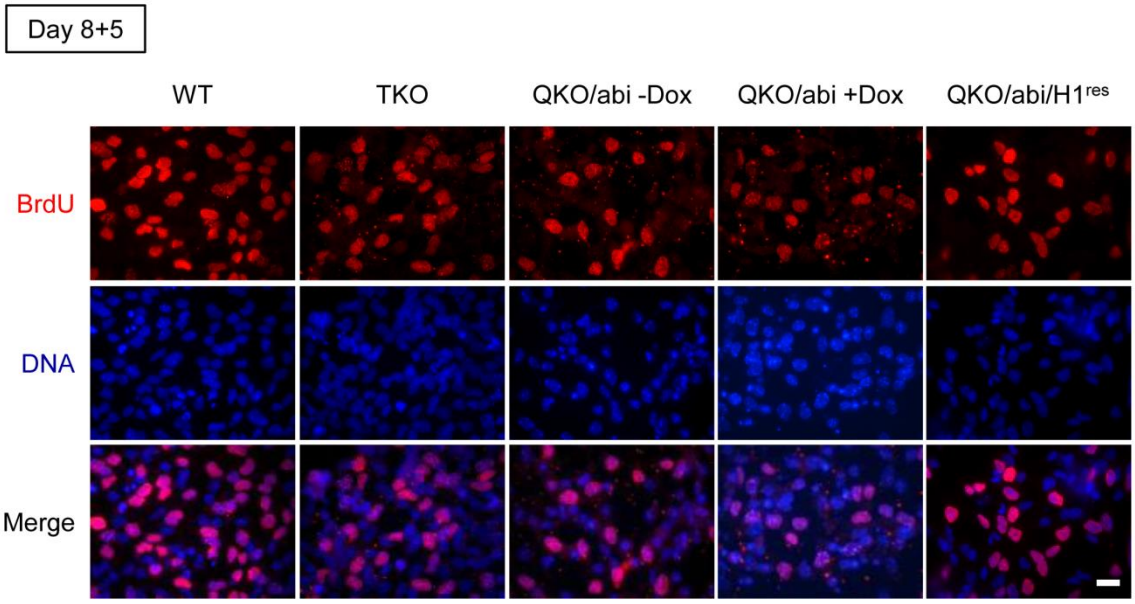

Figure 2.29 H1 depletion leads to a reduction in cell proliferation in neural lineages.
Day 8+5 EBs were pulsed with BrdU for 2 h and immunostained with an anti-BrdU antibody to assess cell proliferation of neural cells. Scale bar: 20 μm.

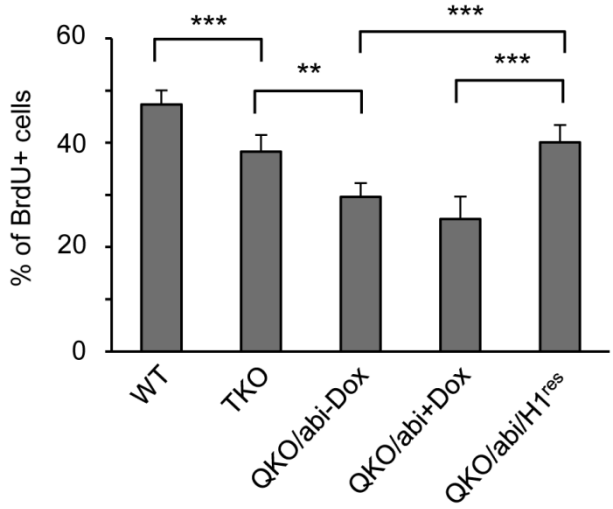

Figure 2.30 Quantification of BrdU-positive cells in day 8+5 EB cultures.
Percentages were obtained by counting cells from at least 4 images of BrdU-immunostained EBs with cell numbers varying from 50 to 90. Data are shown as means ± S.D. **: $p<0.01$; ***: $p<0.001$.

The observed reduction in cell proliferation after H1 depletion may correspond to cellular senescence in neural lineages, a state of irreversible growth arrest (Campisi and d'Adda di Fagagna, 2007; Collado et al., 2007). A previous study suggests that H1 is lost in senescent cells, but it is not clear whether H1 loss also has an impact on cellular senescence (Funayama et al., 2006). To compare the level of cellular senescence in ESCs and day 8+5 EBs, we performed staining of senescence-associated β-Galactosidase (SA-β-Gal), a commonly used marker for senescent cells (Dimri et al., 1995). Although sequential H1 depletion did not cause cellular senescence in ESCs (data not shown), it led to a progressive increase in SA-β-Gal activity in neural lineages, with the strongest staining in QKO/abi+Dox EB cultures (Figure 2.31). H1d overexpression was able to overcome the senescent state.

Collectively, these results suggest that the loss of histone H1 impairs cell proliferation and increases cellular senescence in neural lineages.

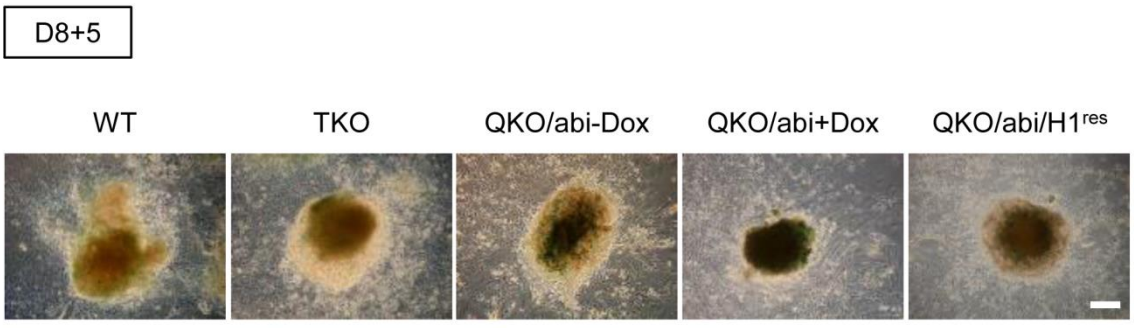

Figure 2.31 Severe H1 depletion leads to cellular senescence in differentiating EBs.
Day 8+5 EBs were stained for senescence-associated β-Galactosidase (SA-β-Gal) activity. Scale bar: 200 μm.

2.4.10 *Oct4* knockdown rescues the defects in neural differentiation caused by H1 depletion

As shown earlier, H1 depletion led to dysregulation of pluripotency-associated genes during neural differentiation. To assess whether the effects of H1 depletion on neural differentiation is mediated through a lack of *Oct4* silencing during differentiation, we sought to determine if knockdown of *Oct4* expression in QKO/abi EBs is able to restore their differentiation. QKO/abi ESCs were transduced with the Tet-On inducible vector encompassing *Oct4* shRNAs to establish QKO/abi/Oct4i ESCs. Upon induction with Dox, *Oct4* expression in QKO/abi/Oct4i ESCs was depleted to less than 30% of that in WT ESCs (Figure 2.32A). Since Oct4 is an essential transcription factor for ESC self-renewal and depletion of *Oct4* expression impaired cell growth of QKO/abi/Oct4i ESCs, we established inducible QKO/abi/Oct4i ESC lines in which knockdown of *Oct4* expression is induced with Dox. We added Dox at day 5 of EB formation and EBs were collected at different time points. qRT-PCR analysis confirmed that *Oct4* expression was successfully depleted in QKO/abi/Oct4+Dox EBs during neural differentiation (Figure 2.32B). Remarkably, while QKO/abi/Oct4i-Dox EBs resembled QKO/abi-Dox EBs, QKO/abi/Oct4i+Dox EBs formed abundant neurites by day 8+5 (Figure 2.33A). Quantitatively, 19% QKO/abi/Oct4i-Dox EBs had 9 neurites on average, whereas *Oct4* knockdown restored neurite outgrowth to 67% of EBs with 27 neurites on average (Figure 2.33B). Immunostaining and qRT-PCR analysis of neural markers corroborated the efficient rescue of both neurogenic and gliogenic processes (Figures 2.34, 2.35, and 2.36). Interestingly, *Oct4* knockdown was accompanied by *Nanog* downregulation during neural differentiation (Figure 2.36). Furthermore, *Oct4* knockdown could

partially rescue the reduction in cell proliferation and cellular senescence in neural lineages, indicating there exist other mechanisms causing these phenomena (Figures 2.37 and 2.38). These results demonstrate that *Oct4* knockdown alone can efficiently rescue the defects in neural differentiation and establish *Oct4* repression as a critical step in this process.

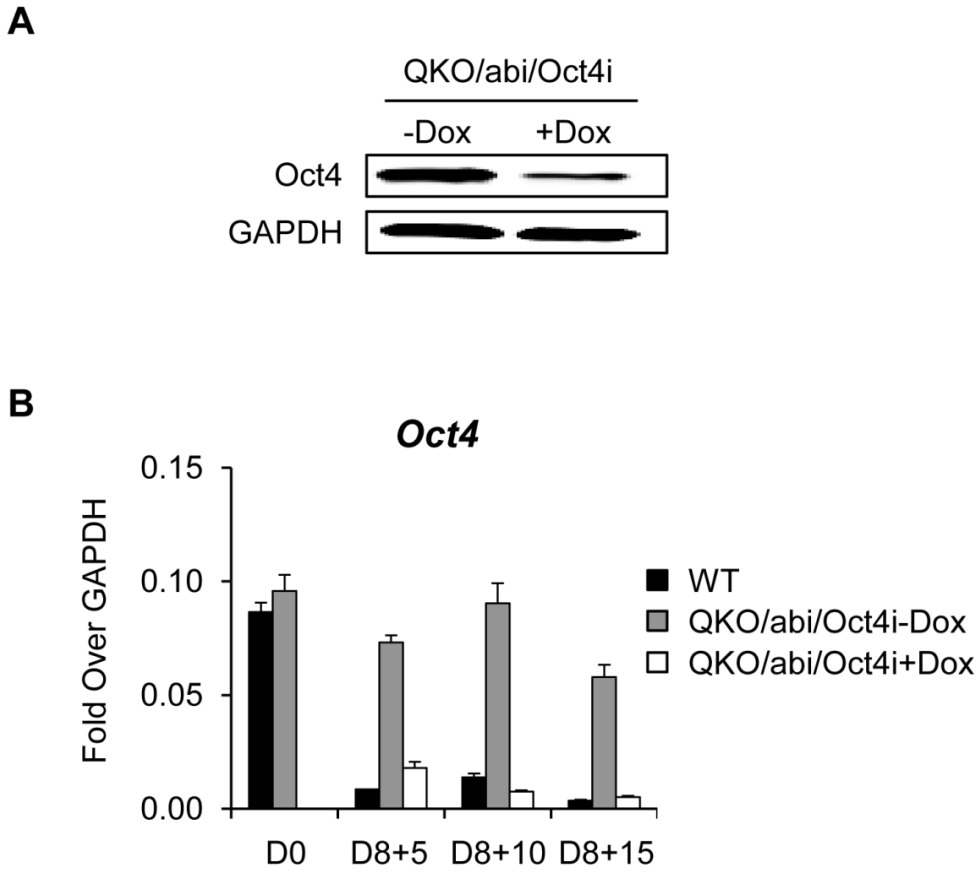

Figure 2.32 *Oct4* knockdown in QKO/abi ESCs and EBs.
QKO/abi ESCs were transduced with pTRIPZ-Oct4shRNA to establish QKO/abi/Oct4i ESCs for inducible *Oct4* knockdown. *Oct4* knockdown efficiency was examined by Western blotting in ESCs (A) and by qRT-PCR in EBs (B).

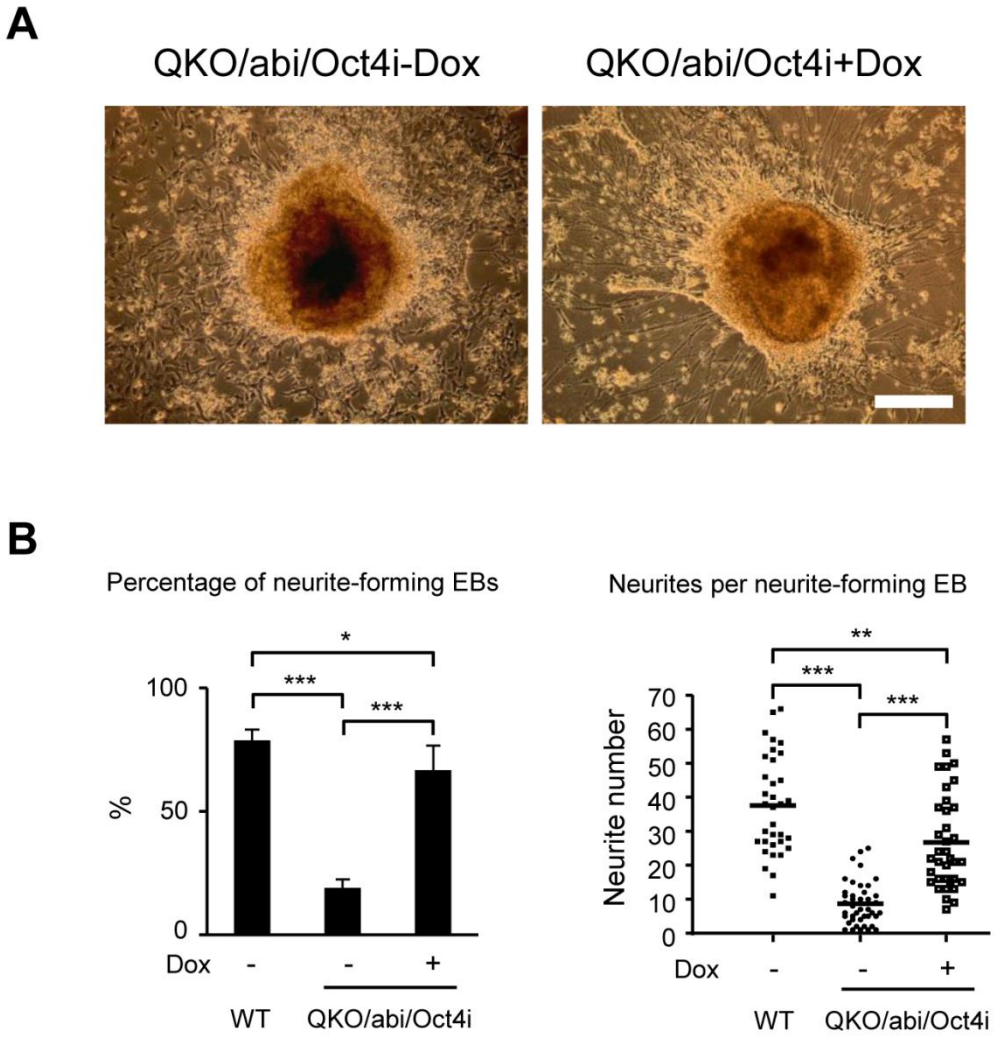

Figure 2.33 *Oct4* knockdown rescues the defects in neurite outgrowth caused by H1 depletion.

A) Phase contrast images of day 8+5 EBs. Scale bar: 200 μm.

B) Left panel: percentage of neurite-forming EBs. Numbers were averaged from at least 4 experiments. Over 100 EBs were counted per experiment. Right panel: numbers of neurites per neurite-forming EB. Neurite number was counted from EBs that produced neurites. Data are presented as means ± S.D. *: $p<0.05$; **: $p<0.01$; ***: $p<0.001$.

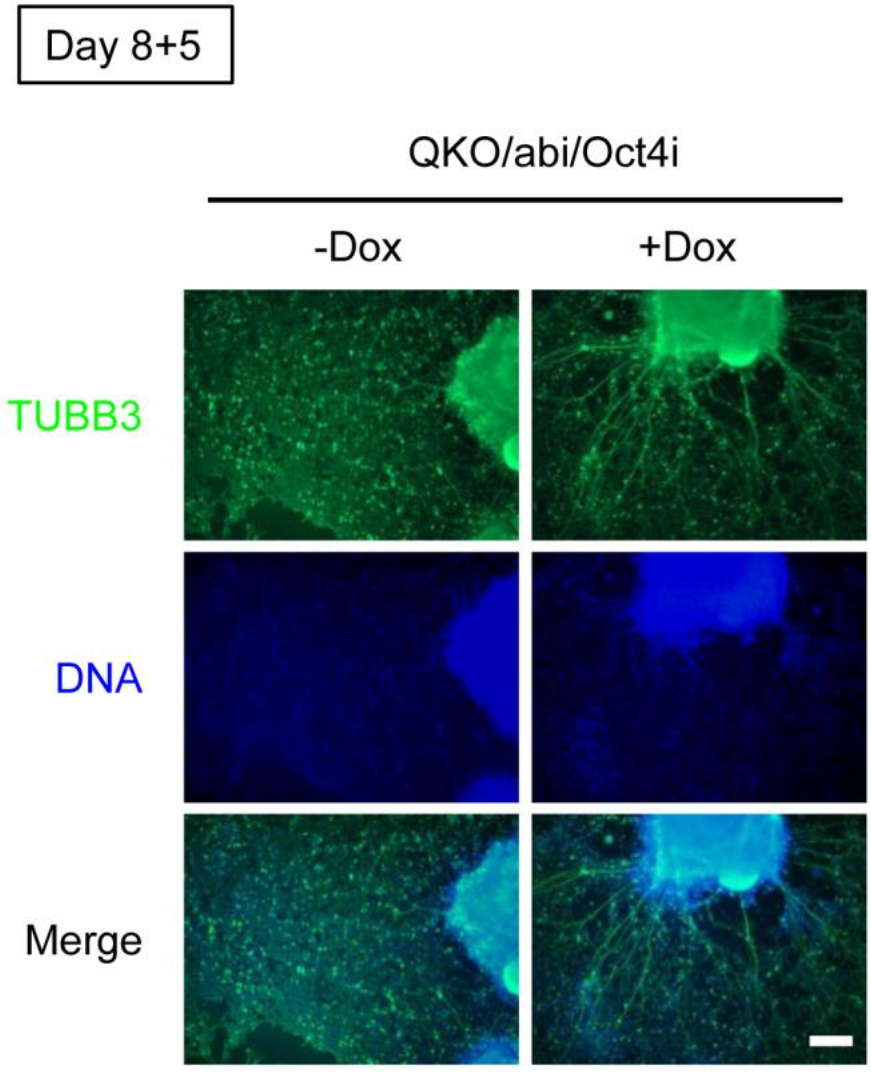

Figure 2.34 Immunostaining of TUBB3 in day 8+5 QKO/abi/Oct4i EBs.
TUBB3 was stained in green color and nuclei were counterstained with Hoechst in blue.
Scale bar: 200 μm.

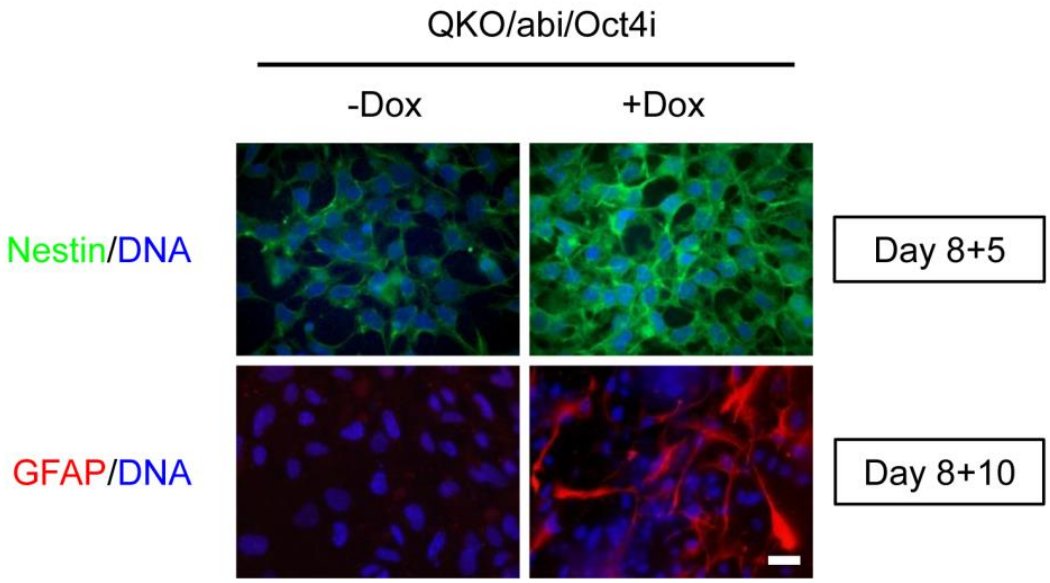

Figure 2.35 Immunostaining of Nestin and GFAP in QKO/abi/Oct4i EBs.
Day 8+5 and 8+10 EBs were immunostained against the neural stem cell marker Nestin (upper panels) and the glial cell marker GFAP (lower panels), respectively. Nuclei were counterstained with Hoechst in blue color. Scale bar: 20 μm.

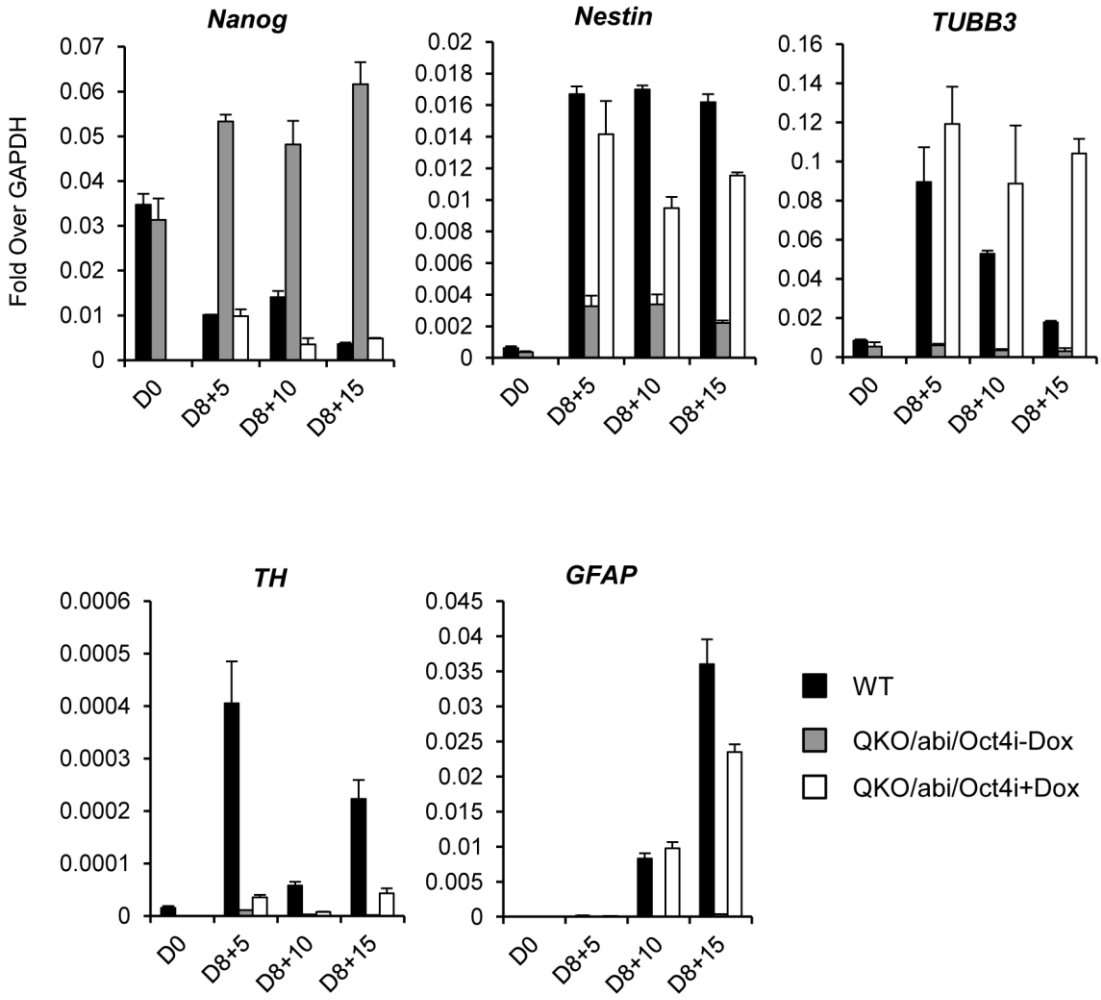

Figure 2.36 qRT-PCR analysis of the expression of *Nanog* and neural lineage-specific genes in QKO/abi/Oct4i EBs during the whole neural differentiation course.
Data were normalized over the expression levels of *GAPDH* and are presented as means ± S.D.

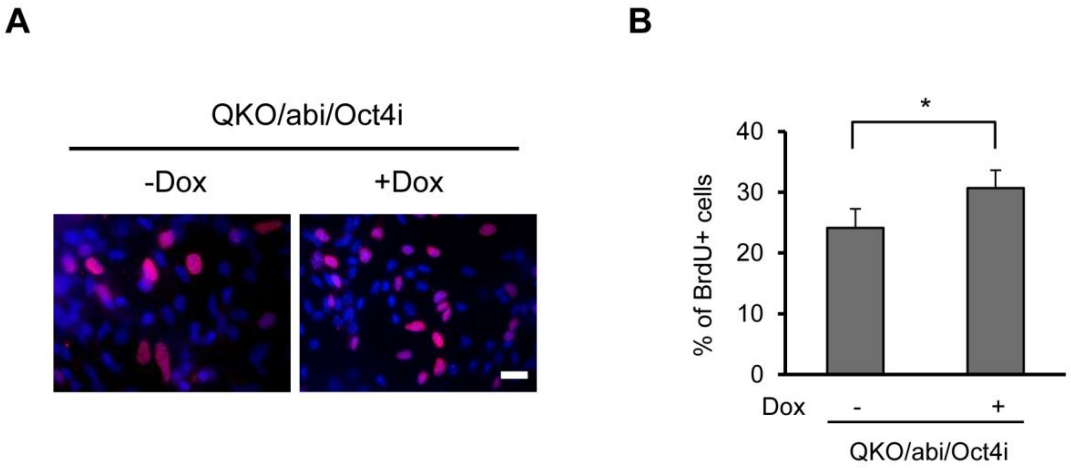

Figure 2.37 *Oct4* knockdown partially rescues the reduction in cell proliferation in neural lineages caused by H1 depletion.
A) BrdU incorporation assay of day 8+5 QKO/abi/Oct4i EBs. Scale bar: 20 μm.
B) Quantification of BrdU-positive cells. Percentages were obtained by counting cells from at least 4 images of BrdU-immunostained EBs with cell numbers varying from 40 to 90. Data are shown as means ± S.D. *: $p<0.05$.

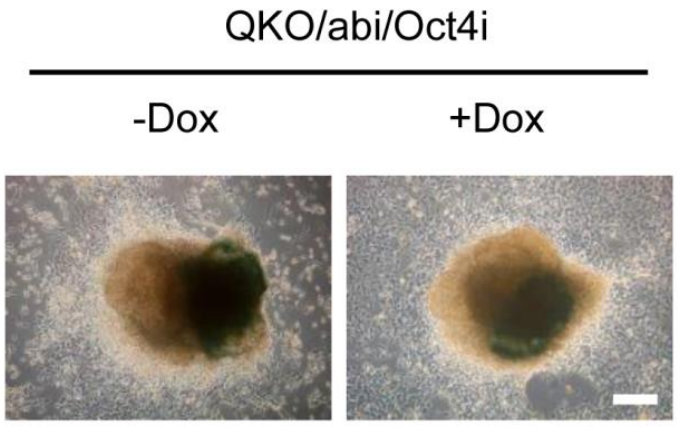

Figure 2.38 *Oct4* knockdown partially rescues cellular senescence in differentiating EBs caused by H1 depletion.
Day 8+5 QKO/abi/Oct4i EBs were stained for senescence-associated β-Galactosidase (SA-β-Gal) activity. Scale bar: 200 μm.

2.5 Discussion

By sequential depletion of major somatic H1 variants, we took the first step to generate a mammalian cellular system with an ultra-low H1 level using combined knockout and knockdown approaches. We first derived H1 QKO ESCs from H1c/H1d/H1e/$H1^0$ quadruple knockout mouse blastocysts, followed by establishing QKO/abi ESCs through knocking down H1a and H1b. The Tet-On inducible RNAi system utilized in this study serves as a convenient and controllable tool for simultaneous depletion of the remaining H1a and H1b variants. This combined approach allowed us to deplete the total H1 level in ESCs by 75% (Figure 2.5). Since ESCs are able to differentiate into all cell lineages from three germ layers, the ESC lines generated in this study provide great systems to investigate the role of histone H1 in ESC differentiation.

Surprisingly, Dox-induced QKO/abi ESCs with an H1/nuc ratio of 0.11 have normal colony morphology, *Oct4* expression, growth rate, and cell cycle profile (Figure 2.6), indicating that such a minimum level of H1 is compatible with ESC self-renewal. Given the presence of remaining 25% histone H1s in these ultra-low H1 ESCs, it remains open whether ESCs can self-renew normally in the face of complete loss of all H1s, which warrants future studies.

It is generally accepted that ESCs possess a relatively "open" chromatin state with globally transcriptional hyperactivity and undergo chromatin condensation upon differentiation (Efroni et al., 2008; Gaspar-Maia et al., 2011). ESCs have an H1/nuc ratio of 0.46 (Fan et al., 2005), approximately 1 H1 per 2 nucleosomes, versus that up to 0.75~0.8 in adult cells (Fan et al., 2003; Woodcock et al., 2006). Depletion of H1c, H1d,

and H1e impairs ESC differentiation and disrupts embryonic development (Fan et al., 2003; Zhang et al., 2012a). The ultra-low H1 (QKO/abi) ESCs generated here allowed us to better examine the role and mechanisms of H1 and chromatin structure in regulating ESC differentiation. Using a neural differentiation protocol that we optimized for improved efficiency, we observed a dosage effect of the total histone H1 level, rather than a variant specificity, on silencing pluripotency genes and neural differentiation of ESCs as well as cell proliferation and senescence in differentiating EBs. The fact that individual deletion of $H1^0$, or H1c, or H1d, or H1e, does not affect ESC differentiation (this thesis and Zhang et al., 2012b) and that QKO/abi/$H1^{res}$ cells have restored neural differentiation further support the dosage effect of somatic H1 variants on neural differentiation.

In contrast to the normal cell proliferation of ultra-low H1 ESCs, EBs exhibit a progressive decrease in cell proliferation with an increasing reduction of the total H1 level as shown in BrdU incorporation assay (Figures 2.29 and 2.30). Senescence-associated β-Galactosidase (SA-β-Gal) staining further demonstrated that severe H1 depletion elicits a cellular senescence state in neural lineages (Figure 2.31). These results suggest that loss of histone H1 impairs cell proliferation and leads to cellular senescence in neural lineages. It would be interesting to examine the chromatin structure and gene expression profiles of these cells in differentiating EBs. Such studies will provide insights into how changes in chromatin structure lead to cell cycle defects and cellular senescence in differentiated cells.

The dosage effect of H1 depletion on differentiation is also apparent on the defects in silencing pluripotency-associated genes such as *Oct4* and *Nanog* during neural

differentiation, with more severe defects associated with more severe depletion (Figure 2.18). The pluripotency factors orchestrate a regulatory network to govern pluripotency and promote self-renewal of ESCs (Liang et al., 2008; Loh et al., 2006; Nichols et al., 1998; Niwa et al., 2000; Silva et al., 2009). These pluripotency factors are rapidly downregulated upon ESC differentiation and forced expression of *Oct4* has been shown to block ESC differentiation (Thomson et al., 2011). To determine if the failure in differentiation of ultra-low H1 ESCs is mediated through sustained *Oct4* expression, we performed inducible *Oct4* knockdown in QKO/abi ESCs. Notably, *Oct4* knockdown alone in QKO/abi ESCs effectively rescued the defects in neural differentiation in neurite formation and the expression of neural markers (Figures 2.33, 2.34, 2.35, and 2.36). Knockdown of *Oct4* expression in these ultra-low H1 cells also partially restored cell proliferation rate and mitigated cellular senescence in EBs (Figures 2.37 and 2.38). Sustained *Oct4* expression is likely to inhibit lineage-specific expression programs and activate genes involved in maintaining stem cell pluripotency. These results establish *Oct4* repression by H1 as a critical step and an important mechanism for the role of H1 in neural differentiation of ESCs.

Genome-wide epigenetic profiling studies have revealed that during neural differentiation the chromatin in stem cells undergo transition from a highly dynamic state to a more restrictive epigenetic landscape that dictates lineage-specific gene expression programs (Hawkins et al., 2010; Xie et al., 2013). Chromatin compaction state is dependent on nucleosome repeat length and the stoichiometry of linker histone H1 (Robinson et al., 2008; Routh et al., 2008). Our results suggest that chromatin condensation serves as one of the crucial determinants for efficient neural differentiation.

The differentiation defects of H1-depleted cells appear to largely result from a failure in silencing of *Oct4* as shown in the dramatic rescue of the defects in ultra-low H1 EBs by knocking down the Oct4 level. Future studies to compare the gene networks regulated by H1 depletion with that by *Oct4* knockdown during neural differentiation should lead to better understanding of the interplay among regulatory networks controlled by chromatin structure and pluripotency factors.

2.6 References

Alami, R., Fan, Y., Pack, S., Sonbuchner, T.M., Besse, A., Lin, Q., Greally, J.M., Skoultchi, A.I., and Bouhassira, E.E. (2003). Mammalian linker-histone subtypes differentially affect gene expression in vivo. Proc Natl Acad Sci U S A *100*, 5920-5925.

Allan, J., Hartman, P.G., Crane-Robinson, C., and Aviles, F.X. (1980). The structure of histone H1 and its location in chromatin. Nature *288*, 675-679.

Campisi, J., and d'Adda di Fagagna, F. (2007). Cellular senescence: when bad things happen to good cells. Nat Rev Mol Cell Biol *8*, 729-740.

Cao, K., Lailler, N., Zhang, Y., Kumar, A., Uppal, K., Liu, Z., Lee, E.K., Wu, H., Medrzycki, M., Pan, C., *et al.* (2013). High-resolution mapping of h1 linker histone variants in embryonic stem cells. PLoS Genet *9*, e1003417.

Cestelli, A., Castiglia, D., Di Liegro, C., and Di Liegro, I. (1992). Qualitative differences in nuclear proteins correlate with neuronal terminal differentiation. Cellular and molecular neurobiology *12*, 33-43.

Chapman, G.E., Hartman, P.G., and Bradbury, E.M. (1976). Studies on the role and mode of operation of the very-lysine-rich histone H1 in eukaryote chromatin. The isolation of the globular and non-globular regions of the histone H1 molecule. In Eur J Biochem, pp. 69-75.

Clausell, J., Happel, N., Hale, T.K., Doenecke, D., and Beato, M. (2009). Histone H1 subtypes differentially modulate chromatin condensation without preventing ATP-dependent remodeling by SWI/SNF or NURF. PLoS One *4*, e0007243.

Collado, M., Blasco, M.A., and Serrano, M. (2007). Cellular senescence in cancer and aging. Cell *130*, 223-233.

Davey, C.A., Sargent, D.F., Luger, K., Maeder, A.W., and Richmond, T.J. (2002). Solvent mediated interactions in the structure of the nucleosome core particle at 1.9 a resolution. J Mol Biol *319*, 1097-1113.

Dimri, G.P., Lee, X., Basile, G., Acosta, M., Scott, G., Roskelley, C., Medrano, E.E., Linskens, M., Rubelj, I., Pereira-Smith, O., *et al.* (1995). A biomarker that identifies senescent human cells in culture and in aging skin in vivo. Proc Natl Acad Sci U S A *92*, 9363-9367.

Dominguez, V., Pina, B., and Suau, P. (1992). Histone H1 subtype synthesis in neurons and neuroblasts. Development *115*, 181-185.

Efroni, S., Duttagupta, R., Cheng, J., Dehghani, H., Hoeppner, D.J., Dash, C., Bazett-Jones, D.P., Le Grice, S., McKay, R.D., Buetow, K.H., *et al.* (2008). Global transcription in pluripotent embryonic stem cells. Cell stem cell *2*, 437-447.

El Gazzar, M., Yoza, B.K., Chen, X., Garcia, B.A., Young, N.L., and McCall, C.E. (2009). Chromatin-specific remodeling by HMGB1 and linker histone H1 silences proinflammatory genes during endotoxin tolerance. Mol Cell Biol *29*, 1959-1971.

Fan, Y., Nikitina, T., Morin-Kensicki, E.M., Zhao, J., Magnuson, T.R., Woodcock, C.L., and Skoultchi, A.I. (2003). H1 linker histones are essential for mouse development and affect nucleosome spacing in vivo. Mol Cell Biol *23*, 4559-4572.

Fan, Y., Nikitina, T., Zhao, J., Fleury, T.J., Bhattacharyya, R., Bouhassira, E.E., Stein, A., Woodcock, C.L., and Skoultchi, A.I. (2005). Histone H1 depletion in mammals alters global chromatin structure but causes specific changes in gene regulation. Cell *123*, 1199-1212.

Fan, Y., and Skoultchi, A.I. (2004). Genetic analysis of H1 linker histone subtypes and their functions in mice. Methods in enzymology *377*, 85-107.

Funayama, R., Saito, M., Tanobe, H., and Ishikawa, F. (2006). Loss of linker histone H1 in cellular senescence. J Cell Biol *175*, 869-880.

Gaspar-Maia, A., Alajem, A., Meshorer, E., and Ramalho-Santos, M. (2011). Open chromatin in pluripotency and reprogramming. Nat Rev Mol Cell Biol *12*, 36-47.

Giambra, V., Volpi, S., Emelyanov, A.V., Pflugh, D., Bothwell, A.L., Norio, P., Fan, Y., Ju, Z., Skoultchi, A.I., Hardy, R.R., *et al.* (2008). Pax5 and linker histone H1 coordinate DNA methylation and histone modifications in the 3' regulatory region of the immunoglobulin heavy chain locus. Mol Cell Biol *28*, 6123-6133.

Happel, N., and Doenecke, D. (2009). Histone H1 and its isoforms: contribution to chromatin structure and function. Gene *431*, 1-12.

Happel, N., Schulze, E., and Doenecke, D. (2005). Characterisation of human histone H1x. Biol Chem *386*, 541-551.

Hawkins, R.D., Hon, G.C., Lee, L.K., Ngo, Q., Lister, R., Pelizzola, M., Edsall, L.E., Kuan, S., Luu, Y., Klugman, S., *et al.* (2010). Distinct epigenomic landscapes of pluripotent and lineage-committed human cells. Cell stem cell *6*, 479-491.

Jaenisch, R., and Bird, A. (2003). Epigenetic regulation of gene expression: how the genome integrates intrinsic and environmental signals. Nat Genet *33 Suppl*, 245-254.

Khochbin, S. (2001). Histone H1 diversity: bridging regulatory signals to linker histone function. Gene *271*, 1-12.

Kim, M., Habiba, A., Doherty, J.M., Mills, J.C., Mercer, R.W., and Huettner, J.E. (2009). Regulation of mouse embryonic stem cell neural differentiation by retinoic acid. Dev Biol *328*, 456-471.

Krishnakumar, R., Gamble, M.J., Frizzell, K.M., Berrocal, J.G., Kininis, M., and Kraus, W.L. (2008). Reciprocal binding of PARP-1 and histone H1 at promoters specifies transcriptional outcomes. Science *319*, 819-821.

Liang, J., Wan, M., Zhang, Y., Gu, P., Xin, H., Jung, S.Y., Qin, J., Wong, J., Cooney, A.J., Liu, D., *et al.* (2008). Nanog and Oct4 associate with unique transcriptional repression complexes in embryonic stem cells. Nat Cell Biol *10*, 731-739.

Loebel, D.A., Watson, C.M., De Young, R.A., and Tam, P.P. (2003). Lineage choice and differentiation in mouse embryos and embryonic stem cells. Dev Biol *264*, 1-14.

Loh, Y.H., Wu, Q., Chew, J.L., Vega, V.B., Zhang, W., Chen, X., Bourque, G., George, J., Leong, B., Liu, J., *et al.* (2006). The Oct4 and Nanog transcription network regulates pluripotency in mouse embryonic stem cells. Nat Genet *38*, 431-440.

Luger, K., Mader, A.W., Richmond, R.K., Sargent, D.F., and Richmond, T.J. (1997). Crystal structure of the nucleosome core particle at 2.8 A resolution. Nature *389*, 251-260.

Medrzycki, M., Zhang, Y., Cao, K., and Fan, Y. (2012). Expression analysis of mammalian linker-histone subtypes. Journal of visualized experiments : JoVE.

Meshorer, E., Yellajoshula, D., George, E., Scambler, P.J., Brown, D.T., and Misteli, T. (2006). Hyperdynamic plasticity of chromatin proteins in pluripotent embryonic stem cells. Developmental cell *10*, 105-116.

Mitsui, K., Tokuzawa, Y., Itoh, H., Segawa, K., Murakami, M., Takahashi, K., Maruyama, M., Maeda, M., and Yamanaka, S. (2003). The homeoprotein Nanog is required for maintenance of pluripotency in mouse epiblast and ES cells. Cell *113*, 631-642.

Nichols, J., Zevnik, B., Anastassiadis, K., Niwa, H., Klewe-Nebenius, D., Chambers, I., Scholer, H., and Smith, A. (1998). Formation of pluripotent stem cells in the mammalian embryo depends on the POU transcription factor Oct4. Cell *95*, 379-391.

Nishiyama, M., Oshikawa, K., Tsukada, Y., Nakagawa, T., Iemura, S., Natsume, T., Fan, Y., Kikuchi, A., Skoultchi, A.I., and Nakayama, K.I. (2009). CHD8 suppresses p53-mediated apoptosis through histone H1 recruitment during early embryogenesis. Nat Cell Biol *11*, 172-182.

Niwa, H., Miyazaki, J., and Smith, A.G. (2000). Quantitative expression of Oct-3/4 defines differentiation, dedifferentiation or self-renewal of ES cells. Nat Genet *24*, 372-376.

Pina, B., Martinez, P., Simon, L., and Suau, P. (1984). Differential kinetics of histone H1(0) accumulation in neuronal and glial cells from rat cerebral cortex during postnatal development. Biochem Biophys Res Commun *123*, 697-702.

Qian, X., Shen, Q., Goderie, S.K., He, W., Capela, A., Davis, A.A., and Temple, S. (2000). Timing of CNS cell generation: a programmed sequence of neuron and glial cell production from isolated murine cortical stem cells. Neuron *28*, 69-80.

Ramakrishnan, V. (1997). Histone structure and the organization of the nucleosome. Annu Rev Biophys Biomol Struct *26*, 83-112.

Ramakrishnan, V., Finch, J.T., Graziano, V., Lee, P.L., and Sweet, R.M. (1993). Crystal structure of globular domain of histone H5 and its implications for nucleosome binding. Nature *362*, 219-223.

Rasmussen, T.P. (2003). Embryonic stem cell differentiation: a chromatin perspective. Reproductive biology and endocrinology : RB&E *1*, 100.

Robinson, P.J., An, W., Routh, A., Martino, F., Chapman, L., Roeder, R.G., and Rhodes, D. (2008). 30 nm chromatin fibre decompaction requires both H4-K16 acetylation and linker histone eviction. J Mol Biol *381*, 816-825.

Routh, A., Sandin, S., and Rhodes, D. (2008). Nucleosome repeat length and linker histone stoichiometry determine chromatin fiber structure. Proc Natl Acad Sci U S A *105*, 8872-8877.

Silva, J., Nichols, J., Theunissen, T.W., Guo, G., van Oosten, A.L., Barrandon, O., Wray, J., Yamanaka, S., Chambers, I., and Smith, A. (2009). Nanog is the gateway to the pluripotent ground state. Cell *138*, 722-737.

Sirotkin, A.M., Edelmann, W., Cheng, G., Klein-Szanto, A., Kucherlapati, R., and Skoultchi, A.I. (1995). Mice develop normally without the H1(0) linker histone. Proc Natl Acad Sci U S A *92*, 6434-6438.

Sun, D., Melegari, M., Sridhar, S., Rogler, C.E., and Zhu, L. (2006). Multi-miRNA hairpin method that improves gene knockdown efficiency and provides linked multi-gene knockdown. Biotechniques *41*, 59-63.

Th'ng, J.P., Sung, R., Ye, M., and Hendzel, M.J. (2005). H1 family histones in the nucleus. Control of binding and localization by the C-terminal domain. J Biol Chem *280*, 27809-27814.

Thoma, F., Koller, T., and Klug, A. (1979). Involvement of histone H1 in the organization of the nucleosome and of the salt-dependent superstructures of chromatin. J Cell Biol *83*, 403-427.

Thomson, M., Liu, S.J., Zou, L.N., Smith, Z., Meissner, A., and Ramanathan, S. (2011). Pluripotency factors in embryonic stem cells regulate differentiation into germ layers. Cell *145*, 875-889.

Wolffe, A.P. (1997). Histone H1. Int J Biochem Cell Biol *29*, 1463-1466.

Woodcock, C.L., Skoultchi, A.I., and Fan, Y. (2006). Role of linker histone in chromatin structure and function: H1 stoichiometry and nucleosome repeat length. Chromosome Res *14*, 17-25.

Xie, W., Schultz, M.D., Lister, R., Hou, Z., Rajagopal, N., Ray, P., Whitaker, J.W., Tian, S., Hawkins, R.D., Leung, D., *et al.* (2013). Epigenomic analysis of multilineage differentiation of human embryonic stem cells. Cell *153*, 1134-1148.

Yamamoto, T., and Horikoshi, M. (1996). Cloning of the cDNA encoding a novel subtype of histone H1. Gene *173*, 281-285.

Zhang, Y., Cooke, M., Panjwani, S., Cao, K., Krauth, B., Ho, P.Y., Medrzycki, M., Berhe, D.T., Pan, C., McDevitt, T.C., *et al.* (2012a). Histone h1 depletion impairs embryonic stem cell differentiation. PLoS Genet *8*, e1002691.

Zhang, Y., Liu, Z., Medrzycki, M., Cao, K., and Fan, Y. (2012b). Reduction of Hox gene expression by histone H1 depletion. PLoS One *7*, e38829.

Zlatanova, J., and Doenecke, D. (1994). Histone H1 zero: a major player in cell differentiation? FASEB J *8*, 1260-1268.

CHAPTER 3

MUTATION ANALYSIS OF HISTONE H1

The results in chapter 3 have been published in the following article:

Okosun J, Bödör C, Wang J, Araf S, Yang CY, Pan C, Boller S, Cittaro D, Bozek M, Iqbal S, Matthews J, Wrench D, Marzec J, Tawana K, Popov N, O'Riain C, O'Shea D, Carlotti E, Davies A, Lawrie CH, Matolcsy A, Calaminici M, Norton A, Byers RJ, Mein C, Stupka E, Lister TA, Lenz G, Montoto S, Gribben JG, Fan Y, Grosschedl R, Chelala C, Fitzgibbon J. (2014) Integrated genomic analysis identifies recurrent mutations and evolution patterns driving the initiation and progression of follicular lymphoma. *Nature Genetics* 46(2):176-81.

3.1 Abstract

Follicular lymphoma is an incurable malignancy, with a critical event of transformation to an aggressive subtype during disease progression. Okosun *et al.* performed whole-genome or whole-exome sequencing on 10 follicular lymphoma-transformed follicular lymphoma pairs and deep sequencing of 28 genes in an extension cohort, and reported key genetic events and evolutionary processes driving tumor initiation and progression (Okosun et al., 2014). Interestingly, linker histone H1s are among the frequently mutated genes, presenting in 28% of cases. These mutations are clustered in the globular and the C-terminal domains which are directly involved in chromatin binding. To assess the effects and the mechanisms of action of H1 mutations, we took advantage of H1c/H1d/H1e triple knockout (H1 TKO) ESCs to test the functional difference between wild-type human H1c (WT hH1c) and mutant H1c containing the mutation of a.a. 102 from serine to phenylalanine (S102F). WT hH1c and $hH1c^{S102F}$ mutant were introduced into H1 TKO ESCs, and H1 TKO/hH1c and H1 TKO/$hH1c^{S102F}$ stable clones were screened to identify cell lines expressing similar levels of hH1c and $hH1c^{S102F}$ proteins. HPLC analysis of total histones purified from chromatin isolated from these cells indicates that the S102F mutation in hH1c dramatically impairs its association with chromatin. These results suggest that the identified H1 mutations in follicular lymphoma most likely lead to a loss-of-function phenotype by reducing the binding affinity of H1 for chromatin, thus compromising chromatin compaction and the regulation of specific genes.

3.2 Introduction

Follicular lymphoma (FL) is the second most frequent lymphoma and the most common indolent non-Hodgkin lymphoma (NHL) diagnosed worldwide, comprising approximately 35% of all NHLs (The Non-Hodgkin's Lymphoma Classification Project, 1997). Although the survival rate of patients with FL has significantly improved during the past 25 years through improving treatment regimens and supportive care, FL remains an incurable malignancy (Swenson et al., 2005). As majority of affected patients suffer from multiple relapses and eventually develop resistance to standard therapies, follicular lymphoma has become a significant clinical burden. Furthermore, a subgroup of patients undergo transformation into the more aggressive diffuse large B cell lymphoma (DLBCL), which results in poor clinical outcome and shortens patients' survival (Al-Tourah et al., 2008; Montoto et al., 2007; Montoto and Fitzgibbon, 2011).

Tumor cells in FL are malignant transformation of normal germinal center B cells. The chromosomal translocation of t(14;18)(q32:q21) with rearrangement of the *BCL2* gene in juxtaposition to the immunoglobulin heavy chain promoter, represents 85 - 90% of cases (Weiss et al., 1987; Zelenetz et al., 1991). This genetic aberration leads to constitutive expression of *BCL2* and confers a survival advantage to B cells, thus playing a critical role in pathogenesis of FL. However, this translocation alone is considered to be necessary but insufficient for the initiation of FL. Other than *BCL2*, mutations in multiple genes involved in B cell development, immune response, and epigenetic regulation have been identified, including *TNFRSF14* (Cheung et al., 2010; Launay et al., 2012), genes encoding histone acetyltransferases, CREBBP and EP300 (Pasqualucci et

al., 2011), and genes encoding histone methyltransferases, MLL2 (Morin et al., 2011) and EZH2 (Kridel et al., 2012; Morin et al., 2010).

Our understanding in the pathology of FL has been greatly advanced by recent genomic sequencing and case studies which suggest successive disease events occur from a long-existing tumor-initiating progenitor cell compartment (Carlotti et al., 2009; Eide et al., 2010; Ruminy et al., 2008; Weigert et al., 2012). An in-depth characterization and chronicling of the underlying genetic alterations in FL transformation will provide guidance in developing targeting therapeutic strategies. Okosun *et al.* performed whole-genome or whole-exome sequencing of follicular lymphoma - transformed follicular lymphoma (FL-tFL) pairs in match with germline samples from 10 cases (Okosun et al., 2014). The integrated genomic analysis identified key events and evolutionary processes governing the initiation and the transformation of FL, which are confined to recurrent mutations in 28 genes involved in epigenetic regulations, immune response, JAK-STAT signaling, NF-κB signaling, and B cell development (Okosun et al., 2014). Interestingly, 28% of cases were found to contain mutations in at least one histone H1 gene, and *HIST1H1C* and *HIST1H1E* (genes encoding H1c and H1e variants respectively) are the most frequently mutated (Okosun et al., 2014).

Given that histone H1 is a key component of higher order chromatin structure and regulates specific gene expression, it is not surprising to discover the involvement of histone H1 in tumorigenesis. Expression profiling of histone H1 variants in ovarian cancer shows that ovarian adenocarcinomas and adenomas exhibit distinct expression patterns of the somatic H1 genes, which indicates the expression patterns of histone H1 may serve as potential epigenetic biomarkers for ovarian cancer (Medrzycki et al., 2012b).

In addition, frequent mutations in *HIST1H1B* and *HST1H1E* genes have been identified in colorectal cancer through genome-wide analysis (Sjoblom et al., 2006; Wood et al., 2007). Recurrent missense mutations in multiple somatic H1 variants have also been found in follicular lymphoma in similar studies (Li et al., 2014; Lohr et al., 2012; Morin et al., 2011; Okosun et al., 2014). However, it is still unclear how these mutations of histone H1 affect their *in vivo* functions and contribute to tumorigenesis. To address this issue, we sought to characterize the properties of H1 mutations occurred in follicular lymphoma.

3.3 Materials and Methods

3.3.1 Cell culture

ESCs were propagated on mitotically inactivated mouse embryonic fibroblast feeder layers in tissue culture dishes (Corning) coated with 0.1% gelatin (Sigma-Aldrich). Prior to HPLC analysis, ESCs were grown on feeder-free culture dishes for feeder removal. ESC culture media consisted of Dulbecco's modified Eagle's medium (DMEM) (Life Technologies) supplemented with 15% fetal bovine serum (FBS) (Gemini), 100 U/ml penicillin (Life Technologies), 100 μg/ml streptomycin (Life Technologies), 1X MEM nonessential amino acids (Life Technologies), 0.1 mM β-mercaptoethanol (Life Technologies), and 103 U/ml of leukemia inhibitory factor (LIF; ESGRO, Chemicon). Cultures were re-fed with fresh media every other day, and passaged every 2-3 days when reaching 70-80% confluence.

3.3.2 Generation of hH1c and hH1c^{S102F} expressing ESC lines from H1c/H1d/H1e triple knockout ESCs

A point mutation (C305T) in WT hH1c coding region was made using QuikChange II Site-Directed Mutagenesis Kit (Stratagene) following the manufacturer's manual, resulting in Ser102Phe (S102F) mutation in hH1c protein present in follicular lymphoma. To facilitate the screening of ESC clones expressing the WT hH1c or the hH1c^{S102F} mutant, we inserted the FLAG tag sequence at the N-terminus of WT and mutant hH1c genes, allowing Western blotting analysis to quantify the expression levels of hH1c or hH1c^{S102F} using an antibody against FLAG. As we have previously shown,

the N-terminal FLAG epitope does not change the biochemical properties or *in vivo* functions of H1 variants (Cao et al., 2013). FLAG-hH1c or FLAG-hH1c^{S102F} was subsequently inserted into an expression vector containing 5 kb mouse H1d upstream and downstream regulatory regions and the blasticidin resistant gene established previously (Zhang et al., 2012). 20 μg of plasmid DNA was transfected into 2 x 10^7 H1 TKO ESCs by electroporation and a total of 24 clones resistant to blasticidin (Life Technologies) were picked for each construct and screened by Western blotting against the FLAG epitope (Sigma-Aldrich, F1804). ESC clones with similar expression levels of the respective FLAG-hH1c and FLAG-hH1c^{S102F} were selected for subsequent analyses.

3.3.3 Histone extraction and HPLC analysis

ESC chromatin was prepared and histones were extracted from H1 TKO/hH1c and H1 TKO/hH1c^{S102F} ESCs with 0.2 N sulfuric acid (H_2SO_4) according to protocols described previously (Cao et al., 2013; Fan and Skoultchi, 2004; Medrzycki et al., 2012a). Approximately 50 μg of total histones were injected into a C18 reverse phase column (Vydac) on an Äktapurifier UPC 900 system (GE Healthcare). Linker histones and core histones were fractionated with an increasing acetonitrile gradient (Medrzycki et al., 2012a). The effluent was monitored at 214 nm, and the peak areas were analyzed with AKTA UNICORN 5.11 software (GE Healthcare). The areas of A_{214} peaks of H1 variants and H2B were normalized by the number of peptide bonds of respective histone proteins, and the normalized values were used for calculation of H1 to nucleosome (H1/nuc) ratio (Fan and Skoultchi, 2004; Medrzycki et al., 2012a).

3.4 Results

3.4.1 Examination of H1 mutations identified in follicular lymphoma

Through genomic and exomic sequencing on follicular lymphoma-transformed follicular lymphoma (FL-tFL) pairs followed by deep sequencing of target genes, Okosun *et al.* identified fifty-five mutations across linker histone variants, *HIST1H1B* - *HIST1H1E* in 38 patients (29 diagnostic/relapse cases; 9 cases with paired FL-tFL biopsies) (Okosun et al., 2014). Mutations in *HIST1H1E* and *HIST1H1C* were most frequently observed (30 mutations in 23 cases and 12 mutations in 10 cases, respectively). Overall, 28% of the cohort tested had mutations in at least one H1 gene. Sequence alignment of H1 variants and the globular domain of avian H5 (Ramakrishnan et al., 1993) indicated that vast majority of mutations are clustered within the C-terminal domain and the highly conserved globular domain directly involved in DNA binding and chromatin compaction (Brown et al., 2006; Goytisolo et al., 1996; Vyas and Brown, 2012) (Figure 3.1). Therefore, these mutations may change the binding affinity and residence time of the respective H1 variants in chromatin and compromise their functions in chromatin compaction and specific gene regulation.

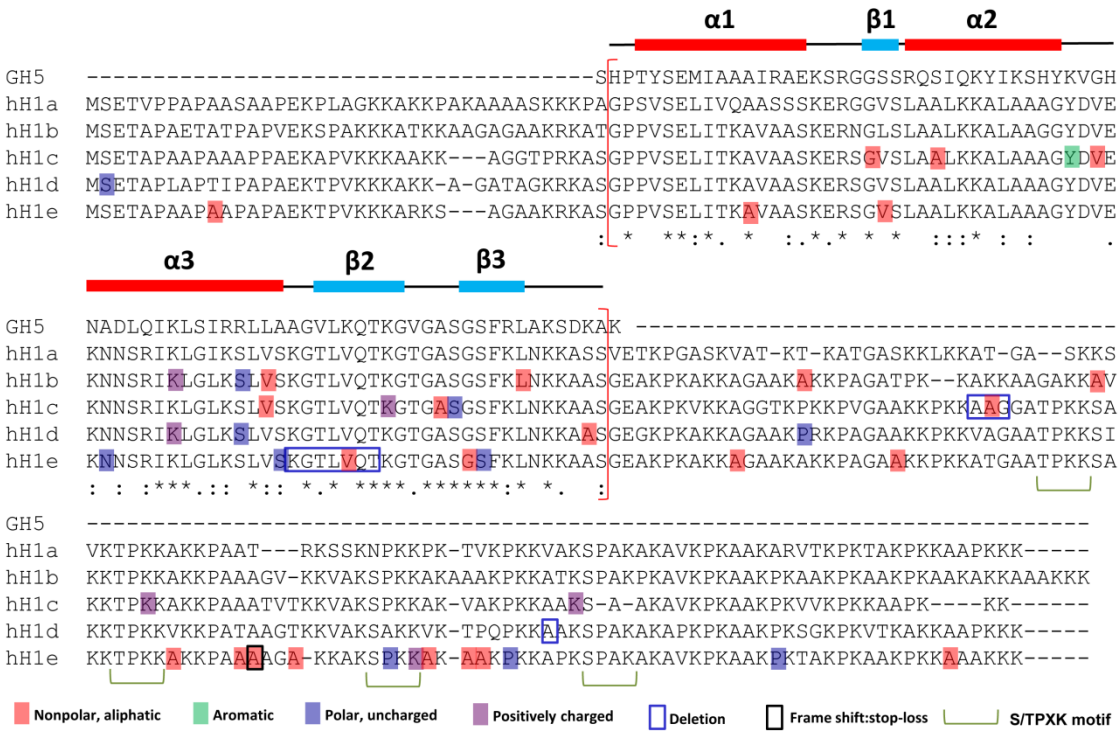

Figure 3.1 hH1a - H1e sequence alignment and the distribution of mutations.
GH5: globular domain of chicken histone H5. H1 globular domain is marked with the red bracket.

3.4.2 Mutation analysis of the human H1c^{S102F} mutation

To ascertain the mechanisms of action of these mutations, we took advantage of H1c/H1d/H1e null ESCs (Fan et al., 2005) to characterize the recurrent mutations in human H1 proteins. We started with the S102F mutation in hH1c. H1 TKO ESCs, lacking the endogenous H1c, H1d, and H1e, provide a clean cellular system for us to compare the differences between the hH1 mutants and their wild-type counterparts in chromatin binding. Expression vectors containing the FLAG-tagged WT hH1c or hH1c^{S102F} mutant were constructed and transfected into H1 TKO ESCs and screened by Western blotting for stable cell lines with high expression of the transfected H1 genes (Figure 3.2A). We have shown previously that N-terminal FLAG tag does not change the biochemical properties or *in vivo* functions of H1 variants (Cao et al., 2013). Thus, we were able to screen different cell clones with semi-quantitative Western blotting using anti-FLAG antibodies to isolate the cell lines with equal expression levels of respective FLAG-hH1c and FLAG-hH1c^{S102F} for subsequent analyses (Figure 3.2B).

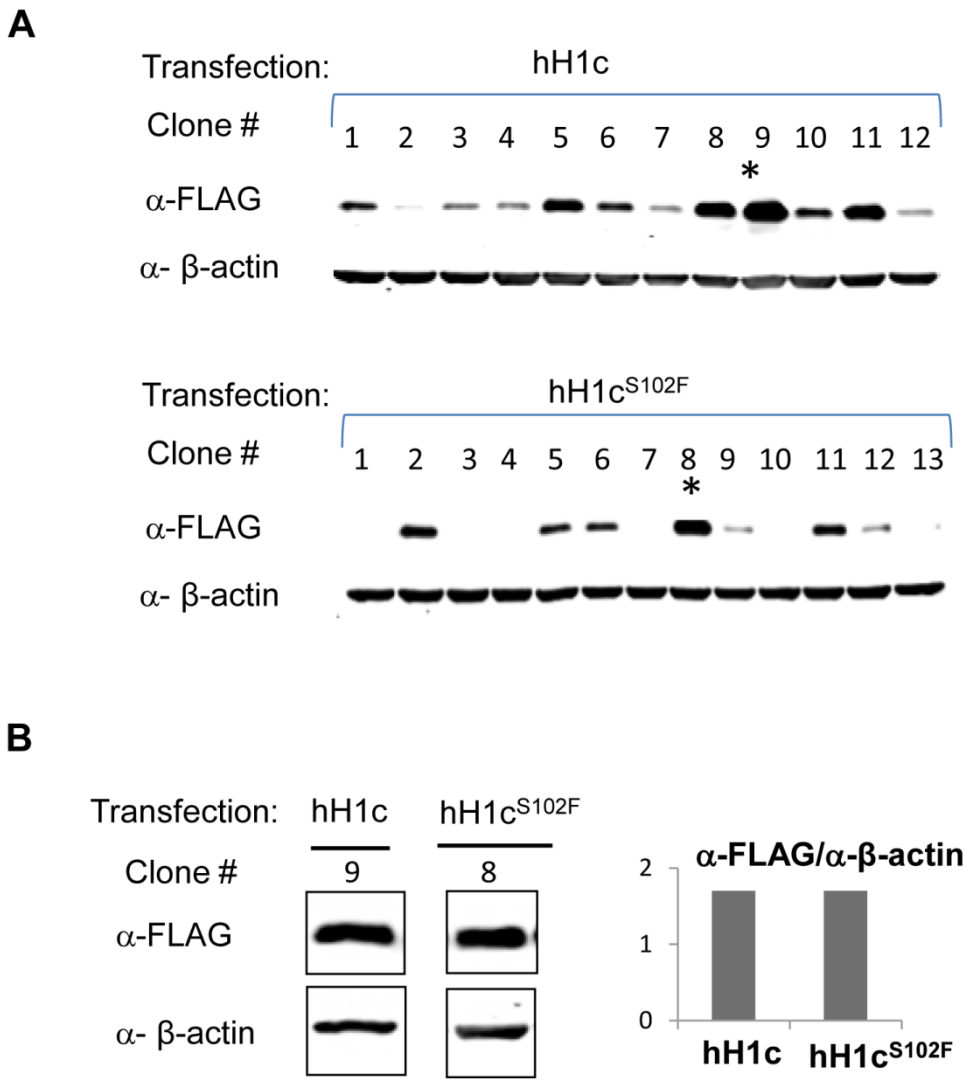

Figure 3.2 Expression of hH1c and its S102F mutant in mouse H1 TKO ESCs.
A) Expression of FLAG tagged human H1c (hH1c) or hH1c^{S102F} mutant in H1c/H1d/H1e triple null embryonic stem cells (H1 TKO ESCs). H1 TKO ESCs were transfected with vectors expressing FLAG-hH1c or FLAG-hH1c^{S102F} mutant. Twenty-four stable ESC clones were picked for each transfection and screened using an anti-FLAG antibody. Representative immunoblots of FLAG-hH1c or FLAG-hH1c^{S102F} expressing cell clones are shown. Immunoblots with anti-β-actin antibody were included as loading controls. Clones indicated with asterisks, demonstrating high expression levels of hH1c or hH1c^{S102F} were used in subsequent analysis.
B) FLAG-hH1c and FLAG-hH1c^{S102F} are expressed at the same levels in selected clones shown, normalized over β-actin.

Next, we purified the chromatin of H1 TKO/hH1c and H1 TKO/hH1c^{S102F} ESC lines, extracted total histones from chromatin, and performed reserve-phase HPLC (RP-HPLC) analysis of the histone extracts. The overexpressed FLAG-hH1c and FLAG-hH1c^{S102F} eluted in separate peaks on HPLC profiles with a delay in elusion time for the FLAG-hH1c^{S102F} peak, indicating a higher hydrophobicity of FLAG-hH1c^{S102F} than FLAG-hH1c (Figure 3.3A). Quantification of individual H1/nucleosome ratios showed a much lower level of chromatin bound FLAG-hH1c^{S102F} (0.046) than that of FLAG-hH1c (0.13), resulting in lack of significant increase in the total H1 level in H1 TKO/hH1c^{S102F} ESCs compared with H1 TKO ESCs (Figure 3.3B). These results suggest that, despite an equal expression level as hH1c, hH1c^{S102F} has drastically reduced binding affinity for DNA and residence time in chromatin, most likely owing to the change in the biochemical property and the interference of DNA binding caused by the mutation. The other H1 TKO/hH1c^{S102F} clone also displayed similar low abundance in chromatin associated histone exacts (data not shown).

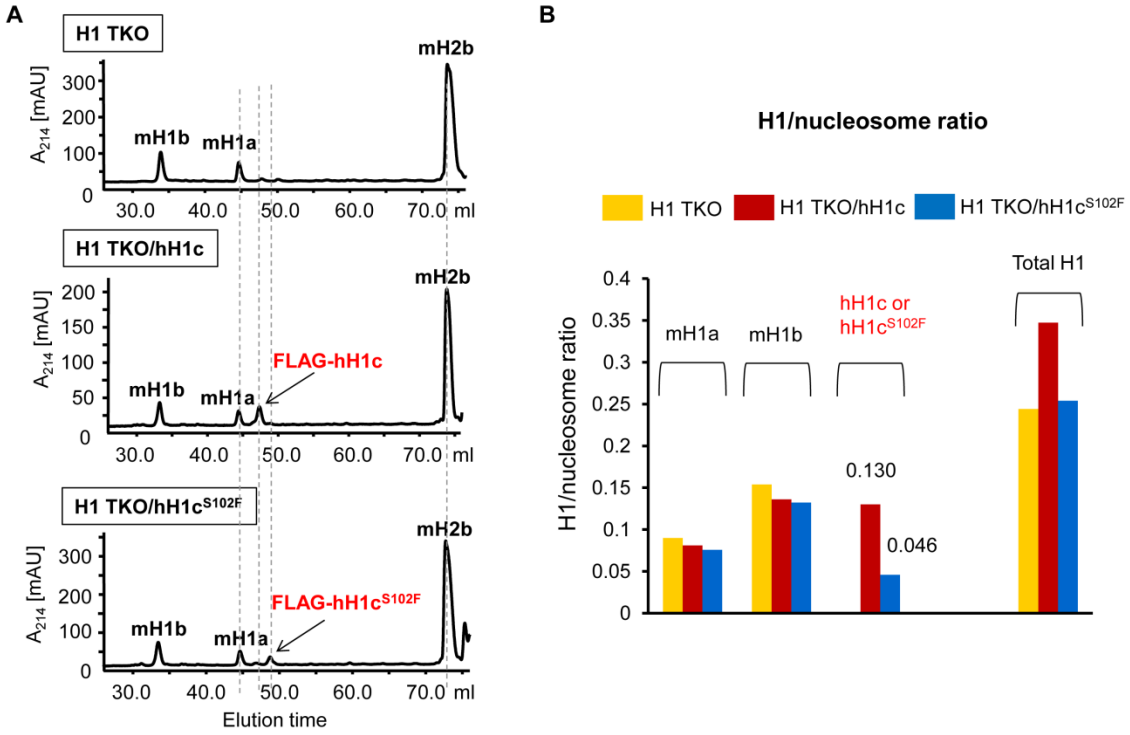

Figure 3.3 Reverse-phase HPLC (RP-HPLC) analysis of mouse H1 TKO ESCs expressing hH1c and hH1c^{S102F}.

A) RP-HPLC profiles of histones extracted from chromatin isolated from histone H1 triple-knockout (TKO) mouse ESCs expressing wild-type or S102F human histone H1. The S102F mutant demonstrated higher hydrophobicity than the wild-type protein. mH1a, mouse histone H1a; mH1b, mouse histone H1b; mH2b, mouse histone H2b; hH1c, human histone H1c.

B) Ratio of individual histone H1 variants (and total histone H1) to the nucleosome of the indicated ESC lines. The ratio is calculated from the HPLC analysis in (A) and demonstrates that the total histone H1 levels in histone H1 triple-knockout ESCs expressing human histone H1c^{S102F} were reduced compared to cells expressing wild-type human histone H1c, as a result of the weaker association of the mutant histone with chromatin (only 35% of wild-type association).

3.5 Discussion

In the current study, Okosun *et al.* reported a comprehensive sequencing effort to identify genetic alterations promoting the initiation and progression of FL (Okosun et al., 2014). This work identified a significant role of epigenetic changes in FL, as well as other co-occurring aberrations in JAK-STAT and NF-κB signaling.

Surprisingly, histone H1 was found to be recurrently mutated in FL, highlighting the potential contribution of higher order chromatin folding in FL tumorigenesis. The mutations are concentrated in the globular and the C-terminal domains normally involved in DNA binding (Brown et al., 2006; Goytisolo et al., 1996; Vyas and Brown, 2012). Indeed, the $hH1c^{S102F}$ mutant displays reduced binding to chromatin, suggesting a loss of function mutation. Other H1 mutations may cause a similar loss-of-function effect as the $hH1c^{S102F}$ analyzed here. Interestingly, many mutations occurred in nonpolar (e.g. alanine and valine) or uncharged (e.g. serine and proline) a.a. residues, which may not directly interact with the negatively charged DNA (Goytisolo et al., 1996; Ramakrishnan et al., 1993). However, these residues are conserved among paralogs, suggesting that they may have important functions in maintaining the protein structure for basic residues to interact with DNA. $hH1c^{S102F}$ may have a different structure leading to its defect in chromatin binding and/or alteration in its genomic localization patterns. It would also be interesting to tease out how H1 mutations affect gene regulation in follicular lymphoma. Other mutations distribute across the intrinsically disordered C-terminal domain, which binds to linker DNA and is important for chromatin condensation (Hansen et al., 2006; Vyas and Brown, 2012). Other than interfering with chromatin binding, mutations in H1

variants may also disrupt the interaction of the respective H1 variant with other specific protein binding partners (McBryant et al., 2010). Further studies along these lines shall help uncover additional mechanisms mediated by H1 mutants in FL.

3.6 References

Al-Tourah, A.J., Gill, K.K., Chhanabhai, M., Hoskins, P.J., Klasa, R.J., Savage, K.J., Sehn, L.H., Shenkier, T.N., Gascoyne, R.D., and Connors, J.M. (2008). Population-based analysis of incidence and outcome of transformed non-Hodgkin's lymphoma. Journal of clinical oncology : official journal of the American Society of Clinical Oncology *26*, 5165-5169.

Brown, D.T., Izard, T., and Misteli, T. (2006). Mapping the interaction surface of linker histone H1(0) with the nucleosome of native chromatin in vivo. Nat Struct Mol Biol *13*, 250-255.

Cao, K., Lailler, N., Zhang, Y., Kumar, A., Uppal, K., Liu, Z., Lee, E.K., Wu, H., Medrzycki, M., Pan, C., *et al.* (2013). High-resolution mapping of h1 linker histone variants in embryonic stem cells. PLoS Genet *9*, e1003417.

Carlotti, E., Wrench, D., Matthews, J., Iqbal, S., Davies, A., Norton, A., Hart, J., Lai, R., Montoto, S., Gribben, J.G., *et al.* (2009). Transformation of follicular lymphoma to diffuse large B-cell lymphoma may occur by divergent evolution from a common progenitor cell or by direct evolution from the follicular lymphoma clone. Blood *113*, 3553-3557.

Cheung, K.J., Johnson, N.A., Affleck, J.G., Severson, T., Steidl, C., Ben-Neriah, S., Schein, J., Morin, R.D., Moore, R., Shah, S.P., *et al.* (2010). Acquired TNFRSF14 mutations in follicular lymphoma are associated with worse prognosis. Cancer Res *70*, 9166-9174.

Eide, M.B., Liestol, K., Lingjaerde, O.C., Hystad, M.E., Kresse, S.H., Meza-Zepeda, L., Myklebost, O., Troen, G., Aamot, H.V., Holte, H., *et al.* (2010). Genomic alterations reveal potential for higher grade transformation in follicular lymphoma and confirm parallel evolution of tumor cell clones. Blood *116*, 1489-1497.

Fan, Y., Nikitina, T., Zhao, J., Fleury, T.J., Bhattacharyya, R., Bouhassira, E.E., Stein, A., Woodcock, C.L., and Skoultchi, A.I. (2005). Histone H1 depletion in mammals alters global chromatin structure but causes specific changes in gene regulation. Cell *123*, 1199-1212.

Fan, Y., and Skoultchi, A.I. (2004). Genetic analysis of H1 linker histone subtypes and their functions in mice. Methods in enzymology *377*, 85-107.

Goytisolo, F.A., Gerchman, S.E., Yu, X., Rees, C., Graziano, V., Ramakrishnan, V., and Thomas, J.O. (1996). Identification of two DNA-binding sites on the globular domain of histone H5. EMBO J *15*, 3421-3429.

Hansen, J.C., Lu, X., Ross, E.D., and Woody, R.W. (2006). Intrinsic protein disorder, amino acid composition, and histone terminal domains. J Biol Chem *281*, 1853-1856.

Kridel, R., Sehn, L.H., and Gascoyne, R.D. (2012). Pathogenesis of follicular lymphoma. The Journal of clinical investigation *122*, 3424-3431.

Launay, E., Pangault, C., Bertrand, P., Jardin, F., Lamy, T., Tilly, H., Tarte, K., Bastard, C., and Fest, T. (2012). High rate of TNFRSF14 gene alterations related to 1p36 region in de novo follicular lymphoma and impact on prognosis. Leukemia *26*, 559-562.

Li, H., Kaminski, M.S., Li, Y., Yildiz, M., Ouillette, P., Jones, S., Fox, H., Jacobi, K., Saiya-Cork, K., Bixby, D., *et al.* (2014). Mutations in linker histone genes HIST1H1 B, C, D, and E; OCT2 (POU2F2); IRF8; and ARID1A underlying the pathogenesis of follicular lymphoma. Blood *123*, 1487-1498.

Lohr, J.G., Stojanov, P., Lawrence, M.S., Auclair, D., Chapuy, B., Sougnez, C., Cruz-Gordillo, P., Knoechel, B., Asmann, Y.W., Slager, S.L., *et al.* (2012). Discovery and prioritization of somatic mutations in diffuse large B-cell lymphoma (DLBCL) by whole-exome sequencing. Proc Natl Acad Sci U S A *109*, 3879-3884.

McBryant, S.J., Lu, X., and Hansen, J.C. (2010). Multifunctionality of the linker histones: an emerging role for protein-protein interactions. Cell research *20*, 519-528.

Medrzycki, M., Zhang, Y., Cao, K., and Fan, Y. (2012a). Expression analysis of mammalian linker-histone subtypes. Journal of visualized experiments : JoVE.

Medrzycki, M., Zhang, Y., McDonald, J.F., and Fan, Y. (2012b). Profiling of linker histone variants in ovarian cancer. Frontiers in bioscience : a journal and virtual library *17*, 396-406.

Montoto, S., Davies, A.J., Matthews, J., Calaminici, M., Norton, A.J., Amess, J., Vinnicombe, S., Waters, R., Rohatiner, A.Z., and Lister, T.A. (2007). Risk and clinical implications of transformation of follicular lymphoma to diffuse large B-cell lymphoma. Journal of clinical oncology : official journal of the American Society of Clinical Oncology *25*, 2426-2433.

Montoto, S., and Fitzgibbon, J. (2011). Transformation of indolent B-cell lymphomas. Journal of clinical oncology : official journal of the American Society of Clinical Oncology *29*, 1827-1834.

Morin, R.D., Johnson, N.A., Severson, T.M., Mungall, A.J., An, J., Goya, R., Paul, J.E., Boyle, M., Woolcock, B.W., Kuchenbauer, F., *et al.* (2010). Somatic mutations altering EZH2 (Tyr641) in follicular and diffuse large B-cell lymphomas of germinal-center origin. Nat Genet *42*, 181-185.

Morin, R.D., Mendez-Lago, M., Mungall, A.J., Goya, R., Mungall, K.L., Corbett, R.D., Johnson, N.A., Severson, T.M., Chiu, R., Field, M., *et al.* (2011). Frequent mutation of histone-modifying genes in non-Hodgkin lymphoma. Nature *476*, 298-303.

Okosun, J., Bodor, C., Wang, J., Araf, S., Yang, C.Y., Pan, C., Boller, S., Cittaro, D., Bozek, M., Iqbal, S., *et al.* (2014). Integrated genomic analysis identifies recurrent

mutations and evolution patterns driving the initiation and progression of follicular lymphoma. Nat Genet *46*, 176-181.

Pasqualucci, L., Dominguez-Sola, D., Chiarenza, A., Fabbri, G., Grunn, A., Trifonov, V., Kasper, L.H., Lerach, S., Tang, H., Ma, J., *et al.* (2011). Inactivating mutations of acetyltransferase genes in B-cell lymphoma. Nature *471*, 189-195.

Ramakrishnan, V., Finch, J.T., Graziano, V., Lee, P.L., and Sweet, R.M. (1993). Crystal structure of globular domain of histone H5 and its implications for nucleosome binding. Nature *362*, 219-223.

Ruminy, P., Jardin, F., Picquenot, J.M., Parmentier, F., Contentin, N., Buchonnet, G., Tison, S., Rainville, V., Tilly, H., and Bastard, C. (2008). S(mu) mutation patterns suggest different progression pathways in follicular lymphoma: early direct or late from FL progenitor cells. Blood *112*, 1951-1959.

Sjoblom, T., Jones, S., Wood, L.D., Parsons, D.W., Lin, J., Barber, T.D., Mandelker, D., Leary, R.J., Ptak, J., Silliman, N., *et al.* (2006). The consensus coding sequences of human breast and colorectal cancers. Science *314*, 268-274.

Swenson, W.T., Wooldridge, J.E., Lynch, C.F., Forman-Hoffman, V.L., Chrischilles, E., and Link, B.K. (2005). Improved survival of follicular lymphoma patients in the United States. Journal of clinical oncology : official journal of the American Society of Clinical Oncology *23*, 5019-5026.

The Non-Hodgkin's Lymphoma Classification Project (1997). A clinical evaluation of the International Lymphoma Study Group classification of non-Hodgkin's lymphoma. Blood *89*, 3909-3918.

Vyas, P., and Brown, D.T. (2012). N- and C-terminal domains determine differential nucleosomal binding geometry and affinity of linker histone isotypes H1(0) and H1c. J Biol Chem *287*, 11778-11787.

Weigert, O., Kopp, N., Lane, A.A., Yoda, A., Dahlberg, S.E., Neuberg, D., Bahar, A.Y., Chapuy, B., Kutok, J.L., Longtine, J.A., *et al.* (2012). Molecular ontogeny of donor-derived follicular lymphomas occurring after hematopoietic cell transplantation. Cancer discovery *2*, 47-55.

Weiss, L.M., Warnke, R.A., Sklar, J., and Cleary, M.L. (1987). Molecular analysis of the t(14;18) chromosomal translocation in malignant lymphomas. The New England journal of medicine *317*, 1185-1189.

Wood, L.D., Parsons, D.W., Jones, S., Lin, J., Sjoblom, T., Leary, R.J., Shen, D., Boca, S.M., Barber, T., Ptak, J., *et al.* (2007). The genomic landscapes of human breast and colorectal cancers. Science *318*, 1108-1113.

Zelenetz, A.D., Chu, G., Galili, N., Bangs, C.D., Horning, S.J., Donlon, T.A., Cleary, M.L., and Levy, R. (1991). Enhanced detection of the t(14;18) translocation in malignant lymphoma using pulsed-field gel electrophoresis. Blood *78*, 1552-1560.

Zhang, Y., Cooke, M., Panjwani, S., Cao, K., Krauth, B., Ho, P.Y., Medrzycki, M., Berhe, D.T., Pan, C., McDevitt, T.C., *et al.* (2012). Histone h1 depletion impairs embryonic stem cell differentiation. PLoS Genet *8*, e1002691.

CHAPTER 4

CONCLUSIONS AND FUTURE STUDIES

Linker histone H1 and H1 variants play key roles in facilitating chromatin packaging into higher order structures. In this study, we first generated ultra-low H1 ESCs by deriving H1c/H1d/H1e/$H1^0$ quadruple knockout ESCs (H1 QKO ESCs) using mouse genetics followed by depletion of H1a and H1b in H1 QKO ESCs using a Tet-On inducible RNAi system. We adopted this approach to avoid the potential deleterious effects of the minimum H1 level on ESC viability. However, these ESCs, with an H1/nuc ratio as low as 0.11, exhibit normal colony morphology and proliferation rates, indicating that severe depletion of the H1 level is compatible with ESC self-renewal. Given the viability of these ESCs, future studies aim to generate complete H1 null ESCs using genome-editing tools such as CRISPR/Cas- and TALEN- based methods (Cong et al., 2013; Gaj et al., 2013; Mali et al., 2013; Miller et al., 2011) should be feasible. Such experiments will address if there is a minimum threshold of H1 required for ESC self-renewal.

The work in this thesis demonstrated a dosage effect of histone H1 on neural differentiation of ESCs. Neural differentiation gives rise to neural progenitors and defined neural lineages which display distinct cell shapes and express multiple specific markers (Bibel et al., 2004; Doetsch, 2003; Temple, 2001; Zhang et al., 2001), rendering an ideal approach to study the regulatory mechanisms of ESC differentiation. *In vitro* neural differentiation of ESCs with sequential H1 depletion revealed a dosage effect, rather than a variant-specificity, of histone H1 on generation of neural progenitors,

neurons, and glial cells, representing all major events during neurodevelopment. The dosage effect is also apparent in silencing pluripotency-associated genes which are normally rapidly downregulated upon ESC differentiation. Since the H1 content gradually increases during neural differentiation, we surmise that chromatin condensation mediated by H1 plays a fundamental role in *Oct4* silencing, which in turn serves as a critical step for differentiation to proceed successfully. It is likely that, despite a global effect on chromatin compaction, H1 acts locally at key regulatory loci in modulating cell differentiation.

While ESC self-renewal appears unaffected by low H1 content, we found that severe H1 depletion leads to reduced cell proliferation and cellular senescence in differentiating EBs. A previous report shows impaired cell proliferation in chicken lymphocytes with complete H1 knockout (Hashimoto et al., 2010). Together, these studies suggest that H1 is important for the propagation of differentiated cells, which have a much higher H1 content than ESCs. It has also been shown that depletion of certain specific H1 variants induces cell cycle arrest and cellular senescence in human breast cancer cells and fibroblasts (Funayama et al., 2006; Sancho et al., 2008), suggesting potential specificities of H1 variants in cell cycle regulation in different cellular context. Future studies on the molecular mechanisms underlying the cell proliferation defects in differentiated cells upon H1 depletion will illuminate how H1 and higher order chromatin structure are connected to cell cycle progression and cellular senescence. For example, one potential mechanism to investigate is the DNA damage response in differentiating QKO/abi cells. DNA damage responses elicit DNA repair and cell cycle arrest (Lukas et al., 2011). It has been found that H1 depletion in chicken

lymphocytes leads to increased chromosome aberration rates (Hashimoto et al., 2010). Immunostaining of γ-H2AX (Ser139 phosphorylated H2AX), a biomarker for double-strand breaks (Burma et al., 2001; Dickey et al., 2009; Rogakou et al., 1998), can be used to compare DNA lesions in QKO/abi and WT EBs.

Another key finding of this study is that *Oct4* knockdown effectively restores neural differentiation and partially reverses the reduction in cell proliferation and cellular senescence in QKO/abi EBs. Other factors that may rescue neural differentiation in the context of H1 loss remain to be identified. Beside *Oct4* and *Nanog,* the expression of other pluripotency-associated factors, such as Sox2, Sall4, Dax1, Essrb, Tbx3, Tcl1, Rif1, Nac1, and Zfp281 (Chen and Daley, 2008; Ivanova et al., 2006; Ng and Surani, 2011; Wang et al., 2006) may also be affected by H1 loss. These factors regulate each other to form a complex transcriptional regulatory network in promoting ESC self-renewal (Zhou et al., 2007). In addition to pluripotency factors, neurogenic factors controlling lineage commitment including Pax6, Ascl1, Brn2, Ngn2, and Mytl1 (Hsieh, 2012; Kohwi and Doe, 2013; Zhang et al., 2013) may also be dysregulated upon H1 depletion. Expression profiling of QKO/abi and WT cells should offer a better picture of the scope of H1's regulation on pluripotency genes and lineage-specific genes. Whether overexpression of the neurogenic factors could rescue the defects in neural differentiation of ESCs with low H1 levels is also warranted.

A separate addition to my thesis work is the mutation analysis of H1 mutants identified in Follicular lymphoma (FL), the most common indolent non-Hodgkin lymphoma of significant clinical burden. Through whole-genome or whole-exome sequencing of follicular lymphomas and transformed follicular lymphomas, Fitzgibbon

Lab identified recurrent mutations driving the initiation and progression of FL (Okosun et al., 2014). Among the frequent mutations are linker histone H1 variants, with their mutations present in 28% of cases, and *HIST1H1C* and *HIST1H1E* were the most frequently mutated. Majority of the mutations are concentrated to the conserved globular domain and the intrinsically disordered C-terminus, which are essential for binding of H1 to chromatin. Mutation analysis of $hH1c^{S102F}$ demonstrated that this mutation increases hH1c's hydrophobicity and reduces its binding affinity for chromatin, thus likely acts through a loss-of-function mechanism by compromising hH1c's functions in chromatin compaction and regulation of key genes, contributing to malignant transformation of B lymphocytes. Future studies to characterize mutations of other sites and variants will provide a more comprehensive picture about the impact of H1 mutations. It will also be worthwhile to investigate how H1 mutations affect gene regulation in B cells for better understanding the mechanisms of H1 mutations in tumorigenesis.

References

Bibel, M., Richter, J., Schrenk, K., Tucker, K.L., Staiger, V., Korte, M., Goetz, M., and Barde, Y.A. (2004). Differentiation of mouse embryonic stem cells into a defined neuronal lineage. Nature neuroscience *7*, 1003-1009.

Burma, S., Chen, B.P., Murphy, M., Kurimasa, A., and Chen, D.J. (2001). ATM phosphorylates histone H2AX in response to DNA double-strand breaks. J Biol Chem *276*, 42462-42467.

Chen, L., and Daley, G.Q. (2008). Molecular basis of pluripotency. Hum Mol Genet *17*, R23-27.

Cong, L., Ran, F.A., Cox, D., Lin, S., Barretto, R., Habib, N., Hsu, P.D., Wu, X., Jiang, W., Marraffini, L.A., *et al.* (2013). Multiplex genome engineering using CRISPR/Cas systems. Science *339*, 819-823.

Dickey, J.S., Redon, C.E., Nakamura, A.J., Baird, B.J., Sedelnikova, O.A., and Bonner, W.M. (2009). H2AX: functional roles and potential applications. Chromosoma *118*, 683-692.

Doetsch, F. (2003). The glial identity of neural stem cells. Nature neuroscience *6*, 1127-1134.

Funayama, R., Saito, M., Tanobe, H., and Ishikawa, F. (2006). Loss of linker histone H1 in cellular senescence. J Cell Biol *175*, 869-880.

Gaj, T., Gersbach, C.A., and Barbas, C.F., 3rd (2013). ZFN, TALEN, and CRISPR/Cas-based methods for genome engineering. Trends in biotechnology *31*, 397-405.

Hashimoto, H., Takami, Y., Sonoda, E., Iwasaki, T., Iwano, H., Tachibana, M., Takeda, S., Nakayama, T., Kimura, H., and Shinkai, Y. (2010). Histone H1 null vertebrate cells exhibit altered nucleosome architecture. Nucleic Acids Res *38*, 3533-3545.

Hsieh, J. (2012). Orchestrating transcriptional control of adult neurogenesis. Genes Dev *26*, 1010-1021.

Ivanova, N., Dobrin, R., Lu, R., Kotenko, I., Levorse, J., DeCoste, C., Schafer, X., Lun, Y., and Lemischka, I.R. (2006). Dissecting self-renewal in stem cells with RNA interference. Nature *442*, 533-538.

Kohwi, M., and Doe, C.Q. (2013). Temporal fate specification and neural progenitor competence during development. Nature reviews Neuroscience *14*, 823-838.

Lukas, J., Lukas, C., and Bartek, J. (2011). More than just a focus: The chromatin response to DNA damage and its role in genome integrity maintenance. Nat Cell Biol *13*, 1161-1169.

Mali, P., Yang, L., Esvelt, K.M., Aach, J., Guell, M., DiCarlo, J.E., Norville, J.E., and Church, G.M. (2013). RNA-guided human genome engineering via Cas9. Science *339*, 823-826.

Miller, J.C., Tan, S., Qiao, G., Barlow, K.A., Wang, J., Xia, D.F., Meng, X., Paschon, D.E., Leung, E., Hinkley, S.J., *et al.* (2011). A TALE nuclease architecture for efficient genome editing. Nat Biotechnol *29*, 143-148.

Ng, H.H., and Surani, M.A. (2011). The transcriptional and signalling networks of pluripotency. Nat Cell Biol *13*, 490-496.

Okosun, J., Bodor, C., Wang, J., Araf, S., Yang, C.Y., Pan, C., Boller, S., Cittaro, D., Bozek, M., Iqbal, S., *et al.* (2014). Integrated genomic analysis identifies recurrent mutations and evolution patterns driving the initiation and progression of follicular lymphoma. Nat Genet *46*, 176-181.

Rogakou, E.P., Pilch, D.R., Orr, A.H., Ivanova, V.S., and Bonner, W.M. (1998). DNA double-stranded breaks induce histone H2AX phosphorylation on serine 139. J Biol Chem *273*, 5858-5868.

Sancho, M., Diani, E., Beato, M., and Jordan, A. (2008). Depletion of human histone H1 variants uncovers specific roles in gene expression and cell growth. PLoS Genet *4*, e1000227.

Temple, S. (2001). The development of neural stem cells. Nature *414*, 112-117.

Wang, J., Rao, S., Chu, J., Shen, X., Levasseur, D.N., Theunissen, T.W., and Orkin, S.H. (2006). A protein interaction network for pluripotency of embryonic stem cells. Nature *444*, 364-368.

Zhang, S.C., Wernig, M., Duncan, I.D., Brustle, O., and Thomson, J.A. (2001). In vitro differentiation of transplantable neural precursors from human embryonic stem cells. Nat Biotechnol *19*, 1129-1133.

Zhang, Y., Schulz, V.P., Reed, B.D., Wang, Z., Pan, X., Mariani, J., Euskirchen, G., Snyder, M.P., Vaccarino, F.M., Ivanova, N., *et al.* (2013). Functional genomic screen of human stem cell differentiation reveals pathways involved in neurodevelopment and neurodegeneration. Proc Natl Acad Sci U S A *110*, 12361-12366.

Zhou, Q., Chipperfield, H., Melton, D.A., and Wong, W.H. (2007). A gene regulatory network in mouse embryonic stem cells. Proc Natl Acad Sci U S A *104*, 16438-16443.